Highly conductive and transparent ZnO thin film using Chemical Spray Pyrolysis technique: Effect of doping and deposition parameters

---

Thesis submitted to

COCHIN UNIVERSITY OF SCIENCE AND TECHNOLOGY

in partial fulfilment of the requirements

for the award of the degree of

Doctor of Philosophy

VIMALKUMAR T. V.

Thin Film Photovoltaic Division

Department of Physics

Cochin University of Science and Technology

Cochin - 682 022, Kerala, India

August 2011

Highly conductive and transparent ZnO thin film using Chemical Spray Pyrolysis technique: Effect of doping and deposition parameters

Ph.D thesis in the field of Thin Film Photovoltaics

Author

Vimalkumar T. V.
Thin Film Photovoltaic Division
Department of Physics
Cochin University of Science and Technology
Cochin - 682 022, Kerala, India
email: vimalcusat@gmail.com

Supervising Guide

Dr. K. P. Vijayakumar
Professor, Department of Physics
Cochin University of Science and Technology
Cochin - 682 022, India
email: kpv@cusat.ac.in

August 2011

Thin Film Photovoltaic Division, Department of Physics, Cochin University of Science and Technology, Cochin - 682 022, Kerala, India.

Dr. K. P. Vijayakumar
Professor
Department of Physics
Cochin University of Science and Technology
Cochin – 682 022

Certified that the thesis entitled ***" Highly conductive and transparent ZnO thin film using Chemical Spray Pyrolysis technique: Effect of doping and deposition parameters"*** submitted by **Mr.Vimalkumar T. V.** is an authentic record of research work carried out by him under my supervision at the Department of Physics in partial fulfilment of the requirements for the award of degree of Doctor of Philosophy of Cochin University of Science and Technology and the work embodied in this thesis has not been included in any other thesis submitted previously for the award of any other degree.

Cochin – 22
Date:

Prof. K. P. Vijayakumar
Supervising Guide

Phone: +91 4842577404. **Fax:**. +91 484 2577595. **Email:** kpv@cusat.ac.in

Declaration

I hereby declare that the thesis entitled *" **Highly conductive and transparent ZnO thin film using Chemical Spray Pyrolysis technique: Effect of doping and deposition parameters**"* submitted for the award of degree of Doctor of Philosophy of Cochin University of Science and Technology is based on the original work done by me under the guidance of **Dr. K. P. Vijayakumar**, Professor, Department of Physics, Cochin University of Science and Technology, Cochin - 682 022 and this work has not been included in any other thesis submitted previously for the award of any other degree.

Cochin – 22
Date:

Vimalkumar T. V.

Dedicated

To my beloved parents & brother

Acknowledgements

This dissertation arose in part out of years of research that has been done since I came to Thin Film Photovoltaic Division. By that time, I have worked with a great number of people whose contribution in various ways to the research and the making of the thesis deserve special mention. It is a pleasure to convey my gratitude to them all in my humble acknowledgment.

In the first place I would like to express my gratitude to Prof. K. P. Vijayakumar for his supervision, advice, and guidance from the very early stage of this research as well as throughout the work. Above all and the most needed, he provided me unflinching encouragement and support in various ways. I am indebted to him more than he knows.

I gratefully acknowledge Prof. C. Sudha Kartha for her advice, supervision, and crucial contribution, which made her a backbone of this research and so to this thesis.

Words are inadequate to express my gratitude to my beloved teacher Prof. C. Raveendranath (St. Thomas College, Thrissur) for his moral support for the completion of my research work. His support has guided me for the better performance throughout the research.

I am thankful to Prof. M. R. Anantharaman , Head of Department of Physics for all the facilities extended to me in the department. I would like to express my sincere appreciation to all the faculties of Department of Physics, CUSAT and St. Thomas college Thrissur for their help and support for my research. I am thankful to all the office and library staff of Department of Physics, CUSAT.

I am grateful to Dr. Y. Kashiwaba and T. Abe of Department of Electrical and Electronic Engineering, Iwate University Japan for XPS measurements. I am also grateful to Dr. K. B. Jinesh, Nanyang Technological University (NTU) Singapore for his valuable help in the SEM analysis of my sample.

I express my heartfelt thanks to my dearest friends Anita and Dr.Pramitha for their sincere friendship and support right from the beginning of my work .I would like to thank my seniors Dr. S . Ramkumar, Dr. Paulraj, Dr. Teny Theresa John, Dr. P. M. Ratheesh Kumar, Dr. Beena Mary John, Dr. R. Sreekumar, Dr. A. Sreekumar, Dr. R. Jayakrishnan, K. C. Wilson, Dr. K. G. Deepa, Dr. Tina Sebastian, Dr. Meril Mathew, and Dr. V. C.

Kishore for their love and support throughout the different stages of my research and life in the University.

My heartfelt thanks to my loving juniors Sajeesh, Rajesh Menon, Angel, Rajeshmon, Poornima, Jafar, Aneesh George, Santhosh, Deepu, Anas, Nithya, Sreeroop, Rajesh C.S, Subramanyan, Minu, Nimmi and Sona. I express my gratitude to Mphil students Manju, Subin, Seena, Niketha, Anjaly and Bijesh and MSc project students. I express my sincere thanks to all my friends in the Physics department, other departments and hostels in CUSAT for their loving support throughout my life at CUSAT.

I am so grateful to all my friends right from my school days and college days especially Dr. Sajanlal , Dr. Shibu, Alex Andrews and Shanoj for their everlasting love and encouragement. I am also thankful to Narendrettan, Ramakrishnettan, Asokettan, Rajan mash, Biju. K. Marar and Rajeesh for their love

I am indebted to my parents for their love, encouragement and support, for the completion of my dream. I would like to thank my brother Vinilkumar for his love and support. I would like to thank all my friends and well wishers for their support.

I thank God Almighty for being with me in every moment giving me the strength to overcome all the obstacles. Without his blessing, it would not have been possible to complete this endeavour.

Vimalkumar T. V.

Preface

Transparent Conducting Oxide (TCO) films with wide energy band gap (2.7 eV-4.6 eV) usually exhibit high electrical conductivity (10^2 - 10^4 S/m), optical transmittance (in visible region) and reflectance (in IR region). These properties of TCO make them suitable for a variety of applications. The semiconducting transparent films have been widely used in a variety of applications such as gas sensors, solar cells, heat reflectors, protective coating, light transparent electrodes and photocathode in photoelectron-chemical cells.

For most optoelectronic devices including flat panel displays, it is essential to use transparent electrodes consisting of a thin film of a TCO. Although tin-doped indium oxide (commonly called indium tin-oxide, or ITO) thin films deposited by magnetron sputtering (MSP) have been in practical use for most transparent electrode applications, there are many reports on other TCO semiconductors as well as deposition methods. A stable supply of ITO may be difficult to achieve for the recently expanding market of optoelectronic devices because of the cost and scarcity of indium, the principal material of ITO. In addition, recent development in optoelectronic devices have resulted in high demand for thin-film transparent electrodes with specialized properties and present research in the area of thin films of TCO semiconductors is focusing on resolving these problems. For example, the impurity-doped Zinc Oxide (ZnO) has been (almost) developed to be an alternative to ITO. Hence there is a great interest in ZnO thin films with properties suitable for specialized applications.

In the present work we report the preparation details studies on ZnO thin films. ZnO thin films are prepared using cost effective deposition technique viz., Chemical Spray Pyrolysis (CSP). The method is very effective for large area preparation of the ZnO thin film. A new post-deposition process could also be developed to avoid the adsorption of oxygen that usually occurs after the spraying process i.e., while cooling. Studies were done by changing the various deposition parameters for optimizing the properties of ZnO thin film. Moreover, different methods of doping using various elements are also tried to enhance the conductivity and transparency of the film to make these suitable for various optoelectronic applications. The Whole study is presented in the thesis in seven chapters.

Chapter 1 is a brief description on transparent conducting oxides. It includes the introduction, general properties and classification of transparent conducting oxides. It also

gives short description of n-type and p-type TCO materials. This chapter concludes with a list of important applications of TCO and few lines on motivation of the present study.

Chapter 2 is a review on ZnO material touching the important points regarding the structural, electrical and optical properties of ZnO prepared using physical and chemical methods. The various applications of ZnO are also discussed here.

Chapter 3, describes the new method developed to enhance the conductivity of spray pyrolysed ZnO thin film. Two methods were tried to reduce the resistivity of the ZnO film viz., the conventional vacuum annealing method and a "Zero energy process" which involves the isolation of the sample from the oxygen atmosphere immediately after deposition. Structural, compositional, optical and electrical characterization of the film is carried out using X-Ray Diffraction (XRD), X-ray Photoelectron Spectroscopy (XPS), Photoluminescence (PL), electrical resistivity measurement, optical absorption and transmission. After the Zero energy process crystallanity, transmittance and conductivity of the film increased drastically and hence this process was made mandatory for all the films.

Chapter 4 deals with the optimization of deposition parameters like spray rate, molarity, precursor medium and pH of the solution. Samples were prepared at different spray rates from 3 ml/min to 12 ml/min. XRD analysis showed that, with the increase in spray rate, orientation of the grains changed from (101) plane to (002) plane. PL studies proved that intensity of the blue-green emission decreased when the orientation of grains shifted to (002) plane. Resistivity was observed to be least [2×10^{-3} Ω cm] for the sample prepared at 7ml/min. Effect of change of the molarity of Zinc acetate precursor was also studied .The molarity is varied from 0.2 M to 0.6 M. The percentage of optical transmission decreased with increasing molarity and resistivity increased with increasing molarity. Next we tried to find out the effect of varying the precursor medium and this was done by changing the nature and concentration of alcohol in the spray solution. It is observed that the crystallite size, optical transmission and electrical conductivity of the films improved with increase in alcohol concentration. Intensity of the PL emission in blue-green region varied with percentage as well as with the type of alcohol used in the precursor solution. Propanol based samples had lower resistivity than ethanol based samples. The lowest resistivity [2×10^{-2}Ω cm] was obtained for the sample prepared using deionized water and propanol in the ratio 1:1. Effect of pH was studied by varying the pH of the precursor from 3 to 6. On

increasing the acidic nature of the solution, transmittance of the film decreased and the intensity of blue-green emission also decreased.

In order to make ZnO films electrically more conducting, different methods of doping using various elements was tried. **Chapter 5** discusses about the different dopant materials used for improving the opto-electronic properties of spray pyrolysed ZnO thin film. First we tried tin and Indium (In) over the spray pyrolysed ZnO thin film through 'ex-situ' doping technique. Lowest resistivity and also better structural properties was obtained for In diffused sample. Next was tried doping of Indium and Aluminum (Al) in spray pyrolysed ZnO thin films through 'in-situ' doping. By in-situ doping the resistivity of the films could be lowered to about 10^{-3} Ω cm, the lowest value being 1.5×10^{-3} Ω cm for 2.5% Al doped sample. Further, optimization of the thickness of Al doped samples were done. By annealing this sample in vacuum [Pressure-2×10^{-5} mbar] at 450^{o}C, resistivity could be further reduced to 6×10^{-4}Ω cm, which is the lowest value obtained for ZnO thin film prepared by chemical methods.

Chapter 6 describes the co-doping of ZnO films using indium and fluorine and also of aluminum and fluorine. In the first case, both indium and fluorine were doped together by adding required quantities of indium nitrate and ammonium fluoride into the spray solution. In the second case, co-doping of aluminum and fluorine were carried out by adding aluminum 2, 4- pentanedionate and ammonium fluoride in the pristine solution. Resistivity and band gap of the films increased with the increase in doping concentration of fluorine in both the cases. On the other hand, the transmittance increased slightly with the increase in the fluorine concentration.

Chapter 7 Summarizes the main results in the thesis. This chapter concludes with a brief coverage of the future scope of the results.

Publications

Journal Publications

- On single doping and co-doping of spray pyrolysed ZnO films: Structural, Electrical and Optical Characterisation, **T. V. Vimalkumar**, N. Poornima, K.B. Jinesh, C. Sudha Kartha and K. P. Vijayakumar, Applied Surface Science 257 (2011) 8334.
- Enhancement of Electrical Conductivity in sprayed ZnO thin film through Zero-Energy Process **T.V. Vimalkumar**, N. Poornima , C. Sudha Kartha , K. P. Vijayakumar. T. Abe and Y. Kashiwaba, Physica B-Condensed Matter 405 (2010) 4957.
- Effect of precursor medium on structural , electrical and optical properties of sprayed polycrystalline ZnO thin films, **T. V. Vimalkumar**, N. Poornima, C. Sudha Kartha and K.P.Vijayakumar, Material Science And Engineering B 175(2010)29.
- On tuning the orientation of grains of spray pyrolysed ZnO thin films, **T. V. Vimalkumar**, N. Poornima , C. Sudha Kartha and K. P. Vijayakumar, Applied Surface Science 256 (2010) 6025.
- Highly conducting spray pyrolysed ZnO thin films through 'Zero Energy Process': Further improvement of electrical and optical properties due to doping, **T.V. Vimalkumar**, N. Poornima, C. Sudha Kartha , K. P. Vijayakumar. T. Abe and Y. Kashiwaba (to be communicated).
- Spatial mapping of deep level PL emission from spray pyrolysed ZnO thin films, N.Poornima, **T. V. Vimalkumar**, C. Sudha Kartha and K. P. Vijayakumar, Applied Surface Science (Under Review).

Conference Publications

- Mono and Dual-doping effect of spray pyrolysed ZnO thin film-**T.V. Vimalkumar**, C. Sudha Kartha and K. P. Vijayakumar, National Seminar on Horizon in Thin film Technology, HTFT , TOC-H Institute of Science & Technology, Arakkunnam, Ernakulam (2011).

- Spatial PL mapping of deep level emission from spray pyrolsed Zinc oxide thin films N. Poornima, **T. V. Vimalkumar,** C. Sudha kartha and K. P. Vijayakumar, National Seminar on Horizon in Thin film Technology, HTFT(2011),TOC H Institute Of Science & Technology Arakkunnam, Ernakulam.
- Characterization of Spray Pyrolyzed ZnO thin films to be used as back contact in solar cell using Photoluminescence. N. Poornima, **T. V. Vimalkumar,** C. Sudha kartha and K. P. Vijayakumar, National Conference on Energy Storage and Conversion .Venkateswara University , Tirupati (2010).
- Doping of ZnO thin films deposited using spray pyrolysis- preparation and characterization- **T.V. Vimalkumar**, C. Sudha kartha and K. P. Vijayakumar, MRSI, Saha Institute , Kolkatta (2009).
- Spray pyrolysed ZnO thin films doped with Al through direct diffusion: Preparation and characterization. **T. V. Vimalkumar** ,C. Sudha Kartha and K. P. Vijayakumar,17 th National Symposium on Ultrasonic (NSU XVII), Bhanarus Hindu University (BHU) , Varanasi (2008).
- Spray Pyrolysed ZnO thin films: Effect of variation of molarity and spray rate, **T. V. Vimalkumar**, C. Sudha kartha and K. P. Vijayakumar, National Conference on semiconductor materials & technology (NC-SMT) Gurukula kangri University, Haridwar (2008).
- Effect of doping and annealing on the physical properties of spray pyrolysed ZnO thin films, **T.V. Vimalkumar**, C. Sudha kartha and K. P. Vijayakumar, National Seminar on Recent Advances in Thin Film Technology.ITM , Gwalior (2007).
- Thermal performance and Energy Efficiency analysis of Line- focusing Type Solar Collectors, **T. V. Vimalkumar** ,C. Sudha Kartha and K. P. Vijayakumar,18 th Annual General meeting of MRSI National Physical Lab-New Delhi (2007).
- Copper solar air heater for better thermal energy conversion to drying needs. A.Sreekumar, **T. V. Vimalkumar** and K. P. Vijayakumar, Discussion meeting on Materials for Future Energy systems, Material Research Society of India (Mumbai Chapter-2006).

Contents

Chapter 1
Transparent Conducting Oxide

1.1 Introduction

Transparent conducting oxides (TCOs) are a special class of materials that can simultaneously be both optically transparent and electrically conducting and, as such, are a critical component in almost all thin-film photovoltaic devices. TCOs are generally based on a limited class of metal oxide semiconductors such In_2O_3, ZnO and SnO_2, which are transparent due to their large band gap and can also tolerate very high electronic doping concentrations to yield conductivities of 1000 S/cm or higher.

TCO's consists of a group of materials that can be thought of as 'conjugate property materials' in which one property, [in this case conductivity], is strongly coupled to a second property, namely, the extinction coefficient. In this regard, it can be stated that materials like metals, that are highly conductive, will not normally transmit visible light, while highly transparent media like oxide glasses behave as insulators. The challenge for achieving materials that are both electrically conducting and optically transparent is to understand the fundamental material structure/property relationships that control these properties so that they may be decoupled such that the material retains transparency while becoming electrically conductive. To an extent, many phenomenological approaches based upon well-understood physical principles have been reported to achieve materials having these properties. More recent studies push the envelope of the earlier work through understanding, at a fundamental level, the microscopic nature of the conductivity process in order to discover the role of chemical structure, bonding, and film morphology on charge transport.

The first realization of a TCO material occurred a century ago when a sputtered film of cadmium metal experienced incomplete thermal oxidation upon post-deposition heating in air [1]. Certain metal oxide systems can show n-type electrical conductivity provided the charge-compensating electrons can be promoted to the conduction band of the material from defect levels lying close to the conduction band minimum. Since this early discovery, appreciable values of electrical conductivity had been achieved in many single, binary,

ternary and quaternary metal oxide systems [2–7]. Even though optical transmission through these materials in the visible region of the spectrum was quite good, electrical conductivities still remain considerably lower than that of metals.

For most optoelectronic devices especially the ones with flat panel displays, it is essential to have a transparent electrode with TCO. Although tin-doped indium oxide (commonly called indium-tin oxide, or ITO) thin films deposited using magnetron sputtering have been in practical use for most of the transparent electrode applications, there are many reports on other TCO's as well as deposition methods [8–13]. A stable supply of ITO for the fast expanding market for optoelectronic devices may be difficult because of the cost and scarcity of indium, the principal material of ITO. In addition, recent developments in optoelectronic devices require thin-film transparent electrodes with specialized properties. Recent research on materials and techniques for making TCO's is mainly focused on resolving these problems. For example, there are several research groups working all over the world aiming at the modification of zinc oxide (ZnO) as an alternative to costly ITO[10, 14, 15]. Recent developments in optoelectronic device applications make it necessary to have improvements in the physical and chemical properties of TCO films used as thin-film transparent electrodes. In order to develop TCO films suitable for specialized applications. Minami et al. reported new TCO semiconductors in 1994, ZnO–SnO_2 multi-component oxides, that not only had the advantages of ZnO but also those of SnO_2 [16]. In addition, TCO films using multi-component oxides composed of combinations of binary compound TCO materials and/or ternary compound TCO materials were developed. Several examples of multi-component oxides composed of combinations of binary compound TCO materials, such as ZnO–$In2O_3$, $In2O_3$–SnO_2 and SnO_2–ZnO systems are at present developed and studies elaborately.

1.2 Reviews of TCO

The research progress for TCO materials have been repeatedly reviewed from time to time. Holland [17] reviewed the early work of TCO film in 1958. Vosser [18] and Hacke [19] reported comprehensive reviews to the mid 1970s. Manfacier [20], Jarzebsk[21] and Chopra et al. [22] published reviews covering all the important works in this area up to the

early 1980s. Hartnagal et al. [9] reviewed the growth technique, properties and application of TCOs. Some critical issues related to new TCO material, such as criteria for application and theoretical model were addressed in the MRS Bulletin [24]. Exarhos et al. [25] summarised up-to date TCO research with an emphasis on the microscopic description of electronic conduction properties and guidelines for designing new TCO materials. S.Calnan et al. [26] reviewed importance of carrier mobility in doped TCOs. In this article strategies used to improve the carrier mobility in degenerately doped TCO thin film were reviewed. T.Minami et al. [5] reported the present status and prospects for further development of poly crystalline or amorphous TCO semiconductor used for practical thin film transparent electrode application.

1.3 General properties of TCO

TCOs are unique materials that combine optical transparency (band gaps > 3.1 eV) and electrical conductivity (carrier concentration of at least 10^{19} cm^{-3}). Band gap > 3.1 eV ensures that visible light photons cannot excite electrons from the valence band (VB) to the conduction band (CB).

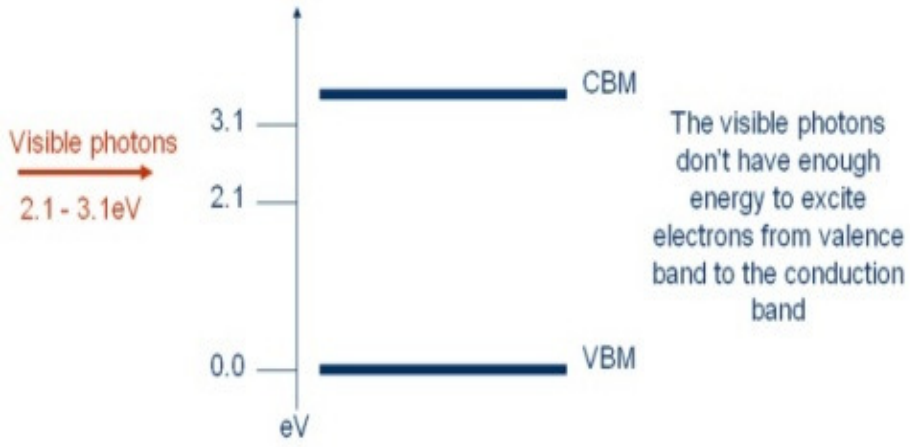

These transparent materials are thus made electrically conducting by the introduction of defects, [intrinsic or extrinsic] into the system. TCOs can be classified as n-type or p-type, according to the defects and type of conduction of the material. These defects form split off acceptor (unoccupied) levels above the valence band maximum (VBM) in the case of p-type conduction, and donor (occupied) levels below the conduction band minimum (CBM) in the case of n-type conduction.

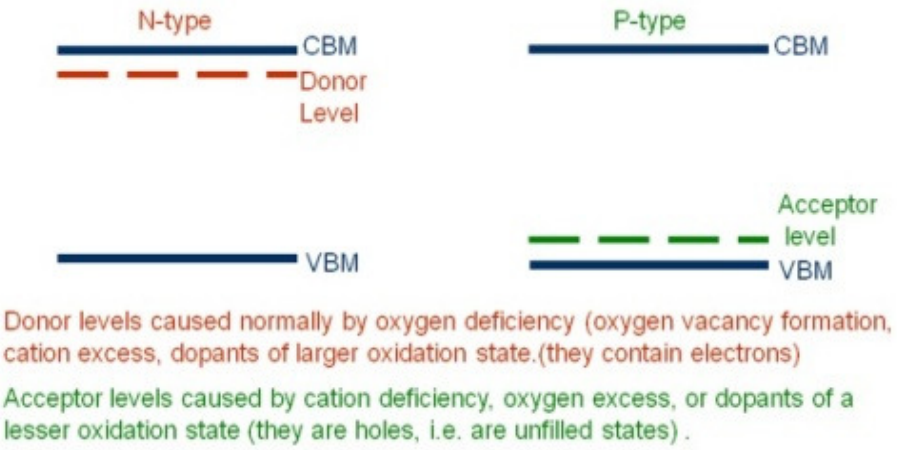

N-type TCOs (SnO_2, ZnO, In_2O_3 etc) are already utilized in a range of technological applications. However p-type TCOs have proved to be harder to manufacture. Most of the wide band gap binary oxides have valence bands dominated by O 2*p* states. Hence on acceptor formation, the acceptor states (holes) are localized on oxygen ions, leading to low conductivity. Designing p-type TCOs with good conductivity has therefore still remains as a major challenge for materials scientists. Cu_2O is a known p-type TCO, in which good p-type conductivity is caused by favourable mixing between Cu (I) $3d^{10}$ and the O 2*p* states, causing a more delocalized VB. However Cu_2O is not transparent as it has a band gap of 2.17 eV. In 1997, Kawazoe et al. [4] first reported p-type conductivity in $CuAlO_2$, which crystallizes in the "delafossite" structure. $CuAlO_2$ combines the p-type conduction properties of Cu_2O, with the wide band gap of Al_2O_3, producing for the first time, a native p-type TCO. They had realised that a suitable cation is needed to mix with the O 2*p* states, like in the case of Cu_2O, and identified Cu(I) and Ag(I) as the best candidates

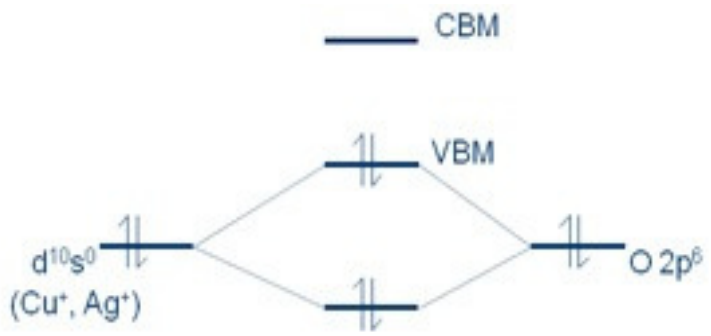

It has been shown that Cu based TCOs are superior to Ag based TCOs, and many other Cu based TCOs have been synthesized, including delafossites $CuInO_2$ [27], $CuGaO_2$ [28], $CuScO_2$ [29], $CuCrO_2$ [30], $CuYO_2$ [31] and the $SrCu_2O_2$ [32]. To date, the p-type material with the highest conductivity is Mg doped $CuCrO_2$ [33].

1.3.1. Electrical conductivity

TCOs are wide band gap (E_g) semiconducting oxides, with conductivity [σ] in the range $10^2 - 1.2\times10^6$ (S), which is due to doping either by oxygen vacancies or by extrinsic dopants. In the absence of doping, these oxides become very good insulators, with $\rho > 10^{10}$ Ω cm. Most of the TCOs are n-type semiconductors. Electrical conductivity of n-type TCO thin films depends on the electron density in the conduction band and on their mobility: $\sigma=\mu n e$, where μ is the electron mobility, n is its density, and e is the electron charge. The mobility is given by:

$$\boldsymbol{\mu=e\tau/m^*} \quad \text{..... (1.1)}$$

Where **τ** is the mean time between collisions, and $\boldsymbol{m^*}$ is the effective electron mass. However, as **n** and **τ** are negatively correlated, the magnitude of **μ** is limited. Due to the large energy gap (E_g > 3 eV) separating the valence band from the conducting band, the conduction band cannot be thermally populated at room temperature (kT~0.03 eV, where k is Boltzmann's constant). Hence, stoichiometric crystalline TCOs are good insulators [34].

To explain the TCO characteristics, various population mechanisms and several models describing the electron mobility were proposed. Some characteristics of the mobility and the processes by which the conduction band is populated with electrons were shown to be interconnected by electronic structure studies [35].For example, the mobility is proportional to the magnitude of the band gap.

In the case of intrinsic materials, the density of conducting electrons has often been attributed to the presence of unintentionally introduced 'donors' usually identified as metallic interstitials or oxygen vacancies that produced shallow donor or impurity states located close to the conduction band. The donors are thermally ionized at room temperature, and move into the host's conduction band. However, experiments have been inconclusive as to which of the possible dopants was the predominant donor [36]. Extrinsic dopants have an important role in populating the conduction band and some of them have been unintentionally introduced. Thus, it has been conjectured in the case of ZnO that interstitial hydrogen, in the H^+ donor state, could be responsible for the presence of carrier electrons [37]. In the case of SnO_2, the important role of interstitial Sn in populating the conducting band, in addition to that of oxygen vacancies, was conclusively supported by first-principle calculations of Kiliç and Zunger [38]. They showed that Sn-interstitials and O-vacancies, which dominated the defect structure of SnO_2 due to the multi-valence of Sn, produced shallow donor levels, turning the material into an intrinsic n-type semiconductor [39]. The electrons released by these defects were not compensated because acceptor-like intrinsic defects consisting of Sn voids and O interstitials did not form spontaneously. Furthermore, the released electrons did not make direct optical transitions in the visible range due to the large gap between the Fermi level and the energy level of the first unoccupied states. Thus, SnO_2 could have a carrier density with minor effects on its transparency.

Electrical conductivity [σ] is intrinsically limited due to two reasons. First, n and μ cannot be independently increased for practical TCOs with relatively high carrier concentrations. At high electron density, carrier transport is limited primarily by ionized impurity scattering i.e., the Coulomb interactions between electrons and the dopants. Higher doping concentration reduces carrier mobility to a degree so that the conductivity cannot be increased. More over it decreases the optical transmission at the near-infrared edge. With

the increase in dopant concentration, the resistivity reaches a lower limit, beyond which it cannot decrease. But the optical window becomes narrower. Ellmer also showed that in ZnO films, deposited using various methods, resistivity and mobility were nearly independent of the deposition method and limited to about 2×10^{-4} Ω cm and 50 cm^2/Vs, respectively [40,41]. In ITO films, the maximum carrier concentration was about 1.5×10^{21} cm^{-3}[42]. This is a universal property of other semiconductors too [43,44]. Scattering by the ionized dopant atoms that are homogeneously distributed in the semiconductor is only one of the possible effects that reduce the mobility. Recently developed TCO materials, including doped and undoped binary, ternary, and quaternary compounds, also suffer from the same limitations. Only some exceptional samples had resistivity of $\leq1\times10^{-4}$ Ω cm.

In addition to the above mentioned effects that limit the conductivity, high dopant concentration could lead to clustering of the dopant ions [45] which increases significantly the scattering rate. It could also produce 'nonparabolicity' of the conduction band, which has to be taken into account for degenerately doped semiconductors with filled conduction bands [46].

1.3.2 Optical properties

As mentioned above, besides high conductivity (~10^6 S/m), good TCO thin films should have very low absorption coefficient in the near UV-VIS-NIR region. Transmission in the near- UV region is limited by E_g, as photons with energy larger than E_g are absorbed. A second transmission edge exists at the NIR region, mainly due to reflection at the plasma frequency. Ideally, a wide band gap TCO should not absorb photons in the transmission "window" in the UV-VIS-NIR region. However, there are no "ideal" TCOs thin films, and even if such films could be deposited, reflection and interference would also affect the transmission. Hence, 100% transparency over a wide region cannot be obtained.

Optical properties of TCOs transmission *[T]*, reflection *[R]*, and absorption *[A]*, are determined by its refraction index *n*, extinction coefficient *k*, band gap E_g, and geometry. Geometry includes film thickness, thickness uniformity, and film surface roughness. *T, R* and*, A* are intrinsic, depending on the chemical composition and solid structure of the material, whereas the geometry is extrinsic. There is a negative correlation between the carrier density and position of the IR absorption edge; but there is positive correlation

between the carrier density and the UV absorption edge, as E_g increases at larger carrier density (Moss-Burstein effect). As a result, the TCO transmission boundaries and conductivity are interconnected.

Width of visible transmission window of a TCO film deposited on a transparent substrate is affected not only by the optical parameters of the TCO film but also by the optical properties of the substrate. Refractive index n_{sub} of the most common substrates are ~1.45 for fused silica and ~1.6 for various glasses. Extinction coefficient of the substrate (k_{sub}) is generally < 10^{-7}. Hence light absorption would take place only in the film, where generally $k_{film} > k_{sub}$. For films thicker than 100 nm, several interference bands could be formed, producing maximal and minimal values of T when either the wavelength or thickness is varied. When $k_{film} \approx 0$,the peak transmission (T_{max}) is equal to the transmission of the substrate. Hence, assuming that the sample is in air, T_{max} = 90% and 93% for films deposited on glass and fused silica, respectively. The minimum sample transmission (T_{min}) in air is expressed by:

$$T_{\min} = \frac{4n^2 n_{sub}}{(1+n^2)(n^2+n_{sub}^2)} \quad \text{..... (1.2)}$$

As most TCO films have values of n in the VIS in the range 1.8 – 2.8, T_{min} will be in the range 0.8 – 0.52. T_{min} and is closely approximated by the relation,

$T_{min} = 0.051n^2 - 0.545n + 1.654$.

As n in the visible region decreases with wavelength, T_{min} increases with wavelength. But it will not exceed ~0.8. When the film extinction coefficient is not negligible and affects the transmission, $T_{max} < T_{sub}$, and T_{min} also decreases. By decreasing the TCO film thickness, T is increased. But the sheet resistance increases.

1.3.3 Work function

Energy difference between Fermi energy level and vacuum level corresponds to the work function (Φ) which is the minimum amount of energy needed to remove an electron from the metal. In metals, work function and ionization energy are the same. Condition of the surface can strongly affect the work function. Presence of minute quantity of contamination (less than a monolayer of atoms or molecules), or the occurrence of surface reactions (oxidation or similar) can change the work function substantially. Changes of the order of 1 eV are common for metals and semiconductors, depending on the surface condition. These changes are due to the formation of electric dipoles at the surface, which change the energy an electron needs to leave the sample. Due to the sensitivity of the work function to chemical changes on surfaces, its measurement can give valuable insight into the condition of a given surface. In a nondegenerate semiconductor (having a moderate doping level), the Fermi level is located within the band gap. This means that work function is now different from the ionization energy (energy difference between valence bands maximum (VBM) and vacuum level). In a semiconductor, the Fermi level becomes a somewhat theoretical parameter since there are no allowed electronic states within the band gap. This means that Fermi distribution needs to be considered, which is a statistical function that gives the probability to find an electron in a given electronic state. Fermi level refers to the point on the energy scale where the probability is just 50%. Work function of untreated ITO is generally equated at ~4.7eV [47], where the plasma cleaning of the TCO in O_2 generally increased the work function by about 0.1- 0.3 eV.

1.3.4 Thermal and Chemical stability

Thermal stability temperature is a threshold temperature, above which TCO films show appreciable change or degradation in its properties. The reported thermal stability temperatures for ZnO, SnO_2 and Cd_2SnO_4 are 250, 500 and 700^oC, respectively [12]. Above these temperatures, chemical decompositions of the films occur, which degrade the quality of the films. Many commercial substrates are temperature sensitive (glass < 500^oC, polymer <200 ^oC) and hence, restrict the processing temperature. Moreover, observations of chemical reaction of the TCO films with the substrate and the subsequent layers have been reported in the literature [48]. Thermal stability is essential for the developed TCOs from

the application point of view as these TCOs may be exposed to various extreme environments. Chemical stability of a TCO is determined by its ability to resist corrosive environment and treatment. For applications such as amorphous Si solar cells, sensitivity of TCO to reducing atmospheres is an important concern. ITO undergoes heavy reduction when exposed to hydrogen environments. Comparatively, doped ZnO films are much more stable in reducing atmospheres and plasmas containing hydrogen species [12, 5]. Therefore, ZnO based TCOs may be preferred for the applications involving hydrogen plasma processing. In contrast, for oxidizing atmospheres, especially at high temperatures, ITO shows better stability compared to other TCOs.

1.3.5 Surface morphology

Surface texture should be such that it nicely scatters the sunlight so as to increase the path length of light inside the cell. The texture, however, does not mean the steep and rugged surface because it makes the smooth and junction formation difficult. One of the smooth, coherent texture was reported on CVD deposited SnO_2: F film in 1990 [49]. Also the chemical stability of ZnO on top of the textured SnO_2: F has been clarified to be better than SnO_2:F bare surface [50]. It consists of regular, smooth surface microcrystals with good coherence and is recognised as standard texture for a-Si solar cells.

TCO coated substrates for use in solar cell comprises of three main features

1) Resistivity as low as possible to minimise the loss due to Joule heat

2) Absorption of sunlight (Covering from near UV to near infrared) as low as possible to better conversion efficiency

3).A proper texture to confine as much sunlight as possible in the junction region of the cell.

The second requirement is now recognised as more important because the light utilization ratio of near infrared/ visible in increasing in a-Si:H/mc-Si:H tandem structures recently available on the market. This means that the TCO having higher mobility is better because of lower absorption in the infrared.

1.3.5.1 Function of TCO texture

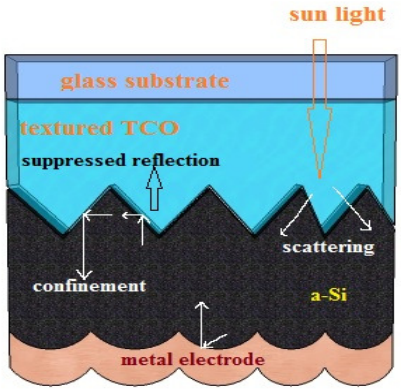

Fig.1.1 Three functions of TCO texture

Effect of texture can be explained in more detail as shown in Fig1.1. **The first** is reduction of reflection (or suppression of reflection) provided by the rugged structure with characteristic length equal to somewhat smaller than the quarter wavelength of the average sunlight. This give rise to graded refractive index layer which serves as anti reflection (AR) layer at the interface (TCO/a-Si). Taking into account the refractive index 2.0 of tin oxide and that of a-Si c.a 4.0, this material combination well satisfy the amplitude condition of the AR coating. **Second** is strong scattering power to extend the travelling length of light in i-layer where photoelectron and holes are generated. Multiple passage of light increases the electron–hole pair generation. The generated electron- hole pair must be separated as soon as possible and this is caused by the electric field between p- and n-layers. Accordingly the separation efficiency goes up as the i-layer thickness decreases. This trade-off relation suggests that there is an optimum thickness of i-layer. Multiple scattering of the light helps semiconductor to generate more electron–hole pairs so that its thickness can be reduced and the separation field is strengthened. Thickness reduction may also serve as saving the Si raw materials.

Third is light confinement. The sunlight yet not absorbed in the photoactive i-layer suffers from diffuse scattering and sent back again into the active i-layer where it takes part in the electric power generation .The higher the diffuse back scattering broader the wavelength region covered by the texture, its contribution to the power generation is enhanced.

1.4 TCO Materials

Three oxides have emerged as commercially important transparent conductors: indium oxide, tin oxide, and zinc oxide. Properties and crystal chemistry of the transparent conducting indium oxide family of materials is discussed in some detail in the following sections because it is probably having the highest performance and hence the best-understood/ studied material in the TCO class. By volume, however, the most deposited TCO today is SnO_2, which is used in IR-efficient architectural window applications. ZnO is also primarily used in window coatings (multilayer stacks with Ag), but recent processing-related improvements and low cost make it an attractive replacement for high-cost In-based TCOs

If an oxide is completely stoichiometric, it can only be an ionic conductor. Such a material is obviously of no interest as transparent conductors because of high activation energy required for ionic conductivity. However, real oxides are hardly, if ever, completely stoichiometric. The oxides used for transparent conductors are invariably with anion vacancy. Consider the formation of an oxygen vacancy in perfect crystal. In the process of removing an oxygen atom, two electrons of oxygen ions are left in the crystal. If both these electrons are localized at the oxygen vacancy, the charge is same as in the perfect crystal and the vacancy has zero effective charge. Such a vacancy is neutral. If one or both of the localized electrons are excited and transferred away from the vacancy, the vacancy is left with an effective positive charge with respect to the perfect crystal. The charged vacancy becomes 'electron trapping site'. But in the process one or more electrons are made available for conduction. If the cation is multivalent (e.g. Sn), the creation of too many oxygen vacancies results in the structure change from SnO_2 to SnO. Somewhere in such a transition, there occurs a compositional change where excess of oxygen in the SnO structure will exist. Cation vacancies resulting from excess oxygen have the opposite effect. They produce holes rather than electron. Creation of an anion vacancy results in a cationic valence charge. Clearly, for conduction to be efficient, volume fraction of trap must be small. Binary oxides used for transparent conductors are relatively unstable and are relatively easy to oxidise or reduce.

If, instead of creating oxygen vacancies by chemical reduction, one incorporates into the host lattice substitutional cations with a valency higher than that of the host, it has electrically the same effect of creating anion vacancies. Since overall charge neutrality must be preserved, substitution of higher valency cation requires the addition of an electron. Conversely, incorporation of lower valency cation produces a hole. [If one incorporates Sb^{+5} substitutionally in SnO_2, an additional electron is added to the lattice. If instead, In^{3+} is substitutionally added, a hole is produced which, in an n-type semiconductor, becomes a trap.] As with the oxygen vacancies, not all higher valency dopants incorporated into the lattice produce charge carriers. Some simply remain as neutral point defects. Electrically equivalent effects can occur if anion sites are doped with atoms whose valency is lower than that of oxygen. Among the anion dopants employed, F^- and Cl^- are the most popular.

Ionic radius of the dopant must be the same or smaller than that of the ion it replaces, and no compounds or solid solutions of dopant oxide with host oxides are formed. Even in the absence of solid solution or compound formation, a dopant may not be usable based on its ionic radius. If the dopant ions are too large, an interstitial, rather than a substitutional site is favoured, and the dopant will act as a scattering site rather than a source of charge carriers.

1.4.1 ITO or Tin –Doped Indium Oxide

ITO is a solid solution of indium oxide and tin oxide, typically 90% In_2O_3, 10% SnO_2 by weight. It is transparent and colourless in thin layer while in bulk form it is yellowish to grey. In the infrared region it is a 'metal like' mirror. ITO is one of the most widely used transparent conducting oxide having electrical conductivity and optical transparency. Thin films of ITO are mostly deposited using electron beam evaporation, physical vapour deposition and sputter deposition techniques.

Tin–doped indium oxide films prepared with the help of various techniques are always polycrystalline and retain a crystal structure of bulk – undoped In_2O_3. However lattice constant values are usually larger than those of bulk-undoped In_2O_3. Increase in lattice constant depends on the deposition parameters like the partial oxygen pressure $p(O_2)$ in the sputtering process [58]. For the lowest value of $p(O_2)$, a_o=10.15 Å while for p (O_2) $>5\times10^{-5}$ Torr, a_o~10.23 Å.Increase in the value of lattice constant up to 10.23 Å has been

observed by many workers [52-54]. ITO film, in general, exhibits a strong (111) or (100) preferred orientation depending on the deposition condition.

1.4.2 Tin oxide (SnO_2)

SnO_2 has tetragonal rutile structure with space group D^{14} ($P4_2/mnm$) [55]. The unit cell contains six atoms –two tin and four oxygen. Each tin atom (cation) is at the centre of six oxygen atoms (anions) placed approximately at the corners of regular octahedron, and every oxygen atom is surrounded by three tin atoms approximately at the corners of an equilateral triangle. The lattice parameters are [56] are a=b=4.737 and c=3.185, while c/a ratio is 0.673. Ionic radii of O^{2-} and Sn^{4-} are 1.40 and 0.71 A respectively [57]. The lattice has 15 optical normal modes of vibration, five of which are Raman active (Frequencies 100-800 cm^{-1}). Seven modes are IR active (frequencies 250-600 cm^{-1}) and two are inactive [58].

If SnO_2 was completely stoichiometric, it would be an insulator or at the most an ionic conductor. However the practical material is never stoichiometric and is invariably anion deficient. This is due to the formation of oxygen vacancies in the otherwise perfect crystal. These vacancies are responsible for making electrons available for the conduction process. In the case of SnO_2, because the cation is multivalent, the creation of too many oxygen vacancies also results in structure change from SnO_2 to SnO.

1.4.3 Indium Oxide(In_2O_3)

In_2O_3 single crystal has the cubic bixebyte structure (also called c-type rare earth oxide structure) and belongs to the space group (T_h^7,Ia^3).The lattice parameter of In_2O_3 is 10.117 A and co-ordination is six fold for the indium atoms and four fold for the O atoms. One can assume that there are two crystallographically non-equivalent In-sites. One of this is associated with an In-O separation of 2.18 Å, and oxygen atom lying nearly at the corners of the cube with two body diagonal opposite corners unoccupied. The other is associated with non-equal In-O separations of 2.13, 2.19 and 2.23 Å, and O atoms lying nearly at the corners of a cube with two face diagonal opposite corners unoccupied.

In_2O_3 is a non-stoichiometric compound under various conditions with In /O ratio larger than 2/3. This non–stoichiometry makes it an n-type semiconductor [or even a semimetal at high electron concentration]. During the crystal growth, large number of native

donors is produced because of the oxygen vacancies. These donors also create an intense 'free carrier absorption' in the infra red reflection spectrum.

1.4.4 Zinc Oxide (ZnO)

Most of the group II-VI binary compound semiconductors crystallize in either cubic zinc–blende or hexagonal wurtzite structure where each anion is surrounded by four cations at the corners of the tetrahedron, and vice versa. Zinc Oxide occurs in the nature as the mineral called 'zincite'. Zinc Oxide crystallizes in the hexagonal wurtzite (B4 type) lattice. Zinc atoms are nearly in the position corresponding to 'hexagonal close pack' structure. Every oxygen atom lies within the tetrahedral group of four zinc atoms and all these tetrahedral points are in the same direction along the hexagonal axis giving the crystal its polar symmetry. The lattice constants are a= 3.24 Å and c= 5.19 Å.

1.5 Important Electrical and Optical Properties of n-type TCO materials

Compound	Structure type	Cell Dimension(Å) a b c	Resistivity (Ω cm)	Band – gap(eV)	Dielectric Constant	Refractive Index
SnO_2	Rutile	4.73 – 3.18	10^{-2} –10^{-4}	3.7—4.6	12(E/a) 9.4(E/c)	1.8-2.2
In_2O_3	C-rare earth	10.11 – –	10^{-2} –10^{-4}	3.5 - 3.75	8.9	2.0-2.1
ITO	C-rare	10.117 – –	10^{-3}–10^{-4}	3.5– 4.6	—	1.8-2.1
Cd_2SnO_4	Sr_2PbO_4	5.56 9.88 3.19	10^{-3}–10^{-4}	2.7—3.0	—	2.05-2.1
ZnO	Wurtzite	3.242 — 5.19	10^{-3}–10^{-4}	3.1 –3.6	8.5	1.85-1.90

1.6 P-type TCO

The first report of a p-type TCO was NiO [59]. In 1997 there was a report of transparent p-type conducting films of $CuAlO_2$ showing considerable improvement over NiO [60]. Although the conductivity of 1 S cm^{-1} was about three orders of magnitude smaller than that of n-type materials, the result was promising. Since then, a number of promising p-type materials have been prepared as a consequence of material exploration efforts following the design concept. Work by the groups of Kawazoe and Hosono over the

last few years has led to the discovery of a number of p-type TCOs [60–63] based on Cu^+ bearing oxides.

1.6.1 Copper-based delafossite structure

Kawazoe and co-workers [60] proposed that one could modify the valence band edge by 'mixing orbitals' of appropriate counter cations that have filled energy levels comparable to O 2p. This would reduce the strong Coulomb force exerted by the oxygen atoms and thereby delocalize the positive holes. Copper was selected as one of the major constituents because of its '3d10 energy level'. Also, its closed d-shell makes it less prone to d–d transitions that could absorb light in the visible range. The chemical formula of delafossites is AMO_2 in which A is the monovalent cation and M is a trivalent cation. Delafossites have a hexagonal, layered crystal structure: the layers of A cations and MO_2 are stacked alternately, perpendicular to the c-axis [64]. As a class, p-type materials now include the copper-based delafossites $CuMO_2$.

1.6.1.1 Copper Aluminum Oxide ($CuAlO_2$)

Structure of $CuAlO_2$ delafossite had been extensively studied by Ishiguro et al. [65] and they proposed an alternative stacking of CuI and layers of nominal AlO_2 composition consisting of $Al–O_6$ octahedral sharing edges. Each copper atom is linearly coordinated with two oxygen atoms to form an O–Cu–O 'dumb-bell unit' placed parallel to the c-axis. Oxygen atoms of the O–Cu–O dumb-bell link all Cu layers with the AlO_2 layers. After the report of p-type semiconducting transparent $CuAlO_2$ thin film, recently a research field in device technology has emerged known as "transparent electronics". For the synthesis of $CuAlO_2$ thin films, the groups of Hosono [66], Gong [67,68], and Chattopadhyay [69-73] used pulsed laser deposition (PLD), "plasma-enhanced metalorganic chemical vapor deposition (PE-MOCVD)" and dc sputtering respectively. Band gap was observed between the valence band edge in the PES spectrum and the conduction band edge in the IPES spectrum, which was about 3.5 eV. The Fermi energy lies almost at the top of the valence band. This observation agrees with the fact that the sample is a p-type semiconductor.

1.6.1.2 Copper Indium Oxide ($CuInO_2$)

Of the copper-based delafossites, the $CuInO_2$ system is particularly interesting because it can be doped to form both p-type (with Ca) and n-type (with Sn), allowing p–n

homojunction to be produced [63, 75]. Thin films of $CuInO_2$ delafossite can also be made both p-type and n-type by doping appropriate impurity and tuning the deposition conditions. This is quite puzzling because $CuInO_2$ has the largest reported band gap of 3.9 eV. No similar trend has ever been observed in any other semiconductors. Using first-principles methods, Nie et al. [76] reported the unusual 'bipolar dopability' observed in this material by the exceptionally large disparity between its fundamental indirect band gap and apparent direct band gap. Unfortunately, the conductivity of $CuInO_2$ films (~10^{-3} S cm−1) has, thus far, been smaller than that of the other p-type TCOs. However, producing phase-pure targets is still challenging and has likely limited the subsequent research on $CuInO_2$. However, the oxygen-rich $Cu_2In_2O_5$ phase of Cu–In–O is easily prepared by solid-state synthesis in air. Therefore, Teplin et al. used $Cu_2In_2O_5$ as a target to deposit single phase undoped and Ca-doped $CuInO_2$ thin films [77].

1.6.1.3 Copper Gallium Oxide ($CuGaO_2$)

$CuGaO_2$ is another p-type TCO with band gap energy of ~3.6 eV [78].This material has a larger lattice constant [a = 2.98 Å], than $CuAlO_2$ (a = 2.86 Å). The lattice constant of the a-axis in $AgInO_2$, which is the only n-type conductive delafossite available at present, is 3.27 Å. Polycrystalline thin film of $CuGaO_2$ has been prepared by an rf sputtering method [79]. The deposited film was obtained in an amorphous state, and was subjected to post-deposition annealing for crystallization at 850 °C for 12 h under nitrogen atmosphere. For $CuGaO_2$ thin film, its activation energy was roughly estimated to be about 0.22 eV. The conductivity at room temperature was about 5.6×10^{-3} S cm^{-1}. Epitaxial $CuGaO_2$ films were prepared on a-Al_2O_3 (001) single-crystal substrates by PLD without post-annealing treatment [78].Electrical conductivity, carrier (positive hole) density, and Hall mobility at room temperature were found to be 6.3×10^{-2} S cm^{-1}, 1.7×10^{18} cm^{-3}, and 0.23 cm^2 V^{-1} s^{-1}, respectively.

1.7 Application of TCOs

TCO's have diverse industrial applications; some of the more important ones will be described in this section. TCO coatings are applied to transparent materials used for work surfaces and closet doors, particularly in clean rooms used for electronics assembly, in order

to prevent harmful static charge build-up. In this application relatively high surface resistances (e.g. kΩ/) can be tolerated.

The architectural use of TCOs is predominately for energy efficient windows. Fluorine doped tin Oxide (FTO) films deposited using chemical vapour deposition (CVD) process, are often used for this application [80,81]. Metal –oxide/Ag/Metal –oxide stacks such as ZnO/Ag/ZnO are common also [82,83]. Windows with tin oxide coating are efficient in preventing radiative heat loss due to their low thermal emittance ~0.15, compared to ~0.84 for uncoated glass [84]. Such "low-e" windows are ideal for use in cold or moderate climate. In addition, pyrolytic tin oxide is also used for heated glass freezer doors in commercial use. In this application, the doors can be defrosted by passing small current through the slightly resistive TCO coating. In 2007, the annual demand for low-e coated glass in Europe was 60×10^6 m^2 and this is projected to increase to about100×10^6 m^2 in a few years [85]. Rapid growth in China is also increasing the demand of low-e glass [86].

Realization of p–n junction composed of TCOs is a requisite for the extension of application of TCOs to transparent semiconductors because a variety of active functions in semiconductors arise from p–n junction. Previous attempts to construct transparent electronic devices have been hampered by the lack of a p-type transparent semiconductor with good performance. To date, the group of copper based delafossites such as $CuAlO_2$ and $CuGaO_2$ and $SrCu_2O_2$, etc., seemed to be potential p-type materials for transparent p–n junctions and due to the development of these materials, it has become feasible to fabricate transparent p–n junctions. Several oxide transparent p–n junctions and LEDs have been successfully fabricated, such as n-ZnO/p-SCO [87–89], n-$CuInO_2$: Sn/p-CuInO2: Ca and n-ZnO/p-$CuAlO_2$ [90]. For these oxide diodes, ZnO was selected as the n-type material due to its advantageous properties in carrier mobility, capability of film deposition at relatively low temperatures and controllability of electrical conductivity.

Amorphous oxide p–n junction diodes are also of interest. When the performance of crystalline devices often suffers from defects inherent to the rigid periodicity of the crystalline lattice, [e.g. grain boundaries and rough interfaces in polycrystalline materials and lattice mismatch at hetero interfaces], amorphous materials and devices are free of these

troublesome effects. Amorphous semiconductors are highly favourable for applications in large-area electronic devices such as solar cells and flat-panel displays because they have several advantages, i.e. homogeneous films can be deposited on a variety of large area substrates at low temperature. Research on p-type transparent amorphous oxide semiconductors and amorphous oxide p–n junction diodes has started to seek materials that meet these advantages. The first 'all-amorphous' oxide p–n junction diode was reported by Narushima et al. [91]. They fabricated a flexible p–n heterojunction diode on plastic substrate using an amorphous $ZnORh_2O_3$ film for the p-layer and a-$InGaZnO_4$ film for the n-layer at room temperature. The diode exhibited distinct rectifying electrical characteristics with threshold voltage (~2.1 V) consistent with the band gap of the a-$ZnORh_2O_3$ film and on–off current ratio of ~10^3.

Transparent heating elements may be constructed from TCO coatings. These are useful as defrosters in aircraft and vehicular windshields. Their advantage over traditional hot air blowers is that they can have a much shorter effective defrosting time and work uniformly over large area. This application requires either the use of very low surface resistance coatings (e.g. ~1 Ω/), or a high voltage power source. Application of TCO coatings to passenger vehicles has proven to be technically successful. However there is a difficulty due to the high cost of a supplemental alternator to deliver the requisite high voltage. If the automobile industry will adopt a higher bus voltage, as has been widely discussed, then this application may prove to be more commercially feasible in the future.

TCO coatings may be used as shielding to decrease electromagnetic radiation interference (EMI) while providing visual access. This may be either to keep radiation from escaping an enclosure to avoid interfering with nearby devices / detection, or from entering an enclosure [to prevent external radiation sources from interfering with electronic devices within]. One potential example is the window of domestic microwave ovens that today use a perforated metal screen, [which obscures clear visual observation], to reduce microwave leakage. Radiation leakage must be minimized to prevent harm to the users, as well as interference to proliferating wireless devices which use the unlicensed spectral band at 2.45 GHz. While transparent conducting films were proposed 50 years ago, an attempt to

introduce microwave windows with TCO coatings into the market was not successful about a decade ago, due to the high cost. Low cost designs are currently being developed.

The three largest applications of transparent conductive oxide thin films, [in terms of the surface area covered and their total value] are flat panel displays, solar cells, and coatings on architectural glass. In general, transparent electrodes are needed for a large variety of electro-optical devices of which flat panel displays and solar cells are the most important examples. In liquid crystal displays (LCDs), TCO films are needed for both the electrodes, in order to allow backlighting to pass through the liquid crystal film while applying voltage to the various pixels. Generally these electrodes are in the form of a pattern of lines, with the alignment of the lines on the two electrodes perpendicular to each other. This allows addressing individual pixels by applying a voltage to the two lines which intersect at a given pixel, and hence patterning the films is required. ITO is the TCO of choice in this application, both because of its electro-optical properties, and the relative ease of acid etching.

The best LCDs utilize an active matrix comprising one amorphous silicon transistor which occupies a corner of each pixel and because the silicon is opaque, there is reduction of light transmission. Recently transparent field effect transistors (FETs) have been developed based on the zinc oxide, but using a Cr gate. Most solar cells use TCO films as a transparent electrode. Major considerations in the choice of the TCO for this application, besides the conductivity and transparency, are electronic compatibility with adjacent layers in the cell, processing requirements, and stability under environmental conditions. Often tin oxide based films are chosen for this application, where patterning is not required, but environmental stability is essential.

1.8 Importance of the present work

Current photovoltaic technologies as well as next-generation approaches to PVs, will place specific demands on the transparent contact layers beyond transparency and low resistivity .To date, the industry standard in TCO is ITO, or tin-doped indium-oxide. This material boasts a low resistivity of ~10^{-4} Ω-cm and a transmittance of greater than 80%. However ITO has the drawback of being expensive. Indium, the film's primary metal, is

rare (6000 metric tons worldwide in 2006), and its price fluctuates due to market demand (over $800 US per ingot in 2006). For this reason, doped binary compounds such as aluminum-doped zinc-oxide (AZO) and indium-doped cadmium-oxide have been proposed as alternative materials. Among these, AZO is composed of aluminum and zinc, two common and inexpensive materials, while indium-doped cadmium oxide only uses indium in low concentrations. In many of the novel PV technologies currently under development, such as organic photovoltaics and Grätzel cells, control of the morphology and surface chemistry of the TCOs used is critical to device performance. Examination of current and future PV-TCO materials performance leads to the conclusion that new efforts to develop application specific TCO materials and processes are needed. As new device structures evolve, it will be necessary to expand the tool kit of TCO materials available to achieve very different film properties and surface chemistries.

References

[1] K. Badeker, Ann. Phys. (Berlin) **22** (1907) 749.

[2] K. L. Chopra, S. Major, D. K. Pandya,Thin Solid Films **102** (1983) 1.

[3] H. Hosono, T. Kamiya, M. Hirano, Bull. Chem. Soc. Jpn. **79** (2006) 1.

[4] H. Kawazoe, K. Ueda, J. Am. Ceram. Soc. **82/12** (1999) 3330.

[5] T. Minami, Semicond. Sci.Technol. **20** (2005) S35.

[6] D. S. Ginley, J.D. Perkins, H. Kawazoe, D.M. Newns, A.B. Kozyrev,Proceedings of the Materials Research Society, Materials Research Society (2001) 433.

[7] D. C. Paine, H.-Y. Yeom, B. Yaglioglu, in: G.P. Crawford (Ed.), Flexible Flat Panel Displays,Wiley Interscience, JohnWiley and Sons (2005) 79.

[8] R. Ayouchi, D. Leinen, F. Martin, M. Gabas, E. Dalchiele and J. R. Ramos Barrodo, Thin Sold Films **426** (2003) 68.

[9] H. L Hartnagel, A. L Dawar, A. K Jain, C. Jagadish Semiconducting Transparent Thin Films (Philadelphia, PA: Institute of Physics Publishing) (1995).

[10] T. Minami MRS Bull.**25 (**2000) 38.

[11] A. J. Freeman, K R Poeppelmeier, T O Mason, R P H Channg, T J Marks MRS Bull. **25 (**2000) 45.

[12] R. G. Gordon MRS Bull. **25 (**2000) 52.

[13] T. J. Coutts, D. L. Young , X. Li MRS Bull. **25 (**2000) 58.

[14] T. Minami, H Nanto, S Takata Appl. Phys. Lett. **41 (**1982) 958.

[15] T. Minami, H Nanto, S Takata Japan. J. Appl. Phys.**23 (**1984) L280.

[16] T. J. Minami. Vac. Sci. Technol. A **17 (**1999) 1765.

[17] L. Holland, Vacuum Deposition of Thin Films. Wiley, New York (1958).

[18] J. L.Vossen, Phys. Thin films **9** (1977) 1.

[19] G. Haacke, Annu. Rev. Mater. Sci. **7** (1977) 73.

[20] J. C. Manifacier, Thin Solid Films **90** (1982) 297.

[21] Z .M. Jarzebski, Phys. Status Solidi A **71** (1982) 13.

[22] K. L. Chopra, S. Major, and D.K. Pandya, Thin Solid Films **102** (1983)1.

[24] Transparent Conducting Oxides. in MRS Bulletin. (2000).

[25] G. J. Exarhos and X.D. Zhou, Thin Solid Films **515 (**2007) 7025

[26] S. Calnan and A. N.Tiwari, Thin Solid film **518** (2010)1839.

[27] Jong-Chul Lee**,** Young-Woo Heo**,** Joon-Hyung Lee and Jeong-Joo Kim**,** Thin Solid Films **518** (2009) 1234.

[28] R. Bruce Gall, Nathan Ashmore, Meagen A. Marquardt, Xiaoli Tan and David P. Cann Journal of Alloys and Compounds **391** (2005) 262.

[29] Y. Kakehi, K. Satoh, T. Yoshimura, A. Ashida and N. Fujimura Thin Solid Films **518** (2010) 3097.

[30] G. Dong, M. Zhang, X. Zhao, H. Yan, C. Tian and Y. Ren Applied Surface Science **256** (2010) 4121.

[31] M. Trari, A. Bouguelia and Y. Bessekhouad, Solar Energy Material and Solar Cells **90** (2006) 190.

[32] V. Varadarajan, D. P. Norton and J. D. Budai Thin Solid Films **488** (2005) 173.

[33] T. W. Chiu, K. Tonooka and N. Kikuchi, Vacuum **83** (2008) 614.

[34] P. P. Edwards, A. Porch, M. O. Jones, D. V. Morgan and R. M. Perks, Dalton Trans. 19 (2004) 2995.

[35] H. Mizoguchi and P.M. Woodward, Chem. Mater.**16** (2004) 5233.

[36] D.C. Look, B. Claflin, in: G.J. Brown, M.O. Manasreh, C. Gmachl, R.M. Biefeld, K.

Unterrainer (Eds.), Materials Research Society Symposium Proceedings **829** (2005)B 8.6.1.

[37] C.G. Van de Walle, Phys. Rev. Lett. **85** (2000) 1012.

[38] C. Kiliç and A. Zunger, Phys. Rev. Lett.**88** (2002) 095501-1.

[39] B. Thangaraju,Thin Solid Films **402** (2002) 71.

[40] K. Ellmer, J. Phys., D, Appl. Phys. **33** (2000) R17.

[41] K. Ellmer, J. Phys., D, Appl. Phys. **34** (2001) 3097.

[42] G. Frank and H. Köstlin, Appl. Phys. A **27** (1982) 197.

[43] G. Masetti, M. Severi and S. Solmi, IEEE Trans. Electron Devices **30** (1983) 764.

[44] D. Chattopadhyay and H.J. Queisser, Rev. Mod. Phys. **53** (1981) 745.

[45] P. Ebert, Z. Zhang, F. Kluge, M. Simon, Z. Zhang and K. Urban, Phys. Rev.Lett.**83** (1999) 757.

[46] T. Pisarkiewicz, K. Zakrzewska and E. Leja, Thin Solid Films **174** (1989) 217.

[47] T. Minami ,T. Miyata and T. Yamamota, Surface and Coating Technology **108-109** (1-3) (1998) 583.

[48] T.J. Coutts , J.D. Perkins, D.S. Ginley and a.T.O. Mason. in Proceedings of the Electrochemical Soc. Seattle, Washington (1999).

[49] K. Sato,Y. Gotoh,Y. Hayashi,K.Adachi and H. Nishimura , Report Res.Lab.Asahi Glass **40** (1990) 233.

[50] T.Ikeda, K. Sato,Y. Hayashi,Y. Wakayama,K. Adachi and H. Nishimura, Solar Energy Material and Solar Cells **34** (1994) 379.

[51] J.C.C Fan, F. J. Bachner and G. H. Foley. Appl.Phys.Lett **31** (1977) 773.

[52] S. Kuleszewicz Thin Solid Films **76** (1981) 89.

[53] W.H Lehman and R. Widmer Thin Solid Films **27** (1975) 359.

[54] J. L. Vossen RCA Rev **32** (1971) 269.

[55] Wyckhoff RWG Crystal Structures vol 1, 2nd edn (New York ;Wiley) 1963.

[56] W. H. Baur ,Acta Crystallogr.**9** (1956) 515.

[57] L. Pauling, The nature of chemical bond [New York : Cornell University Press] (1960)

[58] R. S. Katiyar, P. Dawson, M. M. Hargreave and G. R Wilkinson J. Phys.C .Solid State Phys.**4** (1971) 2421.

[59] H. Sato, T. Minami, S. Takata and T. Yamada, Thin Solid Films **236** (1993) 27.

[60] H. Kawazoe, M. Yasukawa, H. Hyodo, M. Kurita, H. Yanagi and H. Hosono, Nature **389** (1997) 939.

[61] H. Yanagi, H. Kawazoe, A. Kudo, M. Yasukawa and H. Hosono, J. Electroceram. **4** (2000) 407.

[62] A. Kudo, H. Yanagi, H. Hosono and H. Kawazoe, Appl. Phys. Lett.**73** (1998) 220.

[63] H. Yanagi, T. Hase, S. Ibuki, K. Ueda and H. Hosono, Appl. Phys. Lett. **78** (2001)1583.

[64] H. Kawazoe, H. Yanagi, K. Ueda and H. Hosono, MRS Bull. **25** (2000) 28.

[65] T. Ishiguro, N. Ishizawa, N. Mizutani and M. Kato, J. Solid State Chem. **41** (1982)132.

[66] H. Yanagi, S. Inoue, K. Ueda, H. Kawazoe, H. Hosono and N. Hamada, J. Appl. Phys. **88** (2000) 4159.

[67] H. Gong and Y. Wang, Appl. Phys. Lett. **76** (2000) 3959.

[68] Y. Wang, H. Gong and L. Liu, Int. J. Modern Phys. B **16** (2002) 308.

[69] A. N. Banerjee, S. Kundoo, and K. K. Chattopadhyay,Thin Solid Films **440** (2003) 5.

[70] A. N. Banerjee, R. Maity and K. K. Chattopadhyay, Mater. Lett. **58** (2003)10.

[71] A. N. Banerjee and K. K. Chattopadhyay, Appl. Surf. Sci. **225** (2004) 243.

[72] A. N. Banerjee, R. Maity, P. K. Ghosh, and K. K. Chattopadhyay, Thin Solid Films **474** (2005) 261.

[73] A. N. Banerjee and K. K. Chattopadhyay, J. Appl. Phys. **97** (2005) 084308.

[75] H. Yanagi, K. Ueda, H. Ohta, M. Orita, M. Hirano and H. Hosono, Solid State Commun. **121** (2002) 15.

[76] X. C.Nie, S. H.Wei and S. B. Zhang, Phys.Rev.Lett. **88** (2002) 066405.

[77] C. W. Teplin, T. Kaydanova, D. L. Young, J. D. Perkins and D. S. Ginley, Appl. Phys. Let. **85** (2004) 3789.

[78] K. Ueda, T. Hase, H. Yanagi, H. Kawazoe and H. Hosono, J. Appl. Phys. **89** (2001) 1790.

[79] J. Pellicer-Porres, A. Segura, Ch. Ferrer-Roca Phys. Rev. B. **69** (2004) 024109 .

[80] R. G. Gordan, MRS Bulletin. **25** (2000) 52.

[81] C. G. Granqvist, Solar Energy Material and Solar Cells **91** (2007) 1529.

[82] H. J. Glaser,Applied Optics **47** (2008) C193.

[83] C. G. Granqvist, A. Azens,P. Hezler,L. B. Kish and L. Osterlund, Solar Energy Materials and Solar cells **91** (2007) 355.

[84] J. Karlsson and A. Roos, Thin Solid Films **392** (2001) 345.

[85] Pilkington and flat glass industry 2008, Pilkigton Group Limited, St.Helens, United Kingdom WA10 3TT, www.pilkington.com

[86] China Low- E Glass Market Report, Research and Markets, www.researchandmarkets.com/reports/c 88669 (2007-2008).

[87] A. Kudo, H. Yanagi, K. Ueda, H. Hosono and H. Kawazoe, Appl. Phys. Lett. **75** (1999) 2851.

[88] H. Ohta, K. Kawamura, M. Orita, N. Sarukura, M. Hirano and H. Hosono, Electron. Lett. **36** (2000) 984.

[89] Y. Nakamura, Y. Yoshida, Y. Honaga and S. Fujitsu, J. Eur. Ceram. Soc.**25** (2005) 2167.

[90] T. Kazuhiko, B. Hiroshi and A. Yoshihiro, Thin Solid Films **445** (2003) 327.

[91] S. Narushima, H. Mizoguchi, K. Shimizu, K. Ueda, H. Ohta, M. Hirano, T. Kamiya and H. Hosono, Adv.Mater. **15** (2003) 1409.

Chapter 2

Zinc Oxide thin film and its applications

2.1 Introduction

Zinc Oxide is a II - VI compound semiconductor. Most of the group II–VI binary compound semiconductors crystallize in either cubic zinc blende or hexagonal wurtzite (Wz) structure where each anion is surrounded by four cations at the corners of a tetrahedron, and vice versa. This tetrahedral coordination is typical of sp^3 covalent bonding nature; but these materials also have substantial ionic character that tends to increase the band gap beyond the one expected from the covalent bonding. ZnO is a compound semiconductor whose 'ionicity' resides at the borderline between the covalent and ionic semiconductors. The crystal structures shared by ZnO are wurtzite (B4), zinc blende (B3), and rock salt (or Rochelle salt) (B1) as schematically shown in Fig. 1. At Room temperature, thermodynamically stable phase is wurtzite. The zinc-blende structure can be stabilized only by the growth on cubic structure while rock salt (NaCl) structure may be obtained at relatively high pressure.

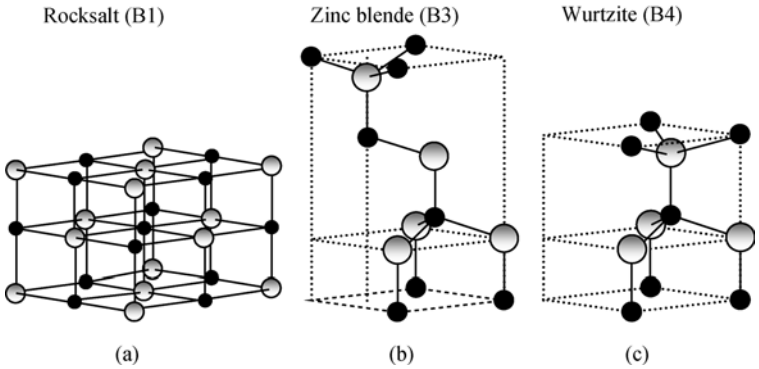

Fig.1. 'Stick and ball' representation of ZnO crystal structures: (a) cubic rock salt (B1), (b) cubic zinc blende (B3), and (c) hexagonal wurtzite (B4). The shaded gray and black spheres denote Zn and O atoms, respectively.

Wurtzite structure has hexagonal unit cell with two lattice parameters a and c in the ratio of c/a=1.66. The structure is composed of two interpenetrating hexagonal-close-packed (hcp) sub lattices, each of which consists of one type atom displaced with respect to each other along the three fold c-axis by the amount of u=3/8=0.375 (in ideal wurtzite structure) in fractional coordinate (the u parameter is defined as length of the bond parallel to the c-axis, in unit of c). Each sub lattice includes four atoms per unit cell and every atom of one kind (group-II atom) is surrounded by four atoms of the other kind (group-VI) or vice versa, which are coordinated at the edges of a tetrahedron. In real ZnO crystal, the wurtzite structure deviates from the ideal arrangement, by changing the c/a ratio or the u value.

2.2 Properties of ZnO

2.2.1 Direct and wide band gap

Band gap of ZnO is 3.44 eV at low temperature and 3.37 eV at room temperature [1]; for comparison, the respective values for wurtzite GaN are 3.50 eV and 3.44 eV [2]. This enhances applications in optoelectronics in the blue / UV region, including light-emitting diodes, laser diodes and photo detectors [3–7].

2.2.2 Large exciton binding energy

The free-exciton binding energy in ZnO is 60 meV [8, 9], compared with 25 meV in GaN [2]. This large exciton binding energy indicates that efficient excitonic emission in ZnO can persist at room temperature and higher. This makes ZnO a promising material for optical devices that are based on excitonic effects.

2.2.3 Large piezoelectric constants

In piezoelectric materials, an applied voltage generates a deformation in the crystal and vice versa. These materials are generally used as sensors, transducers and actuators. The low symmetry of the wurtzite crystal structure combined with large electro-mechanical coupling in ZnO gives rise to strong piezoelectric and pyroelectric properties. Piezolectric ZnO films, with uniform thickness and orientation, have been grown on a variety of substrates using different deposition techniques, including sol–gel process , spray pyrolysis, chemical vapour deposition, molecular-beam epitaxy and sputtering [10–17].

2.2.4 Strong luminescence

Due to strong luminescence in the green–white region of the spectrum, ZnO is also a suitable material for phosphor applications. The emission spectrum has a peak at 495 nm which is broad [half-width of 0.4 eV] [18]. The n-type conductivity of ZnO makes it appropriate for applications in vacuum fluorescent displays and field emission displays. Origin of the luminescence center and luminescence mechanism is not really understood, being frequently attributed to oxygen vacancies or zinc interstitials, without any clear evidence [18]. It has been suggested that zinc vacancies are more likely the cause of green luminescence.

2.2.5 High thermal conductivity

This property makes ZnO useful as an additive (e.g. ZnO is added to rubber in order to increase the thermal conductivity of tyres).This also increases the appeal of ZnO as a substrate for homoepitaxy or heteroepitaxy (e.g. for growth of GaN, which has a very similar lattice constant) [19, 20]. High thermal conductivity translates into high efficiency of heat removal during device operation.

2.2.6 Amenability to wet chemical etching

Semiconductor device fabrication processes greatly benefit from the amenability to 'low-temperature wet chemical etching'. It has been reported that ZnO thin films can be etched with acidic, alkaline as well as mixture solutions. The possibility of low-temperature chemical etching adds great flexibility in the processing, designing and integration of electronic and optoelectronic devices.

2.2.7 Radiation hardness

Radiation hardness is important for applications at high altitude or in space. It has been observed that ZnO exhibits exceptionally high radiation hardness [21, 22], even greater than that of GaN, the cause of which is still unknown.

2.2.8 Strong sensitivity of surface conductivity to the presence of adsorbed species

Conductivity of ZnO thin films is very sensitive to the exposure of the surface to various gases. It can be used as a 'cheap smell sensor' capable of detecting the freshness of foods and drinks, due to the high sensitivity to trimethylamine present in the odour [23].Mechanisms of the sensor action are poorly understood. Recent experiments reveal the

existence of a surface electron accumulation layer in vacuum-annealed single crystals, which disappears upon exposure to ambient air [24–26]. This layer may play a role in sensor action, as well. Presence of this conducting surface channel has been suggested to be related to some puzzling type-conversion effects observed when attempting to obtain p-type ZnO.

2.3 Deposition Techniques

Growth technique played a significant role in controlling the properties of ZnO films, because the same material deposited using two different techniques, usually had different physical properties. This was due to the fact that the electrical and optical properties of the films strongly depended on the structure, morphology and the nature of impurities present. Moreover the films grown using any particular technique might have different properties due to the variation of various deposition parameters and hence the properties can be tailored by controlling the deposition parameters. The specific technique that has been used to grow the ZnO thin films include Chemical vapour deposition (CVD), Spray Pyrolysis, Pulsed Laser Deposition, Sputtering and evaporation of oxide materials. Each process has its own merits and demerits. The purpose of this part is to give the brief account of commonly used technique, particularly suitable for the growth of ZnO thin films.

2.3.1 Chemical Vapor Deposition (CVD)

CVD is one of the important techniques for producing thin film of semiconductor material. This technique involves reaction of one or more gaseous species reacting on a solid surface (substrate). In this process the metallic oxides are generally grown through the vaporisation of the organo-metallic compounds. Vapour containing the condensate material is transported to a substrate surface where it is decomposed usually by the heterogeneous process. Nature of the decomposition process varies according to the composition of the volatile transporting species. The decomposition condition should be such that the reaction occurs only at or near the substrate surface and not in the gaseous state to avoid formation of the powdery deposits which may result in haziness in the films. There are several modifications of this method depending on precursors used .When the metal –organic precursors are used the technique is called MOCVD, metal –organic vapour –phase epitaxy (MOVPE), or organo-metallic vapour – phase epitaxy (OMPVE). In the case of hydride or halide precursors, the technique is named as hydride or halide CVD or VPE.

In the CVD method, ZnO deposition occurs as a result of chemical reactions of vapour-phase precursors on the substrate. These vapours are delivered into the growth zone by the carrier gas. The reactions take place in a reactor where a necessary temperature profile is created in the direction of gas flow. For hydride VPE growth of ZnO, hydrogen (H_2) was employed as a carrier gas [27, 28]. In these cases, the typical pressure was ≤133 Pa and the flow rate was about 40 ml/min. Targets made from ZnO powder were placed in the evaporation zone in which the temperature was around 770 °C. High-quality homoepitaxial ZnO layers were grown on bulk ZnO substrates by using N_2O and diethyl zinc [29]. Two conditions, [proper thermal treatment of substrate prior to the growth to obtain a flat surface and high flow-rate ratios of source materials], were found to be important to obtain high quality layers.

Effect of oxygen partial pressure on the structural perfection as well as optical and electrical properties of ZnO films grown at 600 °C on Al_2O_3 (0001) was studied by Ma et al. [30,31]. It was found that the conduction type in undoped ZnO layers could be controlled by adjusting the oxygen partial pressure during growth. The films grown under oxygen partial pressure lower than 45 Pa showed *n*-type conductivity. With increasing oxygen pressure, the crystallinity of the ZnO layers degraded to polycrystalline with additional (1012) orientation and intrinsic *p*-type ZnO (which should be treated with some caution) was produced as the oxygen partial pressure became higher than 55 Pa. The hole concentration and mobility reached 1.59×10^{16} cm^{-3} and 9.23 cm^2 /V s, and the resistivity was 42.7 Ω cm. Transparent and conductive ZnO thin films were deposited over Si and InP substrates using CVD and characterized using X-ray diffraction (XRD), AFM, optical measurements etc [32]. The main observation was that the preferred orientation of the ZnO crystallite was along (112) for Si and (002) for InP substrates.

Sallet et al. [33] also reported growth of ZnO on (0001) sapphire substrates using MOCVD. Diethylzinc and tertiarybutanol were used as zinc and oxygen sources respectively. In this paper, the authors had given details of growth conditions such as substrate temperature and precursor's partial pressure. Influence of the cleanness state of the MOCVD silica reactor was also emphasized, since it modified both layer quality and crystalline orientation. Moreover, it also affected growth process steps like sapphire thermal treatment and buffer layer deposition. ZnO epitaxial layers were characterized using

scanning electron microscopy [to assess the surface orientation and morphology], X-ray diffraction and photo luminescence. Highly conductive polycrystalline ZnO films were grown using MOCVD technique with dimethyl zinc, dimethyl zinc-triethylamine and tertiary butanol as precursors [34]. Films grown using dimethyl zinc-triethylamine were oriented with the c-axis in the growth direction. Resistivity was of the order of $3x10^{-4}$ ohm cm.

Stoichiometric ZnO films were grown on Si substrate using Plasma enhanced CVD with a zinc organic source and carbon dioxide gas mixture [35]. Substrate temperature was kept at 503 K initially with different gas flow rates and then keeping gas flow rate constant, substrate temperature was varied. Films were oriented along (002) plane at higher substrate temperature, while at low temperature, the films were polycrystalline with different orientation. Room temperature exciton absorption peak was observed in these films, which vanished at lower substrate temperature. This observation was correlated with the crystalline quality of the film. PL studies were also done at room temperature.

Guotong et al. [36] reported growth of ZnO films on C-plane sapphire substrate using plasma-assisted MOCVD. The experimental results show that the high-quality ZnO films have been obtained by annealing. Furthermore, the films with better PL properties are obtained by the final annealing, while the films with higher optical transmission are obtained through annealing during the growth process. Low pressure chemical vapour deposition (LP-CVD) of Al doped ZnO [AZO] thin film was investigated for transparent electrode of thin film solar cell [37]. For LP-CVD, diethylzinc and trimethyl aluminium were used as Zn and Al precursors respectively. Effects of trimethyl aluminium (TMA) precursor flow rate on the structural and optical properties of transparent conducting LPCVD ZnO film was analysed in this work. The haze factor of AZO films drastically increased with the introduction of TMA precursor.

T.Sekiguchi et al. [38] deposited ZnO thin film on sapphire substrate using 'remote plasma-enhanced chemical vapour deposition' with $Zn(C_2H_5)_2$ and CO_2. In the ZnO films grown under the oxygen-rich condition, broad emissions [peaked at 3.8 and 3.0 eV] were observed.

2.3.2 Sputtering

Sputtering is one of the versatile techniques used for the deposition ZnO thin films. Compared to the chemical methods, samples will have better-controlled composition and homogeneity; also this permits to have better control of film thickness. Sputtering process involves the creation of gas plasma by applying voltage between a cathode and anode. Cathode is used as target holder and anode is used as substrate holder. Source material is subjected to intense bombardment by ions and particles are ejected from the surface of cathode. They diffuse away from it and deposit onto a substrate. Sputtering is normally performed at a pressure of 10^{-2} to 10^{-3} Torr. For conducting targets, DC voltage is applied between cathode and anode (DC Sputtering) and for non-conducting samples and insulators, a high frequency generator is connected between the electrodes (RF Sputtering). Magnetron sputtering is useful where high deposition rates and low substrate temperature are required. In magnetron sputtering, a magnetic field is applied to enhance the sputtering rate, which in turns, enhances the deposition rate also.

Highly conductive and transparent AZO thin films were grown using 'off-axis magnetron sputtering' on silica surface and effect of post deposition annealing was discussed in another paper [39]. Optimized ZnO film was having resistivity of 4.5 x10^{-4} ohm cm and optical transmittance of 85 %. Gupta et al. investigated the influence of post deposition annealing on the structural and optical properties of RF sputtered insulating ZnO thin films [40]. The as grown film, deposited over quartz substrate, was in a state of stress with orientation along c- axis. These films became stress-free after annealing in air at 673 K for 1hr. At higher temperature, a process of coalescence was observed which caused a major grain growth. This in turn resulted in the formation of 'micro-crack' and surface roughness. Packing density of 99% was observed for the film annealed at 673 K, which indicated almost a void free film.

Kook et al. [41] reported on the growth of very high quality Al doped n-type ZnO epilayer on sapphire substrate using a RF magnetron sputtering technique combined with a rapid thermal annealing. On increasing annealing temperature up to 900^0C, the PL Intensity (energy 3.2 eV) increased significantly. PL intensity ratio considerably enhanced with increasing the oxygen pressure. Annealing at 900^0C however resulted in improved carrier concentration and mobility about 10^{20} cm^3 and 45-65 cm^2 /Vs.

ZnO and AZO transparent thin films with different thicknesses were prepared using dc magnetron sputtering technique. Deposition was on silicon and Corning glass substrates [42]. Atomic force microscopic characterisation of the films surfaces revealed a granular, polycrystalline morphology with roughness decreasing as the oxygen partial pressure decreases. The films deposited at high O_2 ratio have shown bigger and better grains, whereas those deposited at higher Ar ratio had uniform grain distribution.

ZnO thin films deposited using RF magnetron sputtering method onto unheated glass, silicon, and kapton polymer foil substrates revealed a polycrystalline structure [43]. The influence of deposition arrangement and oxidation conditions on the structural, morphological, and optical properties of the ZnO films was discussed. The crystallites were preferentially oriented along (0 0 2) plane parallel to the substrate surface. Intensity of the (0 0 2) peak for ZnO deposited on kapton polymer foil substrate was higher than that of the other two substrates. This translates into bigger crystallites. All ZnO thin films showed a high transmittance in the visible region. Reflection spectrum of ZnO thin film deposited on Si showed interference maxima and minima due to reflections on the surface the film. Values of the energy gap calculated from the absorption spectra was 3.23 eV for ZnO sample deposited on glass substrate and 3.30 eV for the sample deposited on kapton polymer foil substrate.

AZO films were deposited on quartz substrates heated to 100 or 200^0C under argon gas pressure between 0.08 and 2.7 Pa using RF magnetron sputtering [RF power of 100 W] from a ZnO target with 2 wt.% Al_2O_3. Structural, optical and electrical properties [such as electrical resistivity, carrier concentration and the Hall mobility] were studied as a function of argon gas pressure[44]. As argon pressure during deposition was increased, the grain size decreased and the surface roughness increased leading to higher electrical resistivity. The minimum resistivity of about 2.5×10^{-4} Ω cm was obtained for film grown on quartz substrate heated at 100^0C with RF power of 100 W at argon pressure of 0.13 Pa is comparable to that of ITO films.

Another report, AZO thin films with low resistivity and high transmittance were obtained through middle-frequency alternative magnetron sputtering using a ZnO target mixed with Al_2O_3 of 2 wt% [45]. Lowest resistivity obtained was 4.6×10^{-4} Ω cm for the film with average visible transmittance of 90.0% and sheet resistance of

32 Ω, deposited at 250^0C and 0.8 Pa. Increase of conductivity and optical transmittance was attributed to the improvement of crystallinity with increasing substrate temperature. Resistivity increased and optical transmittance decreased due to deterioration of crystallinity resulting in an increase of surface roughness with the increase of argon gas pressure.

Piezoelectric ZnO film was deposited using RF magnetron sputtering to fabricate an LFE-mode SMR-type FBAR device [46]. Optimal conditions for ZnO deposition were 120 W of RF power and 10 m Torr pressure in the chamber. Suitable substrate rotation was very important for improvement of the *c*-axis-preferred orientation of the films. Electron temperature, plasma density and saturated ion current were approximately 5.5–5.8 eV, $1.0–1.3\times10^{11}$ /$cm^3$and 3.5–4.3 mA/cm^2, respectively. Piezoelectric- active area was 200×200 μm^2, and thicknesses of ZnO film and Au electrode were 1.25 μm and 110 nm, respectively. Series and parallel resonance frequencies of the FBAR device appeared at 1.68 and 1.71 GHz, respectively, which represent 68.4% of the values for a ZnO FBAR of the same thickness without a mass loading effect. Effective coupling coefficient was 0.0432, which corresponds to 54% of the theoretical value for an ideal ZnO FBAR device

Rajesh Das et al. [47] reported that transparent conducting AZO thin films were prepared using RF-magnetron sputtering under different gas ambient at 300^0C. The electrical resistivity varied from 1.23×10^{-1} to 2.8×10^{-4} Ω cm on introducing O_2 and H_2 gas with Ar ambient. Hydrogen plays an important role for creation of oxygen vacancies due to its reducing action which causes the increase of carrier concentration of AZO films. Maximum carrier concentration and Hall mobility, as estimated from Hall effect measurement of the films, were 2.3×10^{21}/cm^3 and 44.4 cm^2 /V s respectively. Photoluminescence (PL) spectra peaks were mainly in the blue emission region; however there was a change from 432 nm (2.87 eV) and 541.5 nm (2.29 eV) with the change of gas ambient. From the X-ray diffraction (XRD) pattern exhibiting only the (002) peak of ZnO, all films were found to be c-axis-oriented. The crystallite size varies from 150 to 288A˚ for different films calculated from (002) orientation of XRD data. Y.B. Xiao et al. [48]studied the properties of Indium Zinc Oxide (IZO) thin films deposited on Polyethylene Terephthalate substrate room temperature with the help of dc magnetron sputtering . Preparation of IZO films were carried out under varying the O_2 concentration and deposition

parameters. As the O_2 concentration in O_2/Ar gas increased from 0.4% to 3.5%, the transmittance of the film increased from 70% to 90% and the resistivity decreased. With increase in dc power, the resistivity increased; but the transmittance decreased. For the variation of gas pressure and target-to-substrate distance, the transmittance showed little change; but the resistivity (5.1×10^{-4} Ω cm) decreased with decrease in gas pressure and increase in target-to- substrate distance.

2.3.3 Pulsed Laser Deposition (PLD)

Pulsed laser deposition (PLD) is one of the sophisticated techniques for depositing transparent semiconducting oxides. Recently PLD technique attained importance among the different techniques employed to fabricate crystalline thin films with good crystallinity. PLD technique involves evaporation of a solid target in a High Vacuum/Ultra High Vacuum chamber, by means of short and high-energy laser pulses. A pulsed laser beam vaporizes the surface of the target, and the vapour condenses on the substrate, producing a film with the same composition as the target. This is the result of the extremely high heating rate of the target surface (10^8 K/s) due to pulsed laser irradiation. It leads to the congruent evaporation of the target irrespective of the evaporating point of the constituent elements or compounds of the target. Because of the high heating rate of the ablated materials, laser deposition of crystalline film demands a much lower substrate temperature than other film growth techniques. For this reason, the semiconductor and the underlying integrated circuit are not damaged from thermal degradation. Main components are a laser, optics, and a vacuum system. It not only involves the physical process of the laser-material interaction of the impact of high-power pulsed radiation on solid target, but also the formation of the plasma plume with high energetic species and even the transfer of the ablated material through the plasma plume onto the substrate surface. The targets used in PLD are small compared to the large size required for sputtering techniques. It is quite easy to produce multi-layered films of different materials by sequential ablation of assorted targets. Besides, by controlling the number of pulses, a fine control of film thickness down to even atomic monolayer can be achieved.

Highly transparent conductive AZO thin films have been deposited on the glass substrate using PLD [49]. Effect of substrate temperature and post deposition annealing treatment on structural, electrical and optical properties of the thin films was investigated.

Resistivity of the film decreased from 1.3×10^{-3} to 6.1×10^{-4} Ω cm with increase of substrate temperature from 170 to 240^0C. Highest mobility value of 11.4 cm^2/VS was obtained for film deposited at 340 ^{0}C. Resistivity of the film further reduced to 4.7×10^{-4} Ω cm by annealing at 400^0C for 2 hr in argon.

The lowest resistivity of 8.54×10^{-5} Ω cm and average transmittance more than 88% in the visible range were obtained in a series of approximately 280 nm thick- AZO films grown on glass substrate at a target-to-substrate distance of 25 mm in a magnetic field applied perpendicular to a plane generated by PLD using an ArF excimer laser[50]. To study the effect of thickness on structural, electrical and optical properties of AZO films, a set of polycrystalline AZO samples with different thicknesses were deposited using PLD [51]. XRD measurement showed that crystal quality of the film was improved with the increase of the film thickness. The optical band gap increased from 3.50 eV to 3.90 eV when AZO film thickness increased from 15 nm to 580 nm.

Choopun et al. [52] studied the influence of oxygen pressure on surface morphology and optoelectronic properties of ZnO films grown on sapphire (0001) by PLD. The films were grown at 750 °C under various oxygen background pressures ranging from 10^{-5} to 10^{-1} Torr. All the ZnO layers grown were found to be *c*-axis oriented. Samples grown under lower oxygen pressure regimes (10^{-5}–10^{-4} Torr) had a *c*-axis lattice parameter 0.25% larger than that of the bulk material.

Preparation of highly conducting and transparent AZO films was reported by Singh et al. [53] which were deposited on quartz and Corning 7059 glass by focusing a XeCl (λ=308 nm and 20-ns pulse width) excimer laser onto a target rotating at 15 rpm. The ZnO target was 2 in. in diameter and doped with 2-wt % Al_2O_3. For all the experiments, a repetition rate of 5 Hz and an energy density of 1.5 J /cm^2 were used. The distance between the target and the substrate was 30 mm, and the deposition time was 30 min. Effects of substrate temperature (from room temperature to 400 °C) and oxygen pressure (from 0.1 to 5 m Torr) were investigated by analyzing the optical and electrical properties of the films. Average transmittance was found to be in the range of 86%–92%, and resistivity varied from 3.56×10^{-3} to 7.0×10^{-3} Ω cm. The lowest resistivity measured was 1.4×10^{-4} Ω cm for the films grown at 300 °C and 1 mTorr oxygen pressure.

Matsubara et al.[54] used oxygen radical-assisted PLD to grow highly transparent and low-resistivity AZO films at room temperature. A KrF excimer laser (λ =248 nm, 30-ns pulse width, and 10-Hz repetition rate) was used for ablation. The oxygen partial pressure during deposition was ($0.7–1.4\times10^{-5}$ Torr) and the applied RF power was 150 W. Distance between the target and the substrate was approximately 6 cm. The minimum resistivity of the obtained transparent films was 5×10^{-4} Ω.cm, while average transmittance in the visible wavelength region was over 86% for ~0.7-μm-thick films.

Craciun et al [55] deposited high-quality ZnO films on glass and silicon substrates using the PLD technique employing a KrF laser (=248 nm) and studied the influence of deposition parameters such as substrate temperature, oxygen pressure, and laser fluence on the properties of the grown films. All the films grown over a rather wide range of deposition conditions were found to be optically transparent, electrically conductive, and *c*-axis oriented. Investigations of the effect of different oxygen partial pressures showed that the best-quality films could be obtained in the higher pressure range.

2.3.4 Chemical Spray Pyrolysis (CSP)

Chemical Spray Pyrolysis (CSP) technique, one of the chemical methods for the preparation of thin films, is widely used one, to deposit variety of thin films. It involves spraying a solution, usually aqueous, containing soluble salts of the constituents of the desired compound, onto a heated substrate. It is quite suitable for depositing large area thin films with good reproducibility. The method has, for many years, been widely used for preparation of transparent conducting oxide films. Spray pyrolysis is based on the pyrolytic decomposition of a metallic compound dissolved in a liquid mixture when it is sprayed onto a preheated substrate. In CSP, doping process is rather simple; just by varying the concentration of the dopant in the solution, one can vary the percentage of doping in the sample. A major drawback of this technique is that it cannot be used for the deposition of very thin films. Another shortcoming lies in the selection of substrate since it is a high temperature process. Effects of substrate temperature on the structural, electrical and optical properties of ZnO films, prepared using CSP technique had been studied [56]. It was found that there was a critical temperature, Tc = 180 ºC, below which the thermal decomposition to ZnO did not occur or was incomplete. Electrical resistivity was of the order of 10^{-3} ohm

cm in dark and it further reduced to 10^{-4} ohm cm after illumination. Band gap was nearly same (3.3 eV) for all samples prepared at different substrate temperatures.

Influence of substrate temperature on the properties of ZnO thin films was also a subject of detailed study and it has been found that resistivity and optical transmittance of the films very much depend on the temperature [57]. Substrate temperature was varied from 573 K to 773 K and spray rate was maintained at 6 ml/min. However films were found to be resistive. Effects of doping and annealing on the electrical, optical and structural properties of ZnO thin films prepared using this simple technique was also investigated [58]. Annealing in argon or vacuum reduced electrical resistivity substantially. The most pronounced change was observed in argon atmosphere. Highest figure of merit was obtained in the case of indium doped ZnO films.

Kuang –Che Hsiao et al. [59] synthesized AZO nano powder using spray pyrolysis technique. Aerosol droplets of the mixture of the zinc and aluminium nitrates [concentration varied from 0.06 to 3.0 M] were pyrolysed in air at temperatures ranging from 500 to 800 °C. The AZO powder had a primary and a secondary particle sizes in the range of 15–30 nm and 1–3 μm, respectively. Particle sizes increased with the reaction temperature and precursor concentration. Relative density of the particles increased with reaction temperature but decreased with precursor concentration. Particles synthesized from high precursor concentration had a tendency to form hollow and/or porous structure

A.E.Manouni et al. [60] reported the structural, optical and electrical characterisation of AZO thin films prepared using CSP technique. The minimum resistivity was obtained for the sample with Al concentration of 1% [1 Ω cm]. All the films were polycrystalline with hexagonal wurtzite structure. The undoped ZnO films had preferred (002) orientation, while the doped samples with Al concentration higher than 2% had (101) and (102) reflection peaks indicating that Al causes a loss of preferential orientation in (002) .

Jiwen Xu et al. [61] prepared the ZnO:Al films on glass substrate at relatively low temperature of 300^0C by ultrasonic spray pyrolysis. Zinc acetate and Aluminum acetate acted as zinc and aluminium sources, which dissolved in ethanol–water solution. The results showed that ZnO: Al films exhibited stronger (1 0 1) preferred orientation and had lenticular-like grain morphology. Resistivity as low as 4.3×10^{-1} Ω cm for as-deposited films

was obtained at the 4 at.% doping concentration, which could be decreased to1× 10^{-2} Ω cm level by post-deposited vacuum annealing. Average transmittance of as-deposited films was nearly 80% in the visible range while that of 4 at.% doped films was reduced to 60% after vacuum annealing at 550–600^{0}C. AZO films were prepared using CSP technique of Zinc acetate and aluminium nitrate[62]. X-ray diffraction analysis showed that the sprayed AZO films were polycrystalline texture with hexagonal structure. All the films exhibited high optical transmission of over 90%. With increase in the film thickness, transmittance decreased. Dependence of the refractive index, n, and extinction coefficient, k, on the wavelength for the sprayed films was also reported. Optical band gap of AZO was between 3.30 and 3.55 eV, depending on the film thicknesses.

H. Gómez-Pozos et al. [63] deposited AZO thin films over sodocalcic glass substrates using CSP technique; in this work, zinc acetate and aluminum pentanedionate were the precursors. The group observed that addition of Al to the starting solution decreased the electrical resistivity of the films up to an optimum value between 2 and 3 at.%; further increase in the [Al/Zn] ratio lead to an increase in the resistivity. After a vacuum-thermal treatment, performed at 400 °C for 1 h, the films showed a resistivity decrease, reaching a minimum value, for the films deposited at 475^{0}C, of 4.3×10^{-3} Ω cm. X-ray diffraction studies showed that the films are polycrystalline and the peaks fit well to the hexagonal wurtzite structure with a preferred orientation along the (002) direction. Optical transmittance at 550 nm ranged between 85 and 90%, depending on the deposition temperature. Slight variations of the band gap were obtained when the substrate temperature was varied.

AZO 'microrods' with increasing [Al]/[Al+Zn] molar ratios up to 20 at.% were prepared on glass substrates[64]. X-ray diffraction studies revealed that all films had hexagonal wurtzite crystal structure with a strong (002) preferred orientation. Surface morphology of the films studied using scanning electron microscopy showed that the undoped ZnO film had hexagonal shaped microrods. Optical studies indicated that the band gap slightly decreased [from 3.23 eV to 3.15 eV as the doping increased from 0 at.% to 20 at.% Al] with increasing Al doping, which could be explained in terms of electron concentration dependence of band gap shift in the Al-doped ZnO films. Doping with Al resulted in the decrease of electrical resistivity (2.9 Ω.cm) up to 15at.%.

Lokhande and Uplane discussed structural, optical and electrical studies on highly oriented (along 100 plane) sprayed ZnO films [65]. The resistivity of the film at room temperature was ~ 10^{-1} ohm cm and the band gap energy was 3.27 eV. Transparent conducting IZO thin films were prepared on soda-lime glass substrates using CSP technique [66]. Dependence of electrical, structural, morphological and optical properties on the preparation conditions was discussed in detail in this paper. Two main variables, viz., substrate temperature and molar concentration, were varied in the ranges of 425–525 °C and 0.05–0.5 M respectively in order to obtain films with low electrical resistivity and high optical transparency in the visible region. Minimum resistivity value of ~ 3×10^{-3} Ω cm was obtained for films deposited from highly concentrated starting solutions, i.e. 0.4 and 0.5 M. Values of the free-carrier concentration and the electronic mobility were estimated using Hall effect measurements. XRD studies proved that the preferential orientation was along the (1 0 1) direction. Surface morphology was clearly affected by the variations in molar concentration, leading to a smoother appearance as the zinc concentration in the starting solution increased. Typical optical transmittance values in the order of 85% were obtained for all the films.

Indium doped ZnO thin films were grown on glass substrates using the CSP technique [67] and effect of acetic acid content in starting solution as well as the substrate temperature was studied .When the acetic acid content in the solution (C_{AA}) is extremely low, the resistivity become relatively high (4×10^{-2} Ω cm). When the C_{AA} was increased at fixed temperature, resistance of the film decreased as low as 4×10^{-3} Ω cm for the film deposited at 525^0C. Another report, IZO thin films were prepared using spray pyrolytic decomposition of zinc acetate with indium acetate in an alcoholic solution [68]. The films were deposited onto soda lime glass substrate, alumina and sodium chloride crystals. Application of 'Reitveld refinement' method to analyse the XRD pattern has been proven to be effective method to obtain more detailed information about the crystallographic structure of the ZnO films. Another report,Indium doped ZnO [IZO] thin films were prepared on Corning glasses substrates again using CSP technique [69]. Doping concentration of 2 at.% was proved to be optimum for indium doped zinc oxide thin films. X-rays diffraction pattern showed that the IZO films were polycrystalline of wurtzite structure with preferential orientation of (0 0 2) direction. Samples having doping level of 2% exhibited

the lowest resistivity of 6×10^{-3} (Ω cm) while undoped ZnO had 17 Ω cm. Optical gaps of the IZO thin films were determined using optical transmission spectra and band gap value increased slightly from 3.28 eV to 3.35 eV due to the indium doping.

Indium doped (2mol %) ZnO films on glass substrate were grown through the spray pyrolysis method at 500 °C [70]. Samples were annealed under N_2 atmosphere between 100 and 600 °C for 5min.The XRD spectra indicated that the *c*-axis became more prominent with increasing annealing temperature. Low resistivity of 4.0×10^{-2} Ω cm with electron mobility of 3.0 $cm^2\ V^{-1}s^{-1}$ and carrier concentration of 7.0×10^{19} cm^{-1} were obtained at annealing temperature of 450 °C. The PL indicated that five distinct peaks, [donor and acceptor bound exciton and its phonon replicas], could be observed in the undoped ZnO film. On the other hand, one broad peak was dominant in the In-doped ZnO film. This peak was due to donor bound exciton of the In interstitial (In_i) or In atom in the Zn site(In_{Zn}). No deep emission bands were observed in the undoped and In-doped ZnO films. This proved that the V_O and/or Z_{ni} defects were few in the ZnO films. The peak energy of the PL spectra was not changed with increasing annealing temperature. However, the PL intensity decreased with annealing temperature.

Gallium, aluminum, and indium-doped ZnO (ZnO:Ga, ZnO:Al, and ZnO:In) films have been deposited using the chemical spray method on sodacalcic substrates [71]. Best electrical properties were observed in the thickest indium-doped ZnO films; the lowest electrical resistivity was of the order of 10^{-3} Ω cm. Optical transmittance value in the visible spectrum was around 87% in the thinnest films. Structural and morphological properties of ZnO:Ga and ZnO:Al films were similar, as in both cases the (0 0 2) orientation was dominant . In the case of ZnO:In films, the (1 0 1) was the preferential growth orientation, and the surfaces seem to be smoother than the corresponding ZnO:Ga and ZnO:Al films.

Highly conducting and transparent gallium doped zinc oxide (ZnO:Ga) layers also were deposited [72]. The ZnO:Ga films grown at a substrate temperature of 350 ^{0}C with gallium concentration of 5.0 at.% had the best physical properties. These layers were highly oriented along the (002) planes and having n-type conductivity type [electrical conductivity ~ 1.32×10^3 Ω^{-1} cm^{-1}]. Transmittance of these films was higher than 85% in the visible region with a high reflectance in the infra-red region.

ZnO and cerium-doped zinc oxide (ZnO:Ce) films were deposited using reactive chemical pulverization spray pyrolysis technique Here chlorides of zinc and cerium were used as precursors [73]. All films were oriented preferentially along the (00 2) direction. Films doped with 0.8 at.% cerium had stronger c-axis orientation perpendicular to the substrate, larger grain, smoother surface morphology and higher transmittance than the others. Thicknesses of films grown from solution with 3.03% and 3.4% cerium concentration were 250 nm and 200 nm, respectively.

2.3.5 Molecular Beam Epitaxy (MBE)

Molecular Beam Epitaxy is a technique for the epitaxial growth via the interaction of one or several molecule or atomic beams that occurs on the surface of a heated crystalline substrate .The solid source materials are placed in evaporation cells to provide an angular distribution of atoms or molecular in beams. The substrate is heated to necessary temperature and, when needed, continuously rotated to improve the growth homogeneity. MBE takes place in the High Vacuum (10^{-8} Pa). The most important aspect of the MBE is the slow deposition rate (typically less than 1000nm per second), which allows the films to grow epitaxially. The term 'beam' means that evaporated atoms do not interact with each other or vacuum chamber gases until they reach the wafer, due to the long mean free path of the atom. MBE is also used for the deposition of some types of organic semiconductors. In this case, molecules, rather than atoms, are evaporated and deposited onto the wafer.

Highly transparent and conductive ZnO films were grown through atomic layer controlled growth on various substrates including glass, sapphire and polyethylene tetraphthalate (PET) at different temperatures [74]. Effect of doping with Ga was also discussed in this report. Thermal annealing of ZnO layers was done in N_2 or O_2 atmosphere and their effects were also studied [75]. Annealing in O_2 atmosphere is necessary compared to N_2 atmosphere in order to suppress the generation of V_O and Zn_i. If the annealing is done in O_2 at temperatures higher than the growth temperature, the electron concentration increases while the annealing in O_2 at temperatures lower than the growth temperature, causes reduction in electron carrier density e.g., from 2.4×10^{18} to $2.5\times10^{17}cm^{-3}$ by the 500^0C annealing. Interestingly the crystallinity is improved.

M.A. Reshchikov et al. [76] observed strong shift of blue and yellow luminescence band with variation of excitation intensity in the ZnO film grown on sapphire using MBE

with hydrogen peroxide as source of reactive oxygen. The group observed the Yellow Luminescence (YL) and Blue Luminescence (BL) bands with nearly Gaussian shape and positions of maxima in the ranges 2.1–2.3 and 2.85–3.15 eV, respectively. Both the PL bands were blue- shifted substantially with increasing excitation intensity. The shifts were attributed to screening of potential fluctuations created by random distribution of charged defects in regions with high degree of compensation. They suggested that BL and YL bands in studied ZnO were caused by diagonal transitions from the potential valleys in the conduction band (or shallow donors located there) to the potential humps in the valence band and to deep acceptor levels located in these humps, respectively. Tsukazaki et al. [77] reported the high-quality ZnO thin film deposition on close lattice–mismatched hexagonal $ScAlMgO_4$ substrate by laser MBE at high growth temperature up to 1000^0C. The FWHM of (0002) XRD rocking curve is less than 18 arc sec for 1 μm thick ZnO films. By using the high quality undoped ZnO films, these authors also demonstrated ZnO p-i-n homojunction for light emitting diodes (LED) applications.

2.3.6 Summary of deposition techniques

Spray Pyrolysis can be employed for the growth of low-cost films for large area application. The technique has high growth temperature and poor uniformity compared to other deposition technique. Some of the major advantage of the spray technique than the others are 1) stoichiometry can be easily varied by varying the concentration of the constituents in spray solution 2) Easiness of doping 3) Spray solution contains soluble salt of constituents of desired compound. For the growth of reproducible device-quality films, CVD, PLD, sputtering have been extensively used in one form or another. The deposition rates of CVD are usually greater than those of sputtering. The sputter deposition technique, although more complex and more expensive, is preferred as it permits better control of film composition and thickness.

2.4 Application of ZnO

2.4.1 Solar cells

There has been interest in recent years directed towards the development of conducting transparent oxide-based solar cell. These oxides offer the possibility of fabrication of solar cell with performance characteristics suitable for large-scale terrestrial applications. Transparent conducting oxides are particularly effective in solar cell applications because of the following advantages.

(a) The conducting transparent film permits transmission of solar radiation directly to the active region with little or no attenuation, so that solar cells based on these materials result in improved sensitivity in the high photon- energy portion of the solar spectrum.

(b) Ease of fabrication of the junction because of lower junction formation temperature.

(c)These films can serve simultaneously as low resistance contact to the junction and anti-reflective coating for the active region.

Oliver kluth et al [78] reported the suitability of the light scattering properties of different texture glass/ZnO surfaces for efficient light trapping in silicon thin film solar cells. AZO substrate with adapted surface texture for different applications and reduced absorption losses contributed to the development of μc-Si:H p-i-n, and a-si:H/μc-si:H stacked p-i-n cell with efficiencies of 9% and 12.1% respectively. J.A. Aranovich et al [79] investigated electrical and photovoltaic properties of heterojunction prepared using spray pyrolysed ZnO films on single crystal p-type CdTe. Under actual sunlight the optimum cell showed an open-circuit voltage of 0.54 V and short-circuit current of 19.5 mA/cm^2 with an efficiency of 8.8%.

$CuInS_2$/ZnO solar cell of 2% efficiency with Voc =280 mV, Isc=13.3 mA/cm^2 and FF=0.38 were prepared using spray pyrolysis [80]. The solar cell performance depends on the $CuInS_2$ deposition parameters and resistivity of $CuInS_2$ and ZnO thin films. Annealing is the most critical parameters for the improving junction behaviour. M.S.Tomer et al. [81] prepared thin film ZnO/$CuInSe_2$ heterojunction solar cell using CSP technique. The cell showed an open-circuit voltage 0.3 V, short circuit current of 23mA/cm^2, a fill factor of 0.29 and electrical conversion efficiency exceeding 2%.

M.C.Kao et al. [82] deposited Zinc Oxide nano crystalline thin film on Fluorine Tin Oxide(FTO) coated glass substrate using sol-gel spin–coating technology and rapid thermal

annealing for the use in dye sensitized solar cells. Efficiency of 2.5% with J_{sc} and V_{oc} 8.2 mA/cm^2 and 0.64 V respectively were obtained when the ZnO film were pre annealed at 300^0C. ZnO layer was deposited as 'diffusion barrier' through DC Magnetron sputtering from pure ZnO target on stain steel substrate [83]. ZnO diffusion barrier had strongly reduced the diffusion of Fe from the stainless steel substrate into CIGS solar cells.

M.Berginski et al.[84] investigated the influence of doping level of the sputter target and substrate temperature on the post etching surface texture of ZnO:Al films and their light trapping ability in silicon thin film solar cells. Kerstin Schulze et al.[85] compared organic solar cell using different transparent conducting oxides as anodes [ITO and 3 kinds of AZO]. These anodes with different work functions were used for small molecule photovoltaic device based on as oligothiophene derivatives as donor and fullerene C60 as acceptor molecule. They concluded that the work function of the anode did not influence the V_{oc} of the photovoltaic device.

S.Y.Myong et al. [86] developed hydrogenated 'protocrystalline silicon' (pc-Si:H)/Hydrogenated 'microcrystalline silicon' (μc-Si:H) double junction solar cell structure employing boron doped ZnO (ZnO:B) intermediate layer. Because the ZnO:B intermediate layer reduced the potential thickness for pc-Si:H absorber in the top cell, this double junction structure was promising candidate to fabricate highly stable Si- based thin film solar cell. T.Dittrich et al. [87] investigated the effect of annealing on the ZnO nanorods/In_2S_3/ CuSCN devices. They compared the charge selective contact of solar cells with extremely thin absorber based on ZnO- nanorod/In_2S_3/ CuSCN before and after thermal annealing by current-voltage measurements at varying temperature and light intensity.

A. Campa et al. [88] reported that the role of ZnO between the CIGS and the back metal contact in terms of optical improvement of the back contact. Simulation results showed significant increase in the reflectance of ZnO/Mo contact compared to Mo contact without ZnO layer. The analysis of improvements in simulated quantum efficiency (QE) and short circuit current (J_{sc}) of a thin film CIGS solar cell, related to TCO/metal indicated that significant amount of reflected light escaped from the substrate due to the insufficient light trapping in thin CIGS absorber.

U. Rau et al. [89] showed the role of i-ZnO layer in ZnO/CdS/CIGS solar cell. Authors proposed that the local series resistance provided by the i-ZnO prevented electrical

homogeneities from dominating the open circuit voltage of the entire device. Lin Ke et al [90] studied the degradation mechanism of ZnO dye sensitized solar cell (glass/ITO/ZnO/dye/electrolyte/Pt) using various characterisation techniques. Extremely Thin Absorber (ETA) cells with the structure of TCO/ZnO rod/In_2S_3/ $CuInS_2$ were prepared with the help of CSP technique [91]. Effects of buffer layer thickness and ZnO nano-rods of length 500–1000 nm were studied. Increasing In_2S_3 layer thickness reduced fluctuations of the cell output parameters and increased V_{oc} and FF; however, certain thicknesses induce losses due to light absorption. The highest conversion efficiency 4.17% at AM1.5 was recorded from small contact area of the cell based on rods with length of 600nm.

2.4.2 Light Emitting Diodes

One of the first [if not *the* first] ZnO-based hybrid hetero structure LEDs was fabricated by Drapak [92] in 1968 who used Cu_2O as the p-type layer. In all the other hybrid structures that followed, the emission observed under forward bias either originated in the p-type layer, or showed a very weak contribution at the ZnO band edge corresponding to extremely small external quantum efficiencies. When p-AlGaN was used to favour hole injection into ZnO thereby promoting emission in that material, strong Electroluminescence(EL) peaking at 390 nm due to excitonic recombination within ZnO has been observed [93,94]. Although these results show that p-AlGaN is a good candidate for fabricating efficient hybrid hetero-structure LEDs with ZnO active layers, 'all-ZnO-based' LEDs incorporating stable p-ZnO are needed for light emitters to compete with those based on nitrides. Reports on 'all-ZnO-based' light-emitting devices have also started to appear [95,96] as p-type ZnO became available. However, production of stable and device-quality p-type ZnO has not been realized despite a large number of publications reporting successful demonstration of p-type ZnO samples, as discussed in detail in the reference [97]. Incorrect interpretation of the van der Pauw–Hall measurements has been suggested [98] as one of the reasons for the controversial reports of p-type conduction in ZnO. In wide band gap semiconductors, doped with a high density of acceptor-type impurities, localization is an endemic problem: carriers are trapped and cannot follow the Lorentz force and the electric force induced by the low fields employed in Hall measurements. High carrier concentrations in p-type ZnO, which are often reported in the literature, are caused by very low Hall voltages. Correspondingly low-mobility values measured are usually indicative of

strong localization in the material which, if present, brings the applicability of conventional Hall measurements under question, particularly at low temperatures. Therefore, the interpretation of Hall effect measurements should be made very carefully.

2.4.3 Photodiodes

There have been many reports regarding the photo response properties of the ZnO-based hetero-junctions. Jeong et al.[99] reported the photoelectric properties of *n*-ZnO/ *p*-Si photodiode (PD) which detect UV photons in the depleted *n*-ZnO and simultaneously detect visible photons in the depleted *p*-Si by employing two related photoelectric mechanisms. I-V measurements obtained while the photodiodes are exposed to radiation in a wavelength range of 310–650 nm showed a linear increase in photocurrent with reverse bias. In the visible range, the photocurrent rose rapidly with bias but saturated beyond a critical voltage. The diodes exhibited high response of 0.5 and 0.3 A/W for UV (310-nm) and red (650-nm) photons, respectively, under a 30-V bias with a minimum near 380 nm which corresponds to the band gap of ZnO.

Ohta et al. [100] also reported on transparent *p-n* hetero-junctions composed of *p*-$ZnRh_2O_4$ and *n*-ZnO thin layers grown using reactive solid-phase epitaxy technique. Polycrystalline $ZnRh_2O_4$ was deposited on a ZnO epitaxial layer at room temperature. Thermal annealing of the bilayer sample at 950 °C in air converted the polycrystalline $ZnRh_2O_4$ layer to what was reported to be an epitaxial single-crystalline layer. The resultant *p-n* hetero-junctions had an abrupt interface and exhibited distinct rectifying *I-V* characteristics with a threshold voltage of ~2 V that is in agreement with the band-gap energy of $ZnRh_2O_4$. Photo voltage originating mainly from the *n*-ZnO layer was also observed.

n-ZnO/p-Si heterojunction photodiodes have been fabricated through sputter deposition of n-ZnO films on p-Si substrates [101]. The substrate temperatures were in the range 300, 400, 480 and 550^0 C with Ar and O_2 in the ratio of 6:1. All the diodes showed typical rectifying behaviour as characterized by the current–voltage (*I–V*) measurement in dark; the photoelectric effects from the diodes were observed under illumination using monochromatic light of wave length of 670 nm. Maximum amount of photo-current was obtained under reverse bias condition from n-ZnO/p-Si heterojunction when the ZnO film was deposited at 480^0C while the ZnO films deposited at 550^0C show the best

stoichiometric and crystalline quality. H. Y. Kim et al. [102] fabricated the n-ZnO/p-Si and n-ZnO/n-Si hetero-junction photodiode using RF sputtering technique varying the substrate temperature and Ar : O_2 ratio. The photoelectric effect was very promising ~~at~~ for the n-ZnO/p-Si structure while the n-ZnO/n-Si showed large dark current.

An optically transparent tin-doped indium oxide/ZnO/NiO n–i–p hetero-structure photodiode was fabricated using ion beam assisted e-beam evaporation [103]. The diode clearly demonstrated rectifying current–voltage (J–V) characteristics with current rectification ratio up to 104 at bias ±2Vand low reverse current of ~100 nA/cm^2 at −5 V. H.T.Hsueh et al [104] reported the deposition of Cu_2O onto vertically aligned ZnO nano-wires using DC sputtering. The average length, average diameter and density of these VLS-synthesized ZnO nano-wires were 1μ m, 100 nm and 23 wires/μm^2 respectively. With proper sputtering parameters, the deposited Cu_2O could fill the gaps between the ZnO nano-wires with good step coverage to form coaxial p-Cu_2O/n-ZnO nano-wires having rectifying current–voltage characteristic. Furthermore, the fabricated coaxial p-Cu_2O/n-ZnO nano-wire photodiodes exhibited reasonably large photocurrent to dark current contrast ratio as well as fast responses.

2.4.4 Gas Sensors

Semiconductor material whose conductance is modulated directly by interaction with an active gas has been studied for many years. There is reversible chemisorption of reactive gases at the surface of the certain metal oxides. The electron concentration in semiconductor sensors varies more less linearly with pressure up to eight decades, while the variation in the mobility was less than a factor of two over the same pressure range. This suggests that gas chemisorption into the surface of the semiconductor materials is useful for the fabrication of gas sensing electronic devices.

ZnO has been widely used for sensing application because of high sensitivity to the chemical environment. The sensing process is governed by oxygen vacancies on the surface that influence the electronic properties of ZnO. Upon oxidation, via adsorption of molecules such as NO_2 at vacancy sites that accept electrons, electrons are withdrawn and effectively depleted from the conduction band, leading to a reduction of conductivity. On the other hand, reducing molecules such as H_2 can react with surface-adsorbed oxygen, leaving behind an electron and hence higher conductivity. The challenge is to sense certain gases

selectively. All experimental result demonstrate that ZnO nano-wire owing to the large surface area, have potential for detecting NO_2[105] NH_3[106], NH_4[107], CO[107], H_2 [108], H_2O[109], O_3 [110]H_2S[111] and C_2H_5OH[112].

The key in the most biological process is the need for a small change of pH created by the release of H^+ ions during the biological reactions. Determination of pH is a prerequisite for many processes. Sensing mechanism for the pH is the polarization induced bound charge by interaction with the polar molecule in the liquids. Application of ZnO nano-rods as the pH sensor for intracellular chemical sensing is under development and room temperature sensitivity as high as ~ 59 mV per decades change in the pH value has been reported [113].

There are two different types of contacts between the particles of sensing materials [114]: the two-dimensional (2-D) contact between "necked particles" and point-to-point contact between ordinary particles. When the particles are necked together significantly and the sizes of the necked part become comparable to the thickness of the resistive electron depleted layer, the conductive channel through the neck determines the total resistivity (neck model). When the particle sizes are significantly larger than the thickness of the electron depleted layer, the conductive channel through the neck becomes too wide for the channel to control the electrical resistivity of the particles chain. In this condition, the point-to-point contacts between the grain boundaries dominate the total resistivity, giving rise to gas sensitivity independent of the particle sizes (grain-boundary model). The sensitivity of a gas sensor is closely related to the degree of diffusion of the gas molecules into the sensing material used to adsorb and desorb them [115,116] as well as to the latter's specific surface areas. In order to maximize its sensitivity, many attempts have been made recently to design the structure of the resistive channels so as to enhance the gas diffusion. Although channels with two-dimensional (2-D) film structures have been widely investigated [117,118] their small specific surface areas limit their adsorption efficiency. Recently, channels with one-dimensional (1- D) structures, such as nano-wires, nano-rods and nano-belts, were proposed [119–121] since they offer a greater degree of diffusion for gas molecules as well as relatively larger specific surface area compared with 2-D structured films. These 1-D structures provide well-defined channels without any grain boundaries which might obstruct the flow of electrons through the channels. Due to these favourable properties, gas sensors

with channels made of 1-D nano-materials have been widely investigated. In addition, sensing materials with zero-dimensional (0-D) structures such as nano-particles (NPs) have also been studied for the use in the channels, due to their larger specific surface area compared to those of the other dimensional structures. However, the relatively high temperature (600 ◦C) of the heat treatment used to stabilize the NPs brings about their agglomeration [122] which causes two critical problems for the gas sensors: the sensitivity decreases, since the gas sensing reaction occurs mainly at the surface of the agglomerates, and the response slows down, since the diffusion of gas molecules into the agglomerates becomes more difficult and slower. Thus, the application of NPs as gas sensing materials has been limited

Controlling and monitoring ethanol is important in some fields [123], such as testing alcohol levels of drivers, monitoring chemical synthesis, etc. SnO_2, ZnO [124,125], γ-Fe_2O_3, α.Fe_2O_3 [126], and other oxides are being investigated widely because of their high sensitivity to ethanol. However, much work needs to be done to improve the sensitivity of those materials to ethanol and further to explore new ethanol-sensitive materials. As the present research results on all kinds of semiconductor metal oxides have shown, ZnO may be one of the most hopeful candidates due to its matured fabrication technology, which can produce all kinds of ZnO nanostructures, such as nano-wires, nano-rods, nano-belts, nano-ribbons.

2.4.5 Transparent Thin Film Transistors [TTFT]

The most important electrical parameters in quantifying TFT performance are the 'drain-current on-to-off ratio' and 'active channel mobility'. In terms of these parameters, the best TTFT performance has been reported by Hoffman et al. [127] Highly transparent ZnO-based TTFT's with optical transmittance (including substrate) of ~75% for visible light have been fabricated by using RF sputtering method. Carcia et al. [128] fabricated ZnO thin film transistors using RF magnetron sputtering on heavily doped *n*-type Si substrates held near room temperature. In this structure, the substrate side was coated with a thermal oxide layer of ~100 nm thick. Ti–Au source and drain electrodes 200 μm wide with a 20μm gap (10-nm Ti followed by 100-nm Au) were deposited and patterned directly on the thermal silicon oxide layer applying traditional photolithography.

J. H. Chung et al. [129] investigated the electrical characteristics of ZnO thin film transistors with respect to the thickness of ZnO active layers. ZnO layers with thicknesses 30 nm to1500 nm were deposited on bottom gate patterned silicon substrate using RF sputtering at room temperature. The leakage current was 9.97×10^{-8}A, channel mobility was 0.16cm^2/Vs and threshold current was 12.7 V. L. Zhang et al [130] also reported the performance of ZnO-TTFTS with different thicknesses of the active layer and optimised the conditions. The leakage current of devices increased from 10^{-10} to 10^{-8} A and on/off ratio decreased from 1.2×10^7 to 2×10^4. Atomic force microscope measurements indicated that as the thickness increased, the surface morphology of the active layer improved noticeably at first and then deteriorated.

R. Navamathavan et al. [131] fabricated the ZnO based thin film transistor using RF magnetron sputtering with and without NH_3 plasma treatment. The electrical properties were observed to be significantly improved for the ZnO TFT with NH_3 plasma treatment. NH_3 plasma treated ZnO TFT exhibited excellent electrical characterisation as evident from sub threshold swing of 0.44 V/dec, minimum off-current of 10^{-11} A, threshold voltage of 14 V, field effect mobility of 34 cm^2/Vs, and on/off ratio of 10^5.

H. Faber et al. [132] compared two different solution based techniques to fabricate ZnO TFTs. Nano-particle dispersions were processed through spin coating with thermal treatment of the semiconductor at 100 ^{0}C. Precursor solutions were deposited and converted in to ZnO layers using spray pyrolysis at a temperature of 370 ^{0}C. Thin film transistor devices (TFTs) based on spray pyrolysis films exhibit higher electron mobility up to 24 cm^2 /V s compared to 0.6 cm^2 /Vs for nano particle based TFTs. The increased mobility is clearly due to improved crystalline arrangement in the spray coated films.

2.4.6 ZnO Nanostructures

One-dimensional semiconductor nano-wires and nano-rods have attracted increasing attention due to their physical properties arising from quantum confinement (such as electronic quantum transport and enhanced radiative recombination of carriers). Nano-wires have promising potential in extensive applications and are the fundamental building blocks for fabricating short-wavelength nano-lasers, field-effect transistors, ultrasensitive nano-sized gas sensors, nano-resonators, transducers, actuators, nano-cantilevers, and field emitters (FEs). These nano-structures are the ideal for studying transport mechanisms in one

dimensional (1D) systems, which are of benefit not only for understanding the fundamental phenomena in low-dimensional systems but also for developing new generation nano-devices with high performance.

Li et al. [133] prepared ZnO nano-needles on a silicon wafer through chemical-vapour deposition. The diameters of the needle tips were in the range of 20–50 nm. High-resolution transmission electron microscopy revealed that the nano-needles were single crystals growing along the (0001) direction and exhibiting multiple tip surface perturbations, and were just 1–3 nm in dimension. Field Emission measurements on the prepared nanostructures showed fairly low turn-on and threshold fields of 2.5 and 4.0 V/mm, respectively. The nano-size perturbations on the nano-needle tips are assumed to cause such excellent field-emission performance. High emission current density, high stability and low turn-on field make the ZnO nano-needle arrays one of the promising candidates for high brightness field-emission electron sources and flat-panel displays.

Park et al. [134] reported on the metal-organic vapour-phase epitaxial (MOVPE) growth of ZnO nano-rods which were well aligned vertically, showing uniformity in their diameters, lengths, and density as revealed from electron microscopy. The mean diameter of the nano rods is ~25 nm. In a study by Kong et al. [135], 'single-crystal nano-rings' of ZnO were grown using the solid-vapour process. The raw material was a mixture of ZnO (melting point of 1975 °C), indium oxide, and lithium carbonate powders at a weight ratio of 20:1:1. It was placed at the highest-temperature (1400 °C) zone of a horizontal tube furnace. ZnO decomposes at such a high temperature into Zn^{2+} and O^{2-} and this decomposition process is the key step for controlling the anisotropic growth of the nano-belts. Zhang et al. [136] reported formation of ZnO tubes by MOCVD at temperatures of 350–450 °C. The tubes obtained were grown epitaxially on sapphire (0001) substrates with the growth along *c* axis parallel to the substrate normal. All of the tubes had hexagonal cross section. Nature of the tubes was found to depend strongly on both the growth temperature and reactor pressure. Growth temperature also greatly influenced the tube formation. In the temperature range of 350–450 °C, density of the tubes increased from 0.04 to 1 μm^{-2} and the outer sizes of the tubes decreased from 1.0 to 0.4 μm with increasing temperature.

T. Devoda et al. [137] presented the results on formation of ZnO nano-rods prepared by spraying aqueous solution containing $ZnCl_2$ and thiourea in different molar

ratios on to SnO_2 covered glass substrate. They observed that addition of thiourea into spray solution has great impact on the size, shape and phase composition of ZnO crystals. Thiourea addition generally leads to the formation of thinner rods with higher aspect ratio compared to those deposited from the $ZnCl_2$ solution. According the XRD, well crystallized (002) oriented pure wurtzite ZnO crystals have been formed. When the content of the thiourea was increased, weak reflection at 2θ of 28.5 ^{0}C was detected in the XRD pattern which could be attributed to the (111) reflections of ZnS sphalerite phase.

M. Krunks et al. [138] reported the growth of ZnO nano-rods arrays from Zinc Chloride solution with pH=2 and 5 on glass/ITO substrate at 480^0 C and 550^0 C through CSP technique. ZnO nano rods deposited at substrate temperature of 550^0 C from aqueous solution indicated the concentration of carriers in the range of 10^{14}-10^{15} cm^{-3} irrespective of the spray solution acidity. Heo et al.[139] measured the temperature and the gas/ ambient dependence of current-voltage characteristics of single ZnO nano-rods grown through catalyst-driven MBE on Au-coated Sapphire substrates. Individual nano-rods were removed from the substrate and placed between ohmic contact pads, kept 3.7 μm apart. Conductivity of the nano-rods increased after a post-growth annealing in hydrogen gas at 400 °C. In the temperature range from 25 to 150 °C, resistivity of nano-rods, treated in H_2 at 400 °C prior to measurement, showed an activation energy of 0.089±0.02 eV and was insensitive to the ambient used (C_2H_4,N_2O,O_2 or 10% H_2 in N_2).

M. Shahjahan et al. [140] reported the fabrication of undoped and Al-doped ZnO nano-wall structures on ordinary glass substrate by low cost spray pyrolysis technique at low deposition temperature of 350 °C. Structural study revealed that the fabricated ZnO nanostructures were polycrystalline in nature and crystallinity of the samples depends on the Al doping concentration. For undoped ZnO, the band gap was obtained as 3.27 eV and the band gap decreased up to 3.06 eV with the increased in Al doping concentration up to 4%.

Yuan-Chung Wang et al. [141] reported a novel method for preparing uniform and aligned ZnO nano-wire arrays embedded in anodic alumina membranes (AAM) through electrophoretic deposition (EPD). EPD is a simple and powerful method to obtain arrays of fibrils and tubules just by controlling the applied voltage. XRD and luminescence results indicated that the prepared ZnO arrays can have similar properties to those prepared by other methods. Shu-Cheng Chin et al. [142] compared the nano-structures of three samples

of ZnO thin film on sapphire under different growth temperature conditions. Although disconnected domain structures (on the scale of 100nm in size) were observed in the samples grown under high-temperature (450^0C) their crystal quality was generally better than the one grown at a low temperature (200^0C). Lattice misfits and threading dislocations were observed within a domain with the separation of around 8 nm.

Nano-crystalline ZnO thin films were grown on inexpensive Soda-lime Silica Glass substrates using 'Chemical Solution Deposition' process with zinc acetate - 2 thoxyethanol - MEA solution [143]. XRD analysis proved that the films were amorphous even when annealed at 100^0C- 200 ^{0}C for 60 minutes, while c-axis oriented ZnO were obtained by pre-firing at a high temperature [400 ^{0}C and 500^0C]. A relatively high transmittance in the visible region and clear absorption edges of the films were observed except for the film annealed at 100^0C.

Z. W. Liua et al. [144] synthesized the ZnO nano-rods with various diameters using PLD technique at the relatively high background pressure of 5–20 Torr and substrate temperature 550 °C– 700°C without a catalyst. The PL properties of the nano-rods produced using various processes have been investigated. Thus, *c*-axis oriented ZnO nano-rods were easily synthesized on the sapphire substrate with the help of the laser ablation technique without using a catalyst. The size control could be accomplished by adjusting the temperature and pressure in the range of 550 °C–700 °C and 5–20 Torr.

2.5 Conclusions

A review of properties, deposition techniques and device applications of ZnO is presented in this chapter. ZnO has some unique properties and some advantages over other wide – gap materials such as GaN which is widely used today for production of short–wavelength light emitting devices. Regarding solar cells, already this material has received some attention, although competition is very stiff; however further studies are required to improve the current density and efficiency. As for the nanostructures, ZnO nano-structures (nano wires and nano-rods) provide a path to a new generation of device, but deliberate efforts have to be expended for ZnO nano-structures especially for large-scale device applications, and to achieve high device density with accessibility to individual nano-devices.

References

[1] A. Mang, K.Reimann and St. Rubenacke Solid State Commun. **94** (1995) 251.

[2] O. Madelung (ed) *Semiconductors—Basic Data 2nd Revised* Edn (1996) (Berlin: Springer)

[3] D .C Look , Mater. Sci. Eng. B **80** (2001) 383.

[4] U Ozgur, Y. I. Alivov, C.Liu, A.Teke, M.A.Reshchikov, S.Dogan, V. Avrutin, S-J.Cho and H Morkoc¸ J. Appl.Phys. **98** (2005) 04130.

[5] S. B.Ogale, Thin Films and Heterostructures for Oxide Electronics (New York: Springer) (2005).

[6] N. H. Nickel and E.Terukov (ed) *Zinc Oxide—A Material for Micro- and Optoelectronic Applications*(2005) (Netherlands:Springer).

[7] C. Jagadish and S. J.Pearton (ed) Zinc Oxide Bulk, Thin Films, and Nanostructures (2006) (New York: Elsevier).

[8] D. C. Reynolds, D.C. Look and B.Jogai,Solid State Commun. **99** *(*1996) 873.

[9] D. M. Bagnall, Y. F.Chen, Z. Zhu, T. Yao, S. Koyama, M. Y. Shen and T. Goto Appl. Phys. Lett. **70 (**1997) 2230.

[10] M. N. Kamalasanan and S. Chandra ,Thin Solid Films **288 (**1996) 112.

[11] F. D. Paraguay, W. L. Estrada, D. R. N. Acosta, E. Andrade and M. Miki-Yoshida, Thin Solid Films **350** (1999)192.

[12] H. Funakubo, N. Mizutani, M.Yonetsu, A.Saiki and K. J Shinozaki. Electroceram. 4**[S1] (**1999) 25.

[13] K. Sakurai, M . Kanehiro, K. Nakahara, T. Tanabe and S. Fujita , J. Cryst. Growth **209** (2000) 522.

[14] T. Yamamoto, T. Shiosaki and A. Kawabata J. Appl.Phys. **51** (1980) 3113.

[15] J. Molarius, J. Kaitila, T. Pensala and M Ylimlammi J. Mater. Sci.: Mater. Electron. **14** (2003) 431.

[16] R. Ondo-Ndong, G. Ferblantier, F. Pascal-Delannoy, A. Boyer and A. Foucaran , Microelectron. J. **34** (2003) 1087.

[17] J. G. E Gardeniers, Z. M. Rittersma and G J Burger J. Appl. Phys. **83** (1998) 7844.

[18] S. Shionoya and W. H. Yen (ed) *Phosphor Handbook By Phosphor Research Society*

(1997) (Boca Raton, FL: CRC Press).

[19] D. I. Florescu, L. G. Mourokh, F. H.Pollak, D. C. Look, G. Cantwell and X. Li, J. Appl. Phys. **91**(2002) 890.

[20] U. Ozgur, X. Gu, S. Chevtchenko, J. Spradlin, S. J Cho, H. Morkoc, F. H. Pollak, H.O Everitt, B. Nemeth and J. E. Nause ,J. Electr. Mater. **35** (2006) 550.

[21] F. Tuomisto, K. Saarinen, D. C. Look and G. C. Farlow Phys. Rev. B **72** (2005) 085206.

[22] D. C. Look, J. W. Hemsky and J. R. Sizelove , Phys. Rev.Lett. **82** (1999) 2552.

[23] H. Nanto, H. Sokooshi and T. Usuda, Solid-State Sensors and Actuators **24–27**(1991) 596.

[24] O Schmidt, P. Kiesel, C. G. Van de Walle, N. M. Johnson, J .Nause and G. H. Dohler Japan. J. Appl. Phys. Part 1 **44** (2005) 7271.

[25] O.Schmidt, A. Geis, P. Kiesel, C.G. Van de Walle, N. M Johnson, A. Bakin, A. Waag and G. H Dohler, Superlatt. Microstruct. **39** (2006) 8.

[26] D. C Look, Surf. Sci. **601** (2007) 5315.

[27]R. A. Rabadanov, S. A. Semiletov, and Z. A. Magomedov, Solid State Phys. **12** (1979)1431.

[28] B. M. Ataev, A. M. Bagamadova, V. V. Mamedov, A. K. Omaev and R. A. Rabadanov, J. Cryst. Growth **198–199** (1999) 1222.

[29] K. Ogata,T. Kawanishi, K. Sakurai, S.-W. Kim, K. Maejima, Sz. Fujita and Sg. Fujita, Phys. Status Solidi B **229** (2002) 915.

[30] Y. Ma, J. Cryst. Growth **255** (2003) 303.

[31] Y. Ma , J. Appl. Phys. **95** (2004) 6268.

[32] M. Purica, E. Budianu, E. Rusu, M. Danila and R. Gavrila, Thin Solid Films **403-404** (2002) 485.

[33] V. Sallet, C. Thiandoume, J. F. Rommeluere, A. Lusson, A. Rivière, J. P. Rivière, O. Gorochov, R. Triboulet and V. Muñoz-Sanjosé, Mater. Lett. **53** (2002) 126.

[34] B. Hahn, G. heindel, E. P. Schoberer and W. Gebhaardt, Semicond. Sci. Technol. **13** (1998) 788.

[35] B. S. Li, Y. C. Liu, Z. Z. Zhi, D. Z. Shen, J. Y. Zhang, Y. M. Lu, X. W. Fan and X. G. Kong, J. Vac. Sci. Technolo. A **20(5)** (2002) 1779.

[36]Guotong Dua, Jinzhong Wanga,, Xinqiang Wanga, Xiuying Jianga,Shuren Yanga, Yan Maa, Wei Yana, Dingsan Gaoa, Xiang Liub, Hui Caob, Junying Xub, R.P.H. Chang,Vacuum **69** (2003) 473.

[37] D. Kim, I. Yun, H.Kim ,Current Applied Physics **10** (2010) S459.

[38]T. Sekiguchi, K. Haga, K. Inaba, Journal of Crystal Growth **214/215** (2000) 68.

[39] M. K. Jayaraj, A. Antony and M. Ramachandran, Bull. Mater. Sci. **25** (2002) 227.

[40] V. Gupta and A. Mansingh, J. Appl. Phys **80(2)** (1996) 1063.

[41] K. Young –Kook Kim, Shigeru Niki, Jin-Yong Oh, June-O-Song, Tae-Yeon Seong and Seong-Ju Park, Journal of applied Physics **97** (2005) 066103.

[42] M. Suchea, S. Christoulakis, K. Moschovis, N. Katsarakis and G. Kiriakidis, Thin Solid Films **515** (2006) 551.

[43]Petronela Prepelita , R. Medianu , Beatrice Sbarcea , F. Garoi and Mihaela Filipescu Appl. Surf. Sci. **256** (2010) 1807.

[44] Yasuhiro Igasaki and Hirokazu Kanma ,Appl. Surf.Sci. **169-170** (2001) 508.

[45] En-Gang Fu, Da-Ming Zhuang, Gong Zhang, Zhao ming, Wei-Fang Yang and Jia-Jun Liu, Microelectronics Journal **35** (2004) 383.

[46] Jae Bin Lee, Hyeong Joon Kim, Soo Gil Kim, Cheol Seong Hwang, Seong-Hyeon Hong, Young HwaShin and Neung Hun Lee, Thin Solid Films **435** (2003)179.

[47] Rajesh Das, Koel Adhikary and Swati Ray, Japanese Journal of Applied Physics **47** (2008) 1501.

[48]Yu Bin Xiao, Seon Mi Kong, Eun Ho Kim and Chee Won Chung , Sol. Ener. Mat. & Solar Cells **95** (2011) 264.

[49]Xin Chen, Wenjie Guan, Guojia Fang and X-Z-Zhao Appl. Surf.sci. **252** (2005)1561.

[50] H. Agur, A. Suzuki, T. Matsushita, T. Aoki and M. Okuda, Thin solid films **445** (2003) 263.

[51] Bin- Zong Dong,Gua-Jia Fang, Jian-Feng Wang, Wen- Jie Guan and Xing –Zhong Zhao,J.Appl. Phy. **101**(2007) 033713.

[52] S. Choopun, R. D. Vispute, W. Noch, A. Balsamo, R. P. Sharma, T. Venkatesan, A. Iliadis, and D. C. Look, Appl. Phys. Lett. **75** (1999) 3947.

[53] A. V. Singh, R. M. Mehra, N. Buthrath, A. Wakahara, and A. Yoshida, J.

Appl. Phys. **90** (2001) 5661.

[54] K. Matsubara, P. Fons, K. Iwata, A. Yamada, and S. Niki, Thin Solid Films **422** (2002)176.

[55] V. Craciun, J. Elders, J. G. E. Gardeniers, and I. W. Boyd, Appl. Phys. Lett. **65** (1994) 2963.

[56] S. A. Studenikin, N. Golego and M. Cocivera, J. Appl. Phys. **83** (1998) 2104.

[57] B. Joseph, K. G. Gopchandran, P. K. Manoj, P. Koshy and V. K. Vaidyan, Bull. Mat. Sci.**22** (1999) 921.

[58] P. Nunes, A. Malik, B. Fernandes, E. Fortunato, P. Vilarinho and R. Martins, Vacuum **52** (1999) 45.

[59] Kuang-Che Hsiao , Shih-Chieh Liao and Yi-Jia Chen Mat. Sci. and Eng: A 447 (2007) 71**.**

[60] A.E. Manouni, F.J. Manjon,M.Mollar,B.Mari,R.Gomez,M.C.Lopez and J.S.Ramos-Barrado,Superlattice and microstructures **39** (2006) 185.

[61] Jiwen Xu, Hua Wang, Ling Yang, Minghong Jiang, Shuai Wei and Tingting Zhang Mat. Sci. and Eng.B 1**67** (2010) 182.

[62] M.A. Kaid and A. Ashour Appl. Surf. Sci. **253** (2007) 3029.

[63] H. Gómez-Pozos, A. Maldonado, M. de la L. Olvera, Materials Letters **61** (2007) 1460.

[64] E.Bacaksiz ,S. Aksu, Salih Yılmaz, M. Parlak and M. Altunbaş, Thin Solid Films **518** (2010) 4076.

[65] B. J. Lohkhande and M. D. Uplane, Appl. Surf. Sci. **167** (2000) 243.

[66] M.A.Lucio-López, M.A. Luna-Arias, A. Maldonado, M. de la L. Olvera and D.R. Acosta, Sol. Energy Mater. Sol. Cells **90** (2006) 733.

[67] L.Castanede ,A. Garcia-Valenznele, E.P. Zironi, J. Canestas- Ortega , M.Terrones and A.Maldonado, Thin Solid Films **503** (2006) 212.

[68] M.Miki- Yoshida , F.Paraguay- Delgado, W-Estrada-lopez and E. Andrade, Thin Solid Films **376** (2000) 99.

[69] C.E. Benouis, M. Benhaliliba, A. Sanchez Juarez, M.S. Aida, F. Chami and F. Yakuphanoglu,Journal of Alloys and Compounds **490** (2010) 62.

[70] K.Yoshino,S.Oyama , M.Kato, M.Oshima1, M. Yoneta and T. Ikari1,Journal of

Physics: Conference Series **100** (2008) 082019.

[71] M. de la L. Olvera, H. Gomez and A. Maldonado,Sol. Ener. Mat. & Solar Cells **91** (2007) 1449.

[72] K.T. Ramakrishna Reddy, T.B.S. Reddy, I. Forbes and R.W. Miles, Surf. and Coat.Tech. **151 –152** (2002) 110.

[73] Z. Sofiani , B. Derkowska, P. Dalasin´ ski , M. Wojdyła , S. Dabos-Seignon,M. Alaoui Lamrani, L. Dghoughi, W. Bała, M. Addou and B. Sahraoui, Opt. Commun. **267** (2006) 433.

[74] A. W. Ott and R. P. H. Chang, Mater. Chem Phys. **58** (1999) 132.

[75] K. Ogata, K. Sakurai, Sz. Fujita, Sg. Fujita and K. Matsushige,Journal of Crystal Growth **214/215** (2000) 312.

[76] M.A. Reshchikov,V. Avrutin, N. Izyumskaya, R. Shimada and H. Morkoc Physica B **401–402** (2007) 374.

[77] A. Tsukazaki Nature.Mater **4** (2005) 42.

[78] O.Kluth, B. Rech and H. Wagner,17 th European Photovoltaic Solar Energy Conference, Germany October **22-26** (2001).

[79] J. A Aranocich,Dolores Golmayo,Alen.L.Fahren bruch and Richard.H.Bube. J.Appl.Phys **51** (1980) 4260.

[80] A. N.Tiwari,D. K. Pandya and K. L. Chopra ,Solar cells **22** (1987) 263.

[81] M. S. Tomar and F. J. Garcia, Thin solid films **90** (1982) 419.

[82] M. C. Kao,H. Z. Chen and S. L. Young, Appl Phys A **98** (2010) 595.

[83] C. Y. Shi, Yun Sun,Qing He,F. Y. Li and J. C. Zhao , Sol. Ener. Mat.& Solar cells **93** (2009) 654.

[84] Michael Berginiski,Jurgen Hupkes , Melaniee Schutle, Gunner Schope , Helmat Stiebig and Mathias Wuttig, J. of Appl. Phys.**101** (2007) 074903.

[85] Kerstin Schulze , Bert Maenning ,Karl leo, Yuto Tomito , Christain May, Jurgen Hupkes, Eduard Brier ,Egon Reinold and Peter Bauerle, Appl. Phys. Lett. **91** (2007) 073521.

[86] S.Y.Myong , Kobsak Sriprabha , Shinsuke Miyajima, Makota Konagia and Akira Yamada, Appl. Phy. Lett. **90** (2007) 263509.

[87] T. Dittrich ,D.Kieven, A.Belaidi, M.Rusu,J.Tornow, K.Schwarzburg and M.Ch.Lux-

Steiner,J. of appl. Phys. **105** (2009) 034509.

[88] A. Campa, J.Krc,J. Malmstrom,M. Edoff,F.Smole and M. Topic, Thin Solid Films **515** (2007) 5968.

[89] U. Rau and Marion Schmidt , Thin Solid Films **387** (2001) 141.

[90] L. Ke,S. B. Dolmanan,Lu Shen, Promoda kumara Pallathadk and Zheng Zhnag. Sol. Ener. Mat. & Solar cells **94** (2010) 323.

[91] M. Krunks , E. Karber, A.Katerski, K. Otto, I. Oja Acik,T. Dedova and A. Mere Sol. Ener. Mat. & Solar Cells **94** (2010) 1191.

[92] I. T. Drapak, Semiconductors **2** (1968) 624.

[93] Y. I. Alivov, E. V. Kalinina, A. E. Cherenkov, D. C. Look, B. M. Ataev, A. K. Omaev, M. V. Chukichev and D. M. Bagnall, Appl. Phys. Lett.**83** (2003) 4719.

[94] A. Osinsky, J. W. Dong, M. Z. Kauser, B. Hertog, A. M. Dabiran, P. P. Chow,S. J. Pearton, O. Lopatiuk and L. Chernyak, Appl. Phys. Lett. **85** (2004) 4272.

[95] A. Tsukazaki, A. Ohtomo, T. Onuma, M. Ohtani, T. Makino, M. Sumiya, K. Ohtani,S. F. Chichibu, S. Fuke, Y. Segawa, H. Ohno, H. Koinuma and M. Kawasaki, Nature Mater. **4** (2005) 42.

[96] A. Tsukazaki, M. Kubota, A. Ohtomo, T. Onuma, K. Ohtani, H. Ohno, S. F. Chichibu and M. Kawasaki, Jpn. J. Appl. Phys.l. **44** (2005) L 643.

[97] V. Avrutin, D. Silversmith and H. Morkoc, IEEE Proc. **98** (2010) 7.

[98] O. Bierwagen, T. Ive,C. G. Van de Walle and J. S. Speck, Appl. Phys. Lett. **93** (2008) 242108-1.

[99] I.-S. Jeong, J.-H. Kim, and S. Im, Appl. Phys. Lett. **83** (2003) 2946.

[100] H. Ohta, H. Mizoguchi, M. Hirano, S. Narushima, T. Kamiya and H. Hosono, Appl. Phys. Lett. **82** (2003) 823.

[101] J.Y. Lee, Y.S. Choi, J.H. Kim, M.O. Park and S. Im, Thin Solid Films **403 –404** (2002) 553.

[102] H.Y. Kim, J. H. Kim,Y. J. Kim, K. H. Chae,C. N. Whang,J. H. Song and S.Im, Optical material **17** (2001) 141.

[103] Kai Wang ,Yuriy Vygranenko and Arokia Nathan,T hin Solid Films **515** (2007) 6981.

[104] H.T. Hsueh, S.J. Chang, F.Y. Hung, W.Y. Weng, C.L. Hsu, T.J. Hsueh,T.Y. Tsai and B.T. Dai Superlattices and Microstructures **49** (2011) 572.

[105] P. S. Cho,K. W. Kim and J. H. Lee,J. Electroceramics **17** (2006) 975.

[106] G. S. Devi,V. B. Subrahmanyam ,S. G. Gudkari and S. K. Gupta, Analytica Chimica Acta **568** (2006) 41.

[107] H. Gong,J. Q. Hu,J. H .Wang,C. H. Ong and F. R. Zhu, Sens.Actuators B,Chem.**115** (2006) 247.

[108] H. T. Wang,B. S.Kang,F. Ren, L. C.Tien,P. W. Sadik,D. P. Norton,S. J. Pearten and J. Lin.Appl.Phys.Lett **86** (2005) 243305-1.

[109] X. H. Wang, Y. F.Ding ,J. Zhang, Z. Q. Zhu. S. Z. You,S. Q. Chen and J. Z .Zhu, Sens.Actuators B, Chem**115** (2006) 421.

[110] S.Christoulakis, M.Suchea, E. Koudoumas,M. katharakis, N. Katsarakis, G. Kiriakidis Appl.Surface.Sci.**252** (2006) 5351.

[111] C. H.Wang, X. F.Chu and M. W. Wu, Sens.Actuators B-Chem.**113** (2006) 320.

[112] T. F. Xue, J. F. Hu, H. W. Qin, Y. Zhou, K. An,L. Zhang, T. Han and Y. X. Li, Rare Metal Mater. Eng. **33** (2004) 1006.

[113] S. M. Al-Hilli, R. T. Al-Mofarji and M. Willander, Appl. Phys. Lett. **89** (2006) 173119-1.

[114] N. Yamazoe, N. Miura, in: S. Yamauchi (Ed.), Chemical Sensor Technology **4** (1992) 27.

[115] N. Matsunaga, G. Sakai, K. Shimanoe and N. Yamazoe, Sens. Actuators B: Chem. **83** (2002) 216.

[116] G. Sakai, N. Matsunaga, K. Shimanoe and N. Yamazoe, Sens. Actuators B:Chem. **80** (2001) 125.

[117] P. Mitra, A.P. Chatterjee and H.S. Maiti, Mater. Lett. **35** (1998) 33.

[118] X.L. Cheng, H. Zhao, L.H. Huo, S. Gao and J.G. Zhao, Sens. Actuators B: Chem. **102** (2004) 248.

[119] J.X. Wang, X.W. Sun, Y. Yang, H. Huang, Y.C. Lee, O.K. Tan, and L. Vayssieres, Nanotechnology **17** (2006) 4995.

[120] C. Baratto, G. Sberveglieri, A. Onischuk, B. Caruso and S. di Stasio, Sens. Actuators B: Chem. **100** (2004) 261.

[121] Q. Wan, Q. H. Li, Y.J. Chen, T. H. Wang, X. L. He,J. P. Li and C. L. Lin, Appl. Phys. Lett. **84** (2004) 3654.

[122] P. Bhattacharyya, P.K. Basu, H. Saha and S. Basu, Sens.Actuators B: Chem. **124** (2007) 62.

[123] P. Song, J.F. Hu, H. W. Qin, L. Zhang and K. An, Mater. Lett. **58** (2004) 2610.

[124] T. J. Hsueh, C. L. Hsu, S. J. Chang and I. C. Chen, Sens. Actuators B: Chem. **126** (2007) 473.

[125] L. J. Bie, X.N. Yan, J. Yin, Y.Q. Duan and Z.H. Yuan, Sens. Actuators B: Chem. **126** (2007) 604.

[126] O. K. Tan, W. Cao, W. Zhu, J.W. Chai and J.S. Pan, Sens. Actuators B: Chem.**93** (2003) 396.

[127] R. L. Hoffman, B. J. Norris, and J. F. Wager, Appl. Phys. Lett. **82** (2003) 733.

[128] P. F. Carcia, R. S. McLean, M. H. Reilly, and G. Nunes, J. Appl. Phys. Lett. **82** (2003) 1117.

[129] J. H.Chung,J. Y. Lee,H. S. Kim,N. W.Jang and J. H. Kim, Thin Solid Films **516** (2008) 5597.

[130] L. Zhang, H. Zhang, Yu Bai, Jun Wei Ma, Jin Cao, Xue Yin Jiang and Zhi Lin Zhang. Solid State Communications **146** (2008) 387.

[131] R. Navamathavan and R. Nirmala and Cheul Ro Lee Vacuum **85** (2011) 904.

[132] Hendrik Faber, Martin Klaummunzer, Michael Voigt, Diana Galli,aBenito F. Vieweg, Wolfgang Peukert, Erdmann Spiecker and Marcus Halik , Nanoscale **3** (2011) 897.

[133]Y. B. Li, Y. Bando and D. Golberg, Appl. Phys. Lett. **84** (2004) 3603.

[134] W. I. Park, D. H. Kim, S.-W. Jung and G.-C. Yi, Appl. Phys. Lett. **80** (2002) 4232.

[135] X. Y. Kong, Y. Ding, R. Yang and Z. L. Wang, Science **303** (2004) 1348.

[136] B. P. Zhang, N. T. Binh, K. Wakatsuki, Y. Segawa, Y. Yamada, N. Usami,M. Kawasaki and H. Koinuma, Appl. Phys. Lett. **84** (2004) 4098.

[137] Tatjana Dedova, Olga Volobujeva, Jelena Klauson , Arvo Mere and Malle Krunks, Nanoscale Res .Lett. **2** (2007) 391.

[138] M. Krunks T.Dedova E.Karber V.Mikli I.Oja Acik , M.Grossberg and A.Mere, Physica B **404** (2009) 4422.

[139] Y. W. Heo , Appl. Phys. Lett. **85** (2004) 2002.

[140] M. Shahjahan ,M. K. R. Khan, M. F. Hossain, S. Biswas and T. Takahashi, J. Vac. Sci. Technol. A **27(4)** (2009) 885.

[141] Yuan-Chung Wang, Ing-Chi Leu,z and Min-Hsiung Hon, Electrochemical and Solid-State Letters **5 (4)** (2002) C53.

[142] Shu-Cheng Chin, Chun-Yung Chi, Yen-Cheng Lu, Lin Hong, Yu-Li Lin, Fang-Yi Jen, C.C. Yang, Bao-Ping Zhang, Yusaburo Segawa, Kung-Jen Ma and Jer-Ren Yang ,J.of Crys. Growth **293** (2006) 344.

[143] Kyu-Seog Hwang and Yun-Ji Lee Seung Hwangbo ,Journal of Ceramic Processing Research.**8** (2007) 305.

[144] Z. W. Liua C. K. Ong T. Yu and Z. X. Shen Appl. Phy. Lett. **88** (2006) 053110.

Chapter 3

Novel method for enhancing the electrical conductivity of ZnO thin film

3.1 Strategies to enhance the conductivity of ZnO thin film

3.1.1 Doping

Doping of ZnO films not only improves their electrical and optical properties, but also makes them highly stable. High quality Gallium doped Zinc Oxide (GZO) films were deposited quartz glass substrate using PLD itself [1]. The film formed at substrate temperature of 300^0C showed electrical resistivity of 8.25×10^{-5} ohm cm, carrier concentration of 1.46×10^{22} cm^{-3} and carrier mobility of 30.96 cm^2/Vs at an oxygen pressure of 0.67Pa. T. Prasada Rao et al.[2] discussed the structural, electrical and optical properties of the transparent conducting GZO prepared using spray pyrolysis; the film had lowest resistivity of 6.8×10^{-3} Ohm cm. Saraswathy et al. [3] deposited ZnO and Indium doped ZnO (IZO) with different indium composition on corning glass substrate. Resistivity decreased initially with doping concentration and subsequently increased. IZO with 1% showed the lowest resistivity 2.41×10^{-2} Ohm cm. Lokhande et al. [4] discussed the structural, optical and electrical studies on highly oriented (along 100 plane) sprayed ZnO film. Resistivity of the film at room temperature was 10^{-1} ohm cm. In one report, it was reported that transparent conducting IZO films were prepared on soda-lime glass substrate having resistivity of 3×10^{-3} ohm cm and transmittance of 80% [5].

A. Suzuki et al. [6] deposited Al doped ZnO (AZO) using PLD, having resistivity of 1.4×10^{-4} ohm cm and average transmittance of 90%. In another report, on AZO films studies on the effect of variation of Al content in the film was reported. Here–lowest resistivity of 8.54×10^{-4} ohm cm and average transmittance of >88% were obtained for the best film [7]. Magnetron Sputtering was used to deposit transparent conducting AZO. The lowest resistivity obtained in this work was 4.6×10^{-4} ohm cm with average transmittance of 90% in the visible range and sheet resistance of 32 ohms for samples deposited at 250^0C and 0.8 Pa [8]. In another report, it was shown that the electrical resistivity of the AZO thin film

decreased after H_2 plasma treatment; the resistivity decreased from 1.23×10^{-3} ohm cm to 8.23×10^{-4} ohm cm and average optical transmittance in the visible region increased slightly from 89.5% to 91.7% [9]. Y. Igasaki and H. Kanma prepared AZO films on amorphous substrate, [heated up to 200 ^{0}C with rf power of 100W] using rf magnetron sputtering from a ZnO target mixed with Al_2O_3 of 2wt% [10]. Resistivity of the film deposited at argon gas pressure of 0.31Pa was ~ 2.5×10^{-4} Ohm cm.

AZO films were also deposited using electron beam evaporation technique [11]. Transmittance measurement showed that the best optical and structural properties were achieved for samples deposited at 200^{0}C. Electrical resistivity was 2.5×10^{-4} ohm cm. AZO films were prepared using RF Plasma evaporation [12] and the influence of the O_2 flow rate and Zn concentration on the properties of the film was investigated. Electrical resistivity decreased with decreasing O_2 flow rate and minimum resistivity of 9×10^{-4} Ohm cm was obtained at O_2 flow rate of 30ml/min, which corresponds to a ratio of 0.069 % of total gas flow rate.L.Dghoughi et al. [13] prepared AZO films again using spray pyrolysis on glass substrate at 450^{0}C using anhydrous Zinc Chloride($ZnCl_2$) and Aluminum Chloride ($AlCl_3$). Film had minimum resistivity of 1.4×10^{-3} ohm cm. C. M. Muiva et al. achieved [14] the lowest resistivity of 2×10^{-2} ohm cm and high transmittance of over 85% at 550 nm .Doping percentage of the films was 2at% of Al.

3.1.2 Post deposition treatment

Influence of substrate temperature and post deposition treatment on the properties of AZO films prepared using PLD technique, was also reported [15]. The experiment result showed that when deposited at 240^{0}C, resistivity of the film was 6.1×10^{-4} ohm cm which was further reduced to 4.7×10^{-4} ohm cm, by post deposition annealing at 673K, for 2 hours in argon atmosphere. M.de la L.Olevera et al discussed the structural, electrical and optical properties of ZnO film using different dopant like Gallium, Aluminium and Indium [16]. The best electrical property was observed in the thickest sample doped with indium. Lowest electrical resistivity was of the order of 10^{-3} ohm cm. Here Major et al. also reported the deposition of low resistive ZnO films doped with indium [17]. Spray pyrolysis technique has been used for the deposition and they could attain a resistivity of 8 to 9×10^{-4} ohm cm.

Another study of the effect of annealing of AZO films revealed that minimum electrical resistivity [$1.7\text{x}10^{-2}$ ohm cm] was obtained for the sample containing 3 at% of Al

and which had undergone annealing at 500^0C in nitrogen with 5% hydrogen [18]. P. Nunes et al. [19] reported the effect of annealing treatment on the performance of IZO samples prepared using spray pyrolysis. The most significant improvement was obtained after annealing in 'forming gas' at 200^0C for 2 hrs .These samples exhibited resistivity of 5.2×10^{-2} ohm cm and high transmittance (T=86%). ZnO were also prepared with the help of Ultrasonic Spray Pyrolysis on indium films [deposited using evaporation] and subsequently subjected to rapid thermal annealing (RTA) in air or vacuum [20]. The resistivity of these samples was 2×10^{-3} ohm cm.

Influence of post deposition annealing on structural and optical properties of RF sputtered [insulating] ZnO films has been investigated by Gupta et al. [21]. The 'as grown' films, deposited on quartz substrates, were highly c-axis oriented. These films became almost stress free after a post deposition annealing at 673K for 1 hr in air. Above 673K, a process of coalescence was taking place which caused major grain growth resulting in '*microcracks*' formation and surface roughness. Grain size increased drastically [from ~18 nm to ~28 nm] with the increase in annealing temperature above 673 K. Studies using SEM showed that 'as- grown' films were columnar in nature. All the film exhibited high transmittance (>75%) in visible region with fundamental absorption edge at about 0.38μm. Aghamalyan et al [22] investigated effect of post deposition annealing in air on the physical properties of ZnO thin films, deposited on sapphire substrates using electron beam evaporation technique. The increase of intensity and decrease of FWHM of the diffraction peak (002)with annealing treatment are related to the improvement of crystal quality of ZnO films after annealing. The unannealed samples have very low resistivity of about 10^{-2} Ω cm. After annealing, electrical resistivity of the films increased from 10^{-2} to 36 Ω cm.

Effect of thermal annealing [in different ambient conditions] on structural and opto-electrical properties of ZnO thin films deposited using sol-gel technique were also studied [23].The samples were annealed in nitrogen, vacuum and open air. The highest carrier concentration was observed for the film annealed at 500^o C for nitrogen and vacuum. The lowest resistivity measured in this study was $2.25\times10^{-1}\Omega$ cm only in the case of vacuum annealed samples. Interestingly samples annealed in nitrogen, vacuum and air, were highly transparent in the visible region. Properties of ZnO films were investigated as the function of annealing temperature in H_2/Ar and vacuum. Resistivity and mobility of ZnO films

decreased with increase of annealing temperature in vacuum and H_2/Ar ambient. Resistivity of the films annealed [at 300 °C] in H_2/Ar and vacuum ambient was ~2186 Ω cm and ~ 798 Ω cm respectively, while annealing in vacuum and H_2/Ar ambient [at 600 °C] resulted in resistivities of ~0.040 Ω cm and ~0.035 Ω cm, respectively. Average optical transmission was >82% and an orientation of the samples was [0 0 2] for all annealed in vacuum and H_2/Ar ambient [24].Various stages have been employed to increase the mobility of TCO film while maintaining high transparency and conductivity as reviewed by Exarhos and Zhous[25].

In yet another paper, the effect of thermal annealing of ZnO thin film in N_2 or O_2 atmosphere and their effects were studied [26]. Electron density increased due to annealing in N_2 atmosphere. But optical properties are improved when annealed in O_2 atmosphere at lower temperature. Crystallinity also improves with the annealing. Mobility of the film increased up to 51 cm^2/V s as annealing temperature increased; but it is low at lower temperatures.

Effects of Al doping and an annealing treatment on electrical and optical properties of ZnO thin films were studied [27]. Here Zinc acetate dihydrate, 2-methoxyethanol were used as the precursor solution and aluminium chloride was used as the dopant material. Electrical conductivity of ZnO films was improved by Al doping and by annealing in a reducing atmosphere. Minimum electrical resistivity was obtained for the doping concentration of 3 at.% Al-doped film, annealed at 500 °C in nitrogen with 5% hydrogen and its value was 1.71×10^{-2} Ω cm. Optical transmission was higher than 80% in the visible range. Musat et al. reported [28] the effect of post-deposition heating temperature and atmosphere on the electrical and optical properties of ZnO: Al thin films, prepared using sol-gel method. For the film doped with 2 wt% Al, the resistivity of 2.9×10^{-3}Ω cm has been achieved after annealing under reducing atmosphere of forming gas. The optical transmission spectra of post – heated and annealed film showed a good transmittance within visible wavelength region.

Post deposition treatment in vacuum or in other ambient conditions can be used to improve the properties of films, which is due to the following reasons. 1)Recrystallization of the amorphous portions of the film.2) Reorientation of existing crystallites 3)Chemisorption

/ desorption of oxygen at the grain boundaries. The conductivity of the film enhanced after the post deposition treatment of the film.

3.2 Experimental details

3.2.1 Chemical Spray Pyrolysis (CSP)

[CSP] technique is based on the pyrolytic decomposition of a metallic compound dissolved in a liquid mixture when it is sprayed onto a preheated substrate. Typical CSP equipment consists of an atomizer, substrate heater, temperature controller and solution container. Additional features of like solution flow rate control, improvement of atomization using electrostatic spray or ultrasonic nebulisation can be incorporated into this basic system to improve the quality of the films. To achieve uniform large area deposition, arrangements for moving either nozzle or substrate or both are used. The schematic diagram of typical spray unit is given below. The atomization of chemical solution into spray of fine droplets is accomplished through spray nozzle with the help of filtered carrier gas.

Due to simplicity of the apparatus and good repeatability of this technique on a large area, it has already become most attractive technique to produce thin films of oxides and sulfides of metals, binary / ternary / quaternary compound semiconductors and superconducting compounds. In addition to its simplicity CSP has a number of advantages; for example it offers an enormously easy way to dope films with any element in any proportion [by just diluting the solution we can go even to concentration which cannot be weighed] which help us to change structural, optical and electrical properties.

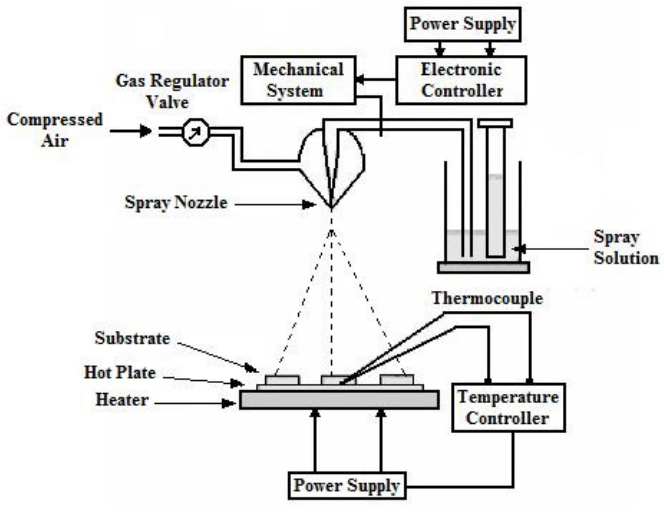

Fig 3.1.Schematic Diagram of chemical spray pyrolysis unit

ZnO thin films can be deposited on soda-lime glass substrates using CSP technique. Spray solution is prepared by dissolving Zn $(CH_3COO)_2.2\ H_2O$ in the solvent usually deionized water (1:1 volume ratio). This salt of Zn is used due to its high vapour pressure at low temperature. Molarity of this solution can be as low as 0.3M. A few drops of acetic acid are to be added to the aqueous solution to prevent the formation of hydroxides. Substrate temperature is usually around 450 to 500 ^{0} C and movement of the spray head is required for uniformity of film. [29]. Air can be directly compressed from the atmosphere; filters are used to remove water vapour and oil particles in order to avoid contamination. Pressure of the gas fed in to the nozzle has to be measured using the mechanical gauge and the pressure can be varied in the range 0-100 psi. The carrier gas pressure and nozzle to substrate distance are held constant. Through this arrangement it is possible to have consistency in the results as well as large area deposition.

The formation of ZnO thin film given by the following equations [30]

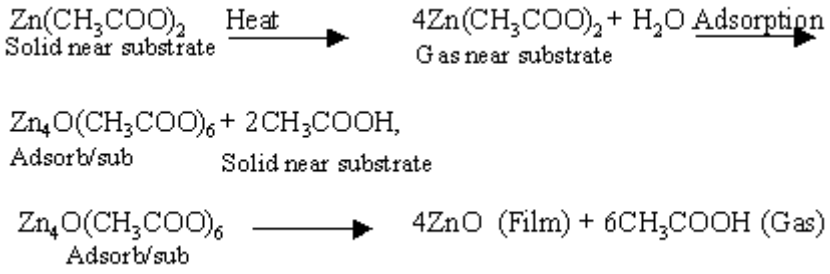

3.2.2 An innovative and original post deposition treatment (Zero- Energy Process) for obtaining low resistive films from CSP technique

Usually in CSP technique, the thin film samples after deposition are left for cooling. It takes about an hour for the samples to come down to room temperature and during this time sample is in open atmosphere with the film surface facing the air. In the case of ZnO films the deposition temperature is of the order of ~500^0 C and there is every chance that oxygen from air will be getting into the films at this high temperature. Unfortunately diffusion of oxygen into the ZnO film will be very much detrimental as far as its electrical properties are concerned. This is because, in order to have highly conducting ZnO films, there should be excess of zinc atoms or oxygen vacancies in the sample and diffusion of oxygen into the film during cooling will naturally damage this condition. For rectifying this we should anneal the ZnO samples in high vacuum for long time-say one hour. But this process is again energy consuming and is not preferred by industries where they require a process which can be easily adapted for the 'production line'. Hence it was felt that during the cooling time, a different process should be incorporated so that the film surface should not come into contact with air.

After the deposition of the ZnO films using CSP technique, the film is kept in the open atmosphere for cooling. It was felt that the cooling of the samples in open atmosphere just after deposition may enhance incorporation of oxygen in the film. Quenching the sample after spraying can reduce the oxygen adsorption. If we avoid air contact while cooling, it can decrease the oxygen adsorption. After the deposition, the samples were quickly removed from the hot plate using a mechanical holder and placed on a plane surface, which is kept at room temperature. In this process the sample was cooled with zinc oxide film surface kept open to the atmosphere. Another set of the samples were prepared and cooled with the film surface in direct contact with the surface of the "base material".

The former set of samples were named as 'zinc oxide-regular cooling (Z-R)' and the latter as 'zinc oxide-inversion cooling (Z-I)' respectively.

No	Base material	Results
1	Metal Sheet	Glass breaks
2	Cardbord	Carbon adsorbed to the surface
3	Thick Chart paper	Air expansion make the base Zig -Zag
4	New wood Material	Uniform Thickness of the film

Table.3.1. Different base materials used for post deposition cooling of ZnO thin film.

We used different base materials for the standardisation of the method and also for the obtaining of good film. Table.3.1 gives the results from the different base materials used for the post deposition cooling. After all these trials, "New wood" was found to be the best base material for the 'inverting the process'. This made the cooling process carried out keeping ZnO film surface in isolation from air atmosphere through a non-vacuum process. This process is relatively "environmental friendly" and is quite useful for large area samples. More over this can be easily incorporated into the production line in any large scale unit. Thus it is a 'zero-energy process' and requires no additional cost.

3.3 Results and discussion

3.3.1 Structural Studies

XRD technique was used here to study the structural changes of the samples taking place after the 'zero-energy process'. XRD is an extremely important technique in the field of material characterization especially to distinguish between crystalline and non crystalline (amorphous) materials. It can be also used to determine the phase content in many minerals and materials. It requires no elaborate sample preparation and is essentially non-destructive. Generally, it gives whole range of information about the crystal structure, orientation, crystallite size, composition (with the help of standards), defects and stresses in thin films. Experimentally obtained diffraction pattern of the sample is compared with 'Joint Council Powder Diffraction (JCPDS)' data for Standards. This gives information of different crystallographic phases, the relative abundance and preferred orientations. From the width of the diffraction peak, average grain size in the film can also be estimated.

Inter-planar spacing *d* was calculated from the X-ray diffraction profiles using the formula,

$$2d \sin\theta = n\lambda \text{ ……..……..(3.1)}$$

where θ is the Bragg angle, *n* is the order of the spectrum and λ is the wavelength of X-rays. Using the *d*-values the set of lattice planes (*h k l*) were identified from the standard data and the lattice parameters were calculated using the following relations.

For the tetragonal systems,

$$\frac{1}{d^2} = \frac{(h^2 + k^2)}{a^2} + \frac{l^2}{c^2} \text{ ……... (3.2)}$$

and for hexagonal systems,

$$\frac{1}{d^2} = \frac{4(h^2 + hk + k^2)}{3a^2} + \frac{l^2}{c^2} \text{ ……... (3.3)}$$

where *a* and *c* are lattice parameters. The grain size (*D*) can be evaluated using Scherrer's formula,

$$D = \frac{k\lambda}{\beta \cos\theta} \text{ ……. (3.4)}$$

where *k* is a constant which is nearly equal to one and β is the "Full Width at Half Maximum (FWHM)", usually measured in radians.

In the present study, XRD analysis was done using Rigaku (D.Max.C) X-Ray Diffractometer, with Cu K_α (λ = 1.5405 Å) radiation and a Ni filter operated at 30 kV and 20 mA. X-ray diffraction pattern of the sample Z-R and Z-I are depicted in the Fig.3.2.Both the films are polycrystalline having hexagonal wurtzite structure (a=3.250, c=5.206Å), with peaks appearing at $2\theta=31.62^0$, 34.42^0, 36.25^0 corresponding to (100), (002) and (101), orientations respectively [JCPDS data card (36-1451)]. When the (002) plane is dominant in the XRD pattern, axis is mainly found to be perpendicular to the surface of the film. The 2-dimensional zinc atom population is highest in the (002) plane of the wurtzite structure [31].

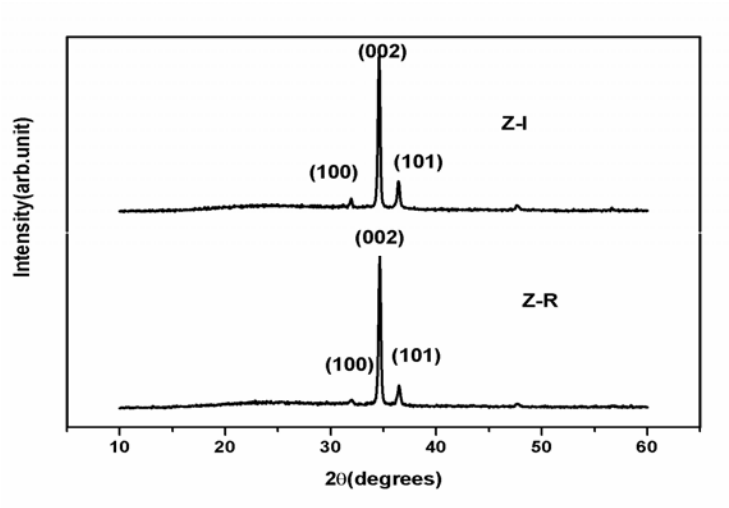

.

Fig.3.2 XRD patterns of Z-R and Z-I samples.

3.3.2 X-ray Photoelectron Spectroscopy (XPS)

'X-ray photoelectron spectroscopy (XPS)' which is also called 'Electron Spectroscopy for Chemical Analysis (ESCA)' is the technique that uses x-rays to knock electrons out of shells / orbitals. The kinetic energy (E_K) of these photoelectrons is determined from the experiment; as the energy of the x-ray radiation ($h\nu$) is already known, the electron binding energy (E_b) can be calculated as,

$$E_K = h\nu - E_b \text{ …….. ....} \quad (3.5)$$

The electron binding energies are dependent on the chemical environment of the atom. XPS is therefore useful to identify the oxidation and / or compound state of an atom. Binding energy of the valance electrons is affected by the chemical environment of the atom. When atomic environment of an atom changes, it alters the local charges surrounding the atom. This charge, in turn, reflects itself as a variation in the binding energy of the valence electrons of the atom. Thus binding energies of valence electrons experience a characteristic shift and this can give important information regarding the valence states/compound formation of the atoms in the sample and one can use this technique to find out whether an element present in a sample is in pure or in compound form. XPS technique is generally a surface analysis technique. However, with facility for physically etching using

sputtering technique, 'depth profile' is also achieved. In XPS spectra, 'intensity' [or 'count'] of the emitted photoelectron signal is plotted as a spectrum of binding energies.

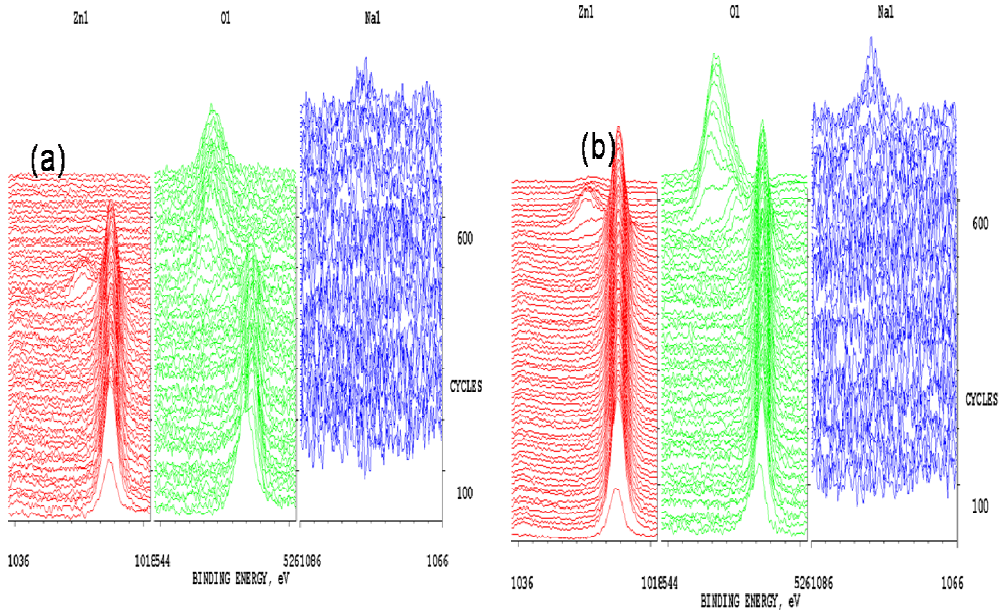

Fig.3.3 XPS of the sample (a) Z-I (b) Z-R

Depth profiling of samples Z-I and Z-R were carried out in the XPS analysis and the results are depicted in Fig. 3.3(a) & 3.3(b) respectively.XPS spectra of the sample were recorded using an ULVAC-PHI unit (model: ESCA 5600 CIM) employing argon ion sputtering (Voltage=3kV, Raster size=3×3 mm^2, pressure 10^{-8}m bar). Al Kα X-ray (1486.6eV) with a beam diameter of 0.8mm and power of 400 W was used as the incident beam. Bottom portion of the figures [near the X-axis] gives the results from surface of the films and the top portion gives results from the substrate-film interface. From the depth profile analysis, one gets details on the variation of atomic percentage as well as atomic states of Zn and O along the thickness of the sample.

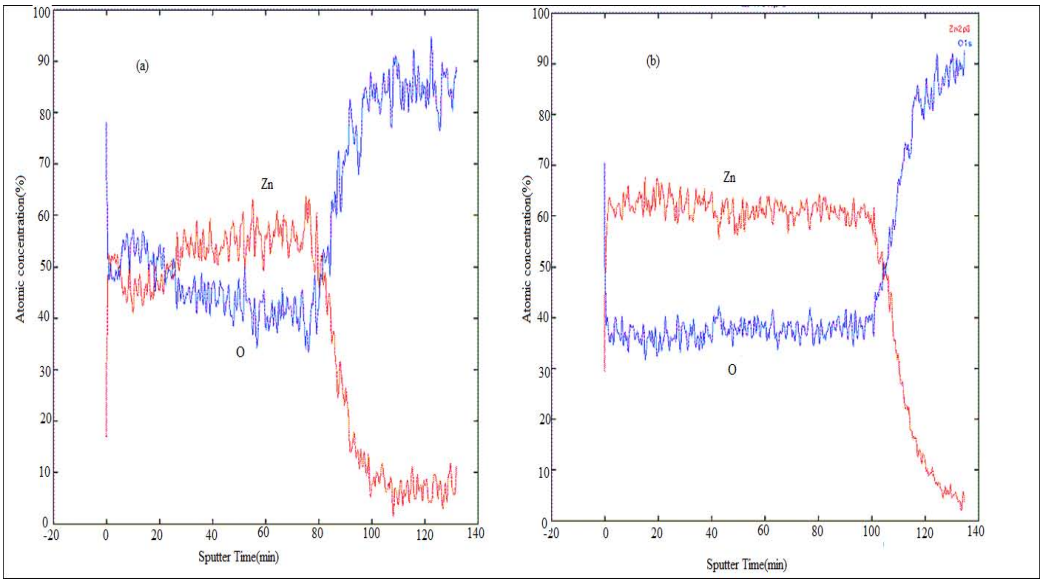

Fig.3.4 Atomic concentrations in ZnO (a) Z-R (b) Z-I (Where the blue line indicate the oxygen concentration and red line indicate the Zinc concentration).

A very clear and interesting observation is that when the samples were cooled in the 'inversion process' concentration of oxygen incorporated into the sample decreased considerably and this occurs along the whole thickness of the sample. Similar results have been observed in vacuum annealed ZnO samples [32]. This proves beyond doubt that the new process of cooling the sprayed samples is just equivalent to vacuum annealing.

Binding energy values are clearly indicating the formation of zinc oxide (1022.95 eV for Zn3p3/2 and 531.02 eV for O1s) only even on the surface which is in contact with the 'base material'. Atomic concentrations of zinc and oxygen were determined for the Z-R and Z-I films (Fig 3.4 (a) & 3.4 (b)). In the case of Z-R, atomic concentrations of Zn and O are not having uniform distribution throughout the thickness of the sample. At the surface of the film, the atomic concentration of zinc is lower as compared to that of oxygen and probably due to this layer, the resistivity of this sample is found to be high. Interestingly towards the interior of the sample [i.e., after sputtering out the sample for 20 min], atomic concentration of zinc [~ 55%] was higher than that of oxygen [~45%]. This is because in this cooling process, incorporation of oxygen from the atmosphere is rather easy in the surface layers of the film and this diffusion goes up to one-fourth of the sample thickness

[i.e. up about 120 nm]. Near the surface of the Z-R sample, [i.e. after sputtering out for ~10 min] the Zn/O ratio was 0.72 while in the depth of the sample [i.e. for sputtering time > 20 min], the Zn/O ratio was 1.71. Thus the Zn/O ratio varied from 0.72 to 1.71 from the surface to the depth of the sample which is not desirable for good electrical properties. But in the case of films which have undergone inversion cooling (Z-I), atomic concentration of zinc was found to be 62% and that of oxygen 35% (Zn/O ratio - 1.77) throughout the whole thickness of the samples. The large decrease in the resistivity of the Z-I samples might be due to the reduction of oxygen concentration in the film [33].

The XPS depth profile study also proved that there is no diffusion of sodium in to the samples from the soda glass substrates even though the ZnO films were deposited at high temperature (Fig 3.3(a) and 3.3 (b)).

3.3.3 Scanning Electron Microscopy (SEM)

SEM is one of the most useful and versatile instruments for the investigation of surface topography, microstructure features, etc. The principle involved in imaging is to make use of the scattered secondary electrons when a finely focused electron beam impinges on the surface of the specimen. The electrons are produced by a thermal emission source, such as heated tungsten filament, or by using field emission cathode. To create SEM image, the incident electron beam is scanned in a raster pattern across the sample surface. Secondary electrons are produced due to the interaction of the primary electron beam. The emitted electrons are detected at each position in the scanned area by an electron detector. Intensity of the emitted electron signal is displayed as brightness on a cathode ray tube. There are two modes of imaging- one is by using Secondary Electrons and the other is by using Backscattering Electrons. Secondary electron imaging provides high resolution imaging of fine surface morphology and for this the samples must be electrically conductive. From the scanning electron microscopic analysis it was found that the crystallite size of the sample increased after the inversion process (Fig.3.5).

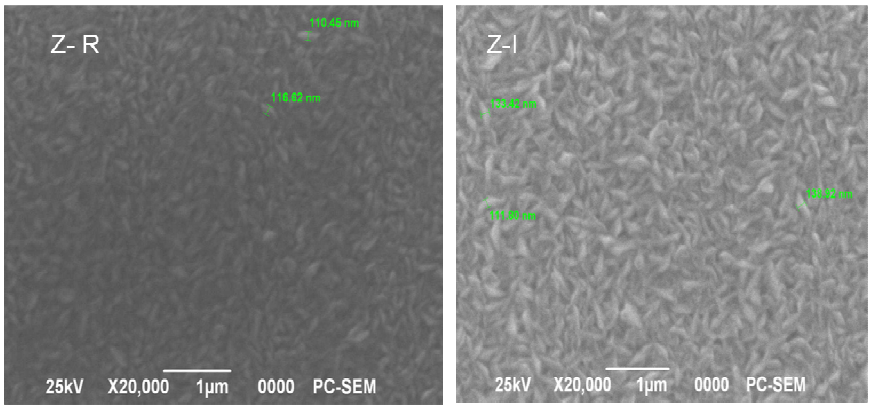

Fig.3.5 SEM micrograph of Z-R and Z-I samples

3.3.4 Stylus profilometer

Thickness of the films measured using stylus profilometer (Dektak 6 M). This instrument takes measurements electro-mechanically, by moving the sample beneath a diamond tipped stylus. The stylus is mechanically coupled to the core of an LVDT (Linear Variable Differential Transformer). The high precision stage moves the sample beneath the stylus according to the user programmed scan length, speed and stylus force. As the stage moves with the sample, the stylus rides over the sample surface. Surface variation causes the stylus to be translated vertically. Electrical signal corresponding to the stylus movement are produced as the core position of the LDVT changes. The LDVT scales an AC reference signal proportional to the position change, which in turn, is conditioned and converted to digital format through a high precision, integrating, analogue to digital converter.

Fig.3.6 given below shows the thickness data plot of Z-I samples deposited over an area, 30cm^2. Thickness was measured from thirty points using thickness profiler and surface mapping was done. It is observed that the thickness variations are prominent only at the edges and the variation is just 10%. Major portion (80% of the sample area) of the film has thickness within the range of 535 nm.

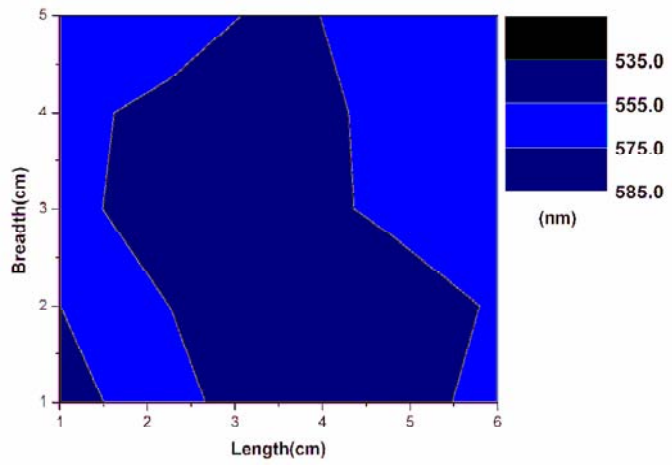

Fig. 3.6 Two dimensional surface mapping of Z-I sample thickness (nano meter scale) over an area of 6 cm ×5 cm.

3.3.5 UV- Vis- NIR Spectroscopy

The most direct and probably the simplest method for determining the band structure of semiconductors is by measuring the optical absorption spectrum. Absorption is expressed in terms of a coefficient (αhυ), which is related to the energy gap E_g according to the equation,

$$\alpha h\nu = A\left(h\nu - E_g\right)^n \quad \ldots\ldots\ldots\ldots\ldots\ldots\ldots\ldots \quad (3.6)$$

where A is a constant, h is the Plank's constant, υ the frequency of the incident beam and n is equal to ½ for a direct gap and 2 for an indirect gap.

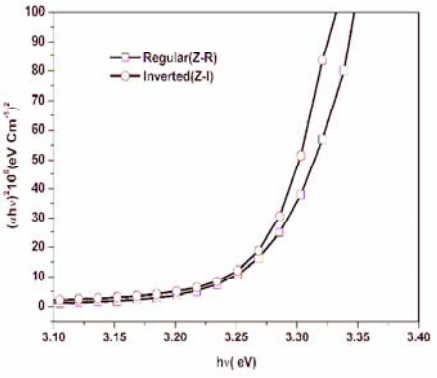

Fig.3.7 $(\alpha h\upsilon)^2$ vs. hυ plot of Z-R and Z-I samples

Absorption and transmission spectra of all the samples were recorded using UV-Vis -NIR spectrophotometer (JASCO -V-570 model). Optical band gap was determined using the $(\alpha h\upsilon)^2$ versus hυ plot by extrapolating the linear portion of the curve to hυ axis. Practically there is no variation of the band gap after the 'inversion process (Fig.3.7).

Optical transmission spectra were recorded for both samples in the wavelength range 200 – 1200 nm (Fig.3.8). Interestingly the percentage of transmission increased in the visible range, after the inversion process. Interference fringe like pattern of transmittance curve established the smooth reflecting nature of the film.

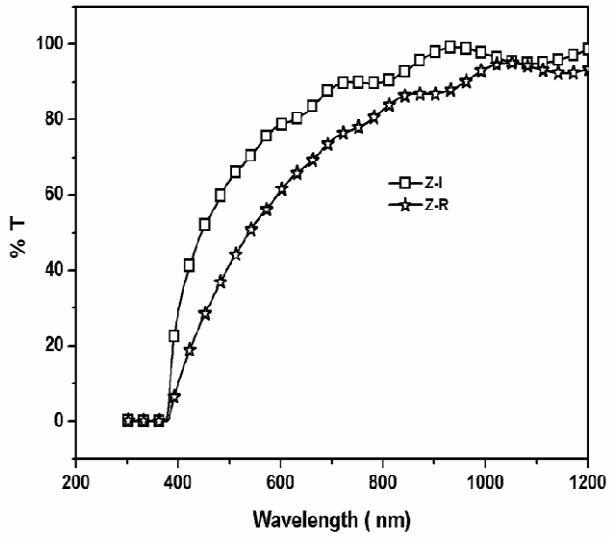

Fig.3.8 Transmission curves for Z-R and Z-I samples

3.3.6 Photoluminescence (PL)

PL measurement is a standard technique to observe defects and impurities in semiconductors. Study of luminescence processes can, not only show the content as well as the behaviour of the defects and impurities in semiconductors, but also can give information on different paths for the radiative recombination. The PL spectrum and its dependence on the irradiation intensity and device temperature can deliver important information for the device characterisation.

PL spectra can be used to determine the band gap energy as well as the energy levels of different defect levels in the band gap region. Hence it can be used for determining the impurity levels and / or activation energy of impurity levels and to study the radiative recombination taking place in semiconductors. Photoluminescence in solids can be classified according to the nature of the electronic transitions producing it. We can have mainly intrinsic and extrinsic emissions. Intrinsic luminescence is further divided into band to band luminescence, exciton luminescence and cross luminescence. In 'band-to-band luminescence', the emission occurs when an electron in the conduction band recombines with a hole in the valence band. This emission can be observed in very pure crystal at higher temperatures while at lower temperature this gets transformed in to 'exciton luminescence'. If there are some impurities having their levels in the forbidden gap, electrons or holes are trapped by them and these recombine with each other via such levels, either radiatively or nonradiatively. 'Cross luminescence' is usually observed in alkaline and alkaline earth halides. Luminescence caused by intentionally incorporated impurities (in most cases metallic impurities) is classified as "extrinsic luminescence". In semiconductors, most important impurities are donors and acceptors that control semiconductor property and these can also act as luminescence activators.

In the present work, the PL studies were performed using 325 nm line of Kimmon He-Cd laser [output power of 20mW] as the excitation wavelength and the emissions were analyzed with the help of Ocean Optics [USB 2000] spectrophotometer.

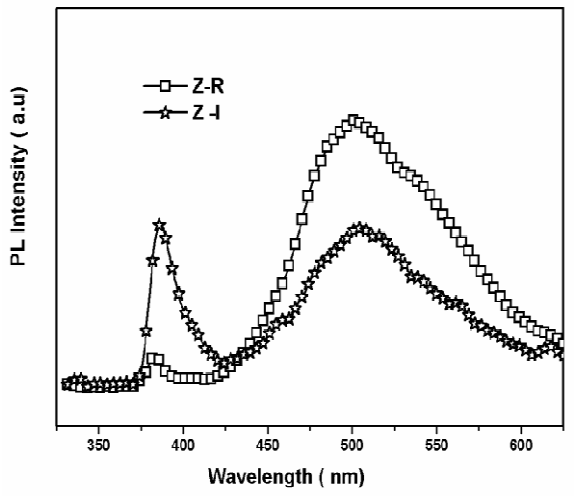

Fig.3.9 Room temperature PL spectra of Z-I and Z-R samples.

Photoluminescence properties depend on the growth conditions including temperature and ambient. In our case the growth temperature was kept constant. The only important parameter here is the ambient condition. In CSP technique, there is strong possibility of samples becoming O-rich as oxygen can easily get incorporated in the sample from the atmosphere. The PL spectra of ZnO have both UV and blue-green emission (Fig.3.8). The green emission is located at ~2.38 eV. In the case of ZnO, majority donors are 'oxygen vacancy' [V_o] and zinc interstitial (Z_{ni}). When the sample is kept in the open atmosphere, the oxygen concentration related to Zn-O bonding increases, reducing concentration of oxygen vacancies. Hence it is rather easy to have higher concentration of Oxygen antisite (O_{zn}) because the Oxygen antisite has relatively low formation energy [34]. In CSP method, air is used as the carrier gas and hence the concentration of oxygen antisite in ZnO prepared using this technique is higher in comparison with samples prepared using other techniques. This results in an intense PL emission due to the transition from the conduction band to antisite oxide (O_{zn}) [35] and this is the blue-green emission, centred around 503 nm. Interestingly the intensity of this emission is very low in the samples which have undergone the "Inversion" process while the 'near band edge' emission [in the UV region] is higher in these samples. It had been reported that the blue-green emission is due to the transition from conduction band to the acceptor level corresponding to the oxygen antisite[O_{Zn}] [36]. Hence it becomes evident that the newly introduced 'cooling under inversion process', reduces the density of the levels due to the antisite of oxygen is considerably.

3.3.7 Electrical properties

The resistivity of some of the ZnO films was determined using the 'two probe' method with the electrodes in planar geometry. Electrical measurements were done after giving electrical contacts using silver paint in the form of two end contacts, having a distance of 1cm between them. In this study, the sheet resistance was calculated by the following equation,

If *l* and *b* are the length and breadth of a rectangular film between the two electrodes and *t* is its thickness then sheet resistance is given by the equation,

$$R_s = \rho l / bt$$

Where ρ is the resistivity in Ohm cm.

If we measure l=b

$$\rho = R\ bt/l$$

$$\rho/t = Rs$$

Rs- Sheet resistance, which is expressed in Ohm per square is given by the above equation

Then resistivity can be calculated as,

$$\rho = R_s d \qquad (3.7)$$

Electrical resistivity values of these two samples are given in the Table. 3.2. The conductivity enhanced by 3 orders of magnitude after the "Inversion- cooling" and the significant enhancement in the electrical conductivity might be due to the increase in the Zn/O ratio after the 'cooling through inversion' process.

Sample Name	Resistivity (Ω cm)
Z-R	80
Z-I	0.02

Table.3.2 Resistivity variation of Z-R and Z-I

3.4 Effect of vacuum annealing

In the present study, both Z-R and Z-I films were annealed at 450^0C for 2h in vacuum (2×10^{-5} m bar) and samples named as Z-R-A and Z-I-A respectively.

3.4.1 Result and discussion

X-ray diffraction patterns of the Z-R-A and Z-I-A are shown in the Fig 3.10. Both the films are polycrystalline having hexagonal wurtzite structure (a=3.250, c=5.206Å), with peaks appearing at $2\theta = 34.42^0$ corresponding to (002) orientation [JCPDS data card (36-1451)]. Among the two types of samples, Z-R-A film was higher intensity peak of (002) plane than Z-I-A.

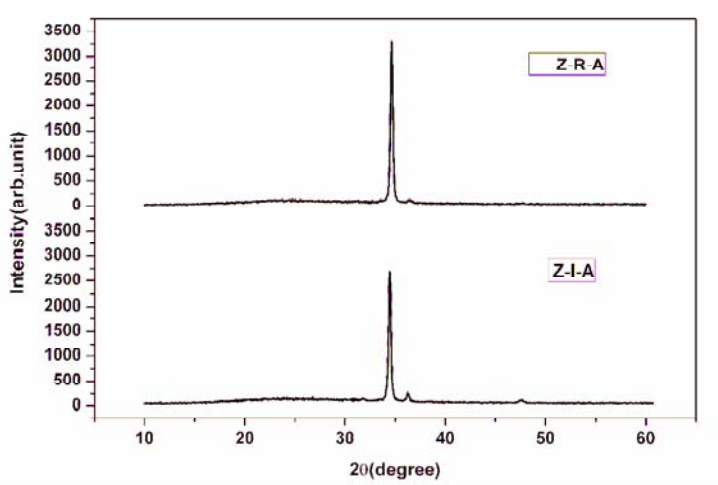

Fig.3.10 XRD patterns of Z-I-A and Z-R-A.

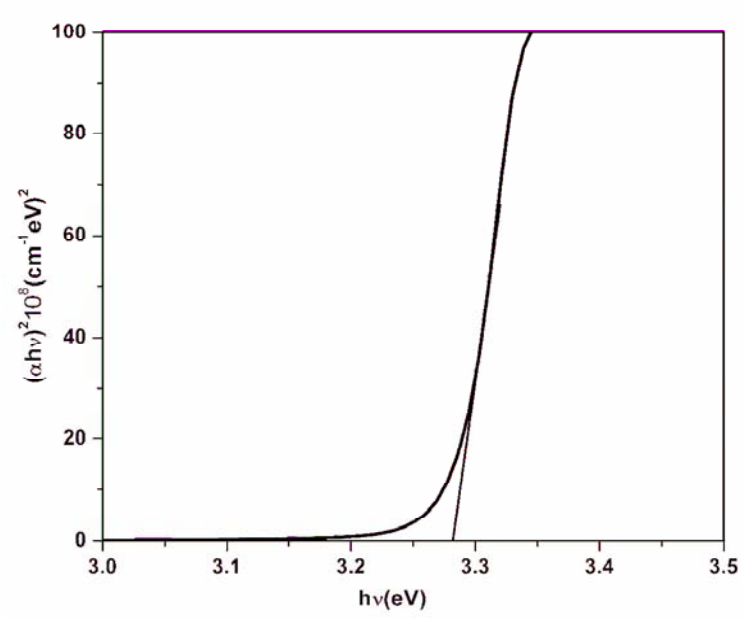

Fig.3.11 $(\alpha h\upsilon)^2$ vs. hυ plot of Z-R-A

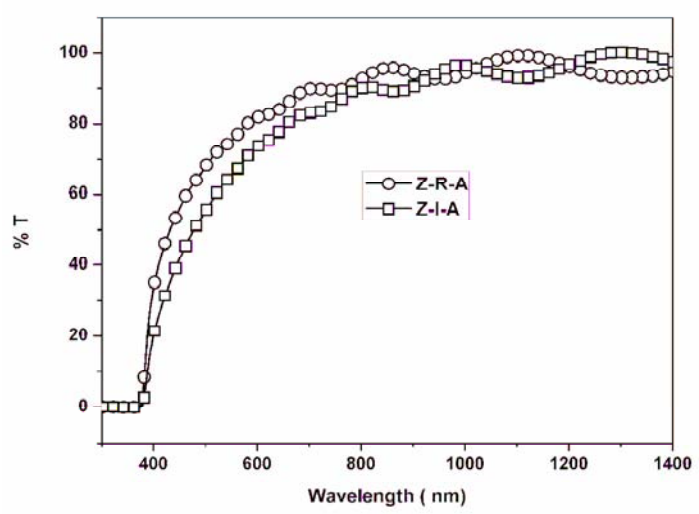

Fig.3.12 Transmission curves of Z-I-A and Z-R-A.

Optical band gap was determined [using the $(\alpha h\upsilon)^2$ versus hυ plot] for the Z-R-A and Z-I-A samples. There is not much variation in the band gap after the vacuum annealing (Fig.3.11). Transmission of both the sets of samples increased after the vacuum annealing. Fig 3.12 shows transmission curve of Z-I-A and Z-R-A. Resistivity of Z-R-A decreased from 80Ω cm to 1.8×10^{-2} Ω cm. But for Z-I-A sample, there is only insignificant decrease of resistivity [from 2×10^{-2} Ω cm to 1.5×10^{-2} Ω cm]. In the case of Z-R samples, after the deposition the film was kept open to the oxygen rich condition. Hence films have absorbed more oxygen atoms during the cooling process. When these samples were annealed in vacuum, desorption of oxygen occurs leading to the annihilation of oxygen acceptor states at the grain boundaries. So there is a drastic decrease of resistivity of the film [37]. Now in the case of Z-I, these are quickly removed from the hot plate and the process of 'Inversion cooling 'is carried out. This process actually isolates the sample from atmospheric oxygen leading to lesser chance of oxygen being incorporated in the film. Further annealing this sample in vacuum condition, only causes the release of remaining few adsorbed oxygen within the film thereby causing a small decrease in resistivity. From the

present electrical study it is clear that the inversion process is one of the best alternatives of vacuum annealing and is very suitable for large area deposition of the samples.

3.5 Conclusions

The newly introduced process of 'cooling under inversion' for ZnO films deposited using CSP technique is capable of reducing resistivity of the ZnO samples by three orders [i.e., from 10^{1} to 10^{-2} Ohm.cm] and is a "zero-energy process" as it does not require any external energy supply. Hence it becomes much useful in industrial applications. The process could also enhance the crystallinity and the optical transmittance. X-ray photo-electron spectroscopy analysis showed that Zn/O ratio increased after inversion and is uniform throughout the thickness of the samples. Room temperature photoluminescence revealed that the intensity of the blue-green emission decreased considerably, indicating the reduction of Oxygen antisite defects. Vacuum annealing does not bring any change in electrical properties of Z-I samples .Thus the process resulted in samples of high electrical conductivity and optical transmission avoiding the post deposition [and energy consuming] processes like vacuum annealing.

References

[1] Sang-Moo- Park,Tomoaki Ikegami and Kenji Ebihara ,Thin Solid Films **513** (2006) 90.

[2] T. Prasada Rao, and M.C. Santhosh Kumar ,Journal of Alloys and Compound**506** (2010) 788.

[3] Saraswathi Chirakkara, K. K. Nanda and S. B. Kripanidhi, Thin Solid Film **519** (2011) 3647.

[4] B. J. Lokhande and M.D Uplane , Appl.Surf.Sci.**167** (2000) 243.

[5] M. A. Lucio- Lopez,M. A Luna – Arias, A .Maldanado,M. de la L. Olevara and D. R. Acosta, Sol. Energy.Mater. Sol. Cells **90** (2006) 733.

[6] A. Suzuki,T. Matsushita,N. Wada,Y. Sakamoto and M. Okunda,Jpn.J.Apl.Phys. **35** (1996) L56.

[7] H. Agura,A. Suzuki,T. Matsushita,T. Aoki and M. Okuda ,Thin solid Films **445** (2003) 263.

[8] En-Gang Fu,Da-Ming Zhuang,Gong Zhang, Zhao ming, Wei-Fang Yang and Jia-Juan

Liu,Microelectronic Journals **35** (2004) 383.

[9] Fang-Hsing Wang, Hung- Peng Chang,Chin-Chung Tseng,Chia-Cheng Huang and Han-Wen Liu, Current Applied Physics **11** (2011) S12.

[10]Y. Igasaki and H. Kanma , Appl.Surf.Sci.**169-170** (2001) 508.

[11] D. R. Sahu, Shin-Yuan Lin and Jow-Lay Huang, Micro electronic Jouranls **38**(2007)245.

[12] Jiro Tsujino, Norio Homma, Tomoaki Sugawara, Isao Shimono and Yoshihiko Abe, Thin Solid Films **407** (2002) 86.

[13] L. Dghoughi, F.Ouachtari,M.Addou,B.Elidrissi,H.Erguig, A.Rmili and A.Bouaoud, Physica.B.Condensed Matter **405** (2010) 2277.

[14] C.M.Muvia,T.S Sathiaraj and K.Maabong, Ceramic International **37** (2011) 555.

[15] X-Chen,W.Guan,G.Fang and X.Z.Zhao,Appl.Surf.Sci.**252** (2005) 1561.

[16] M.de la L.Olevera,H.Gomez and A.Maldonado ,Sol. Energy Material And Solar Cells **91** (2007)1 449.

[17] S. Major, A. Banerji and K.L. Chopra, Thin Solid Films **108** (1983) 333.

[18] Jin- Hong Lee and B Yung- OK Park, Material Science And Engineering B **106** (2004) 242.

[19] P.Nunes,E.Fortunato and R.Martin, International Journal of Inorganic Materials **3** (2001) 1125.

[20] Tae Young Ma and Dae Keun Shim,Thin Solid Films **410** (2002) 8.

[21] Vinay Gupta and Abhi Mansigh, J. Appl.Phys.**80** (1996) 1063.

[22] N.R. Aghamalyan, I A Gambaryan, E.Kh Goulanian, R K Hovsepyan, R B Kostanyan, S I Petrosyan, E S Vardanyan and A F Zerrouk,Semicond.Sci.Technol.**18** (2005) 525.

[23] R. Ghosh, G. K. Paul and D. Basak ,Material Research Bulletin **40** (2005)1905.

[24] J.Kim**,** Myung-chun Kim**,** Jaekeun Yu and Kyeongsoon Park**,** Cur. Appl. Phy. **10** (2010) S495.

[25] G. J. Exarhos, X.-D. Zhou, Thin Solid Films **515** (2007) 7025.

[26] K. Ogata, K. Sakurai, Sz. Fujita, Sg. Fujita and K. Matsushige, Journal of Crystal Growth **214-215** (2000) 312.

[27] Jin-Hong Lee and Byung-Ok Park ,Mat. Sci.and Engineering B **106** (2004) 242.

[28] V. Musat, B.Teixeira, E.Fortunato and R.C.C.Monteiro, Thin Solid Films **502** (2006)

219.

[29] Tina Sebastian, R.Jayakrishnan ,C.SudhaKartha and K P Vijayakumar ,Open Surf. Scie.J.**1** (2009)1-6.

[30] D. F. Paraguay, L.W. Estrada, D. R. Acosta, M. E. Andrade and Miki Yoshida, Thin Solid Films **350** (1999) 192.

[31] S. Amirhaghi, V.Craciun, D. Cracium, J .Elders and I. W. Boyd, Microelectron.Eng. **25** (1994)32.

[32] P. M.Ratheesh Kumar,C. Sudha Kartha, K. P. Vijayakumar, F. Singh,D. K. Avasthi,T. Abe, Y.Kashiwaba,G. S. Okram, M. Kumar and Sarvesh Kumar,J.Appl. Phy **97** (2005) 013509,1-6.

[33] P.M. Ratheesh Kumar, K.P. Vijayakumar and C. Sudha Kartha, J. Mater. Sci. **42**(2007) 2598.

[34] E. C. Lee, Y. S. Kim, Y. G. Jin and K. J. Chang, Physica B **308-310** (2001)912.

[35] E. C. Lee, Y. S. Kim, Y. G. Jin and K. J. Chang, Phys. Rev. B **64** (2001) R85120.

[36] T. B. Hur, G. S.Jeen, Hwang Y-H and H. K. Kim ,J. Appl. Phys. **94** (2003)5787.

[37] P. Nunes,A. Malik, B. Fernandes,E. Fortunato,P. Vilarinho and R .Martins, Vacuum **52** (1999) 45.

Chapter 4
Optimization of deposition parameters on Spray Pyrolysed ZnO thin film

4.1 Introduction

Thin film deposition, using the spray pyrolysis technique, involves spraying a solution / mixture of solutions onto a heated substrate. The solution / mixture of solutions contain compounds of the elements, whose film is required. The droplets, after hitting on the substrate surface, spread into a disk shaped structure and undergo thermal decomposition. The shape and size of the disk depends on the momentum and volume of the droplet. Consequently, the film [which is usually binary / ternary compounds like sulfide, selenide or oxide] will be initially composed of overlapping disks which will finally become grains with specific orientation on the heated substrate. The precursor solution plays an important role in the film formation; for example, nature of the solvent, type of salt [nitrate, halide or acetate etc], concentration of the salt and molar ratio of the required elements in the solution are all influencing the film formation as well as its properties very much. Again the substrate temperature is another important factor affecting crystallinity and grain size / orientation. Therefore the structure and properties of deposited film can be tailored by changing composition of precursor solution and substrate temperature; in the present work the effect of variation of these parameters on properties of ZnO films is studied.

Geometry of the gas and liquid nozzles strongly affect the spray pattern, size distribution of droplets, angle at which droplets meet substrate surface and spray rate, which in turn, determine the growth kinetics and hence the quality of the films. Other factors like surface nature and temperature of the substrate, solution composition, gas and solution flow rates, deposition time and nozzle-to-substrate distance also affect film properties. In general, the films grown at substrate temperature less than 300^0C are amorphous in nature, while at higher temperatures, polycrystalline films are formed. In order to obtain films with good conductivity, it is essential that complex oxidation of the metal be avoided. This is usually achieved by adding an appropriate reducing agent such as propanol, ethyl alcohol or

pyrogallol. Effects of some important spray parameters [as reported in earlier papers] are discussed below.

4.2 Effect of deposition parameters of spray pyrolysed ZnO thin film:

A Review

Aranovich et al. [1] prepared ZnO thin film were produced spray pyrolysis starting with1) aqueous solution of 0.1M $ZnCl_2$, 2) next precursor with similar solution but with a controlled proportion of hydrogen peroxide added and 3) 0.1M Zinc acetate. The rates of flow of solution and air were varied between 1.8 and 3.5cm^3min^{-1} and 8.6-10.6 min^{-1} respectively. It was observed that the substrate temperature and air flow rate significantly affected the crystalline nature and chlorine content of the films. S.A. Studenikin et al. reported the effects of substrate temperature on the structural, electrical and optical properties of ZnO films, prepared using spray pyrolysis technique [2]. It was observed that below the critical temperature, [T_c = 180 ºC], thermal decomposition of ZnO did not occur or was incomplete. The electrical resistivity decreased by one order of magnitude after the illumination of the sample (10^{-3} ohm cm in dark and 10^{-4} ohm cm after illumination). Band gap was nearly same (3.3 eV) for all samples prepared at different substrate temperatures.

Influence of substrate temperature on the properties of Indium doped ZnO thin films was also a subject of study and it has been found that resistivity and optical transmittance of the films very much depend on the temperature [3]. Substrate temperature was varied from 573 K to 773 K and spray rate was maintained at 6 ml/min. However films were found to be resistive (3.5×10^{-1} Ohm cm). Effect of variation of concentration of precursors on the properties of ZnO films was investigated. On increasing the concentration structural properties like growth rate and crystalline quality of the film increased. The texture coefficient of (002) plane also increased with increasing the molarity of the solution [4].

From studies on effect of substrate temperature on the structural and optical properties of ZnO films [5], it was observed that there was a corresponding increase in grain growth and crystallinity of ZnO thin films deposited on glass substrates with the increase in substrate temperature. Prasada et al. [6] discussed the physical properties of ZnO thin films deposited at various substrate temperatures. XRD studies showed that the films deposited at

low temperature (623K) have large stress. XPS analysis revealed the presence of Zn^{2+} and chemisorbed oxygen in ZnO thin films. All the films showed granular, polycrystalline morphology with an increase in grain size as the substrate temperature increased. Variation of direct band gap correlated with the compressive stress of the ZnO thin films.

Dependence of cathodoluminescence of spray-deposited ZnO thin films on deposition parameters [such as substrate temperature, air flow rate and precursors] has been studied in detail [7]. Blue-green emission was observed at substrate temperature of 350 and 400 ^{0}C whereas 'near UV emission' became more dominant than the other transitions (blue-green and red emission) at 450^{0}C. The blue-green emission again appears above substrate temperature 450^{0}C; but red emission appears at different substrate temperature. Structural and luminescent properties of ZnO thin films are also investigated by varying the flow rate region $2.5 \leq f \leq 7.5$ ml/min [Here *f*' was the Air flow rate]. When the spray rate was enhanced, three emissions appeared with dominance for blue-green emission (510nm) [at f =3.75ml/min] and strong intensity of the UV transition (382nm) for f=5 ml/min. At high flow rate [f>6.25ml/min], a degradation of crystallinity leads to decrease of intensity of UV transition and disappearance of both emissions in blue green and red ranges.

Goyal et al. also discussed the development of transparent and conducting ZnO thin films using spray pyrolysis techniques, in which Zn acetate was used as precursor [8]. Structural and electrical studies were conducted and stability of the films in hydrogen plasma was also analysed. Krunks and Mellikove reported the deposition of ZnO thin films using spray pyrolysis technique [9]. Zn acetate dissolved in deionised water and isopropyl alcohol were used as precursors. Growth temperature was in the range of 625 – 675 K and precursor solution was having concentration in the range of 0.1 – 0.2 mol^{-1} for obtaining ZnO films with better optical and electrical properties.

A. Zaier et al. [10] observed the effect of substrate temperature and solution molarity on the structural and opto-electronic properties of spray pyrolysed ZnO thin films. X-ray diffraction pattern indicated that the films were polycrystalline with (002) plane as preferential orientation. UV-Vis spectroscopy confirmed the possibility of getting good transparent samples with an average transmission of about ~ 85% in the visible range. Resistivity of the deposited film was decreased from 44.8×10^4 to $8.4\times10^4\ \Omega$ cm with increase in molarity. Lokhande et al. [11] prepared ZnO thin films after varying

concentration of spray solution [From 0.025 M to 4 M]. XRD studies showed that all the films were polycrystalline having hexagonal wurtzite-type crystal structure with strong orientation along (002) plane except for 0.025 M, which exhibited a strong orientation in along (100) plane. Room temperature electrical resistivity was found to vary in the range 10^2 to 10^{-3} Ω cm, whereas thermoelectric power increased from 1×10^{-6} to 8×10^{-5} V/K.

Optical, electrical and structural properties of polycrystalline [indium doped] spray pyrolysed ZnO thin films from solutions with different pH values were also reported [12]. Different quantities of acetic acid were added to change the pH of the solution. At pH=3.8, film growth with (002) and (101) orientation have a milky appearance. Resistivity of the film decreased as the pH of the solution decreased. In another report, Structural, optical and electrical properties of the ZnO thin films were influenced by the variation of the deposition time [13]. Crystalline quality of the films was improved and grain size increased as thickness was enhanced. But tensile strain decreases with increase in thickness. The electrical conductivity also increased with the thickness.

Structural, optical, chemical and electrical properties of sprayed ZnO films deposited over Pt or silica substrates were determined in temperature range 223 K to 373 K [14]. These films were oriented along (002) direction. The 'band bending' created barriers at grain boundaries and mobility of charge carriers was limited by the thermal field emission of electrons at these barriers.

4.3 Effect of Spray rate

4.3.1 Experimental details

Samples were prepared at different spray rates [varied from 3 ml/min to 12 ml/min] after fixing the precursor volume at 100 ml and substrate temperature at 450^0C in all cases. Here the samples were named as 3ml/min, 5 ml/min , 7 ml/min, 10 ml/min and 12 ml/min. Compressed air was used as the carrier gas. These films were characterized using XRD. Surface morphology of the samples was studied employing scanning electron microscope (JEOL JSM-840). Optical absorbance and transmittance of the sample at normal incidence were studied using UV-Vis-NIR Spectrophotometer. Photoluminescence (PL) studies were conducted with the help of excitation with 325 nm line of Kimmon He-Cd laser [o/p power of 20mW] while the emission was analyzed using Ocean Optics- USB 2000

spectrophotometer. Thickness of the film was measured employing Stylus profiler (Dektak 6M). For electrical measurements 'two probe method' was performed with the help of Keithely 236 source measuring unit [SMU] and metric's Interactive Characterization Unit (ICS). Area of the samples was 30 cm^2.

4.3.2 Structural properties

Fig.4.1 reveals that the samples deposited at the spray rate of 3 ml/min, possessed polycrystalline hexagonal wurtzite structure (a=3.250, c=5.206Å), with peaks appearing at $2\theta=31.77^0$, 34.42^0, 36.25^0 and 47.54^0 corresponding to (100), (002), (101) and (102) phases respectively [JCPDS data card (36-1451)]. But for the spray rate of 6 ml/min, the orientation was shifted to (002) axis. When the (002) plane was dominant in the XRD pattern, axis was mainly found to be perpendicular to the surface of the film. However, when the (101) is dominant, C-axis tilted with respect to the substrate surface. Sang-Hun Jeong et al. [15] and Brett et al. [16] reported that, for modified D.C. planar magnetron-sputtered ZnO films, intensity of c-axis pattern was affected by the flow rate of oxygen. At low flow rate and fixed oxygen partial pressure, (101) plane dominated while at high flow rate (002) plane became dominant. Matsuoka and Ono [17] also observed that the crystallite orientation changes significantly with the flow rate.

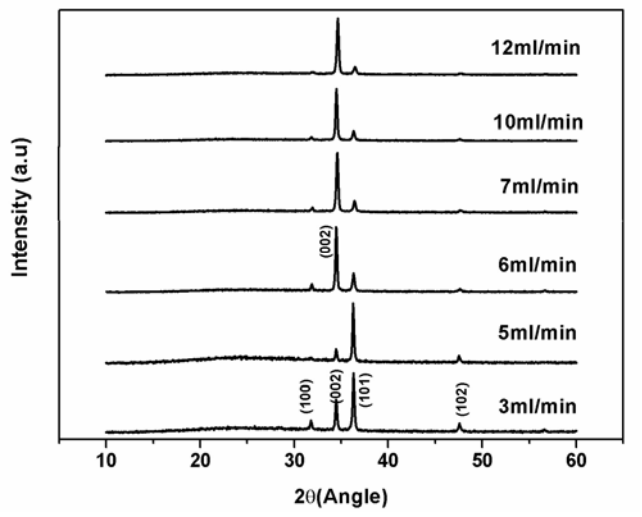

Fig.4.1 XRD pattern of ZnO thin film sample with different spray rate.

Spray rate (ml/min)	Thickness (nm)	Microstrain(ε_s)	Crystallite Size(nm)
3	1400	0.63	38.85
5	950	0.56	38.21
7	750	0.51	33.96
10	900	0.56	37.15
12	1050	0.57	37.97

Table.4.1 Crystallite Size, Thickness, Microstrain as a function of spray rate.

Mean crystallite size was calculated for the (002) diffraction peak using Debye-Scherrer formula D= (0.9 λ)/(β cos θ), where D is the diameter of the crystallite forming the films, λ is the wave length of CuKα line, β is the FWHM , θ is the Bragg angle. This value slightly decreased from 38 nm to 34 nm, when the spray rate increased from 3ml/min to 7 ml/min. After shifting occurred in the preferential axis of orientation, the grain size increased with spray rate. The microstrain developed in the film can be evaluated from the equation, ε_s= [[(λ/D Cos θ)-β)] 1/tan θ] [18]; this also decreased on increasing the spray rate up to 7ml/min after which it increased. These results indicated that the spray rate plays a prominent role in the manner in which the crystal structure of ZnO thin films.

The "texture coefficient [TC]" was calculated for the different planes using the following expression [19].

$$TC(hkl) = \left(\frac{I(hkl)/I_r(hkl)}{\left[\left(1/n\right)\sum I(hkl)/I_r(hkl)\right]} \right) \qquad (4.1)$$

Where ***I(hkl)*** indicates the X-ray diffraction intensity obtained from the film, 'n' is the number of diffraction peak considered and $I_r(hkl)$ is the intensity of reference diffraction pattern [JCPDS data card (36-1451)]. It is clear from the definition that the variation of the texture coefficient implies the film growth in preferred orientation. TC*(hkl)* calculated for different preferred orientations viz., (100), (002),(101) and (102) are listed in table 4.1 with different spray rates. Higher value of TC*(hkl)* indicates that the preferred orientation of the film is along that direction and it is very evident that the value of TC (002) changes with changes in spray rate. The high value of TC (002) indicate the maximum preferential orientation of the film along the (002) plane. If the TC is unity, all the crystallites are oriented randomly in the film whereas for TC is higher than one, the film becomes textured. This implies that all the crystallites are oriented preferentially in the particular direction.TC roughly measures the volume of the grains that are preferentially oriented compared to that of randomly oriented crystallites. In order to know the final texture of the film and to determine preferential orientation of the grains, strain energy and surface energy are to be minimized [20].

Spray rate	Texture Co-efficient			
	(100)	(002)	(101)	(102)
3 ml/min	0.44	1.54	1.20	0.80
5 ml/min	—	0.80	1.37	0.86
7 ml/min	0.21	3.14	0.29	0.30
10 ml/min	0.20	3.18	0.30	0.28
12ml/min	0.15	3.20	0 .23	0.25

Table 4.2.Variation of Texture co-efficient with spray rate

The lattice constants '*a*' and '*c*' were calculated by using the following equation [21]:

$$\frac{1}{d^2_{(hkl)}} = \frac{4}{3}\left[\frac{h^2 + hk + k^2}{a^2}\right] + \frac{l^2}{c^2} \qquad (4.2)$$

The observed '*c*' and '*a*' values are in agreement with the standard values [JCPDS data card (36-1451)]. In thin films, strains originate mainly due to lattice mismatch between the film and the substrate and/or differences in coefficients of thermal expansion of the film and the substrate. Average uniform strain $\boldsymbol{\varepsilon_z}$ in the lattice along the *c*-axis in the randomly oriented ZnO films deposited using different spray rates has been calculated from the lattice parameters with the help of the following expression.

$$\varepsilon_z = \frac{C - C_0}{C_0} \times 100\% \qquad (4.3)$$

where 'C_0' is the lattice constant in unstrained ZnO. For hexagonal crystals, the stress (σ_{film}) in the plane of the film can be calculated using the biaxial strain model [22]:

$$\sigma_{film} = \frac{2C_{13}^2 - C_{33}(C_{11} + C_{12})}{2C_{13}} \varepsilon_z \qquad (4.4)$$

where C_{11} = 209.7GPa, C_{12} = 121.1GPa, C_{13} = 105.1GPa, and C_{33} = 210.9 GPa are the elastic stiffness constants of bulk ZnO. Calculated values of stress ($\boldsymbol{\sigma_{film}}$) in the films, grown at different spray rate and molarity is listed in Table 4.3.

sample name	lattice parameters a (Å)	c(Å)	c /a	Strain %	Stress(GPa)
3ml/min	3.25	5.18	1.59	-0.38	1.72
5ml/min	3.25	5.18	1.59	-0.38	1.72
7ml/min	3.22	5.18	1.60	-0.38	1.72
10 ml/min	3.24	5.20	1.60	-0.11	0.49
12 ml/min	3.22	5.16	1.60	-0.76	3.44

Table.4.3 Variation of lattice parameters, strain, stress as a function of spray rate

From SEM analysis (Fig 4.2 (a) and (b)) it is evident that microstructure is greatly influenced by the spray rate. In the case of 3ml/min, the grains have 'edge like' structure. But when the spray rate is increased, the grains are much better and have uniform orientation. This observation compliments the results from XRD studies.

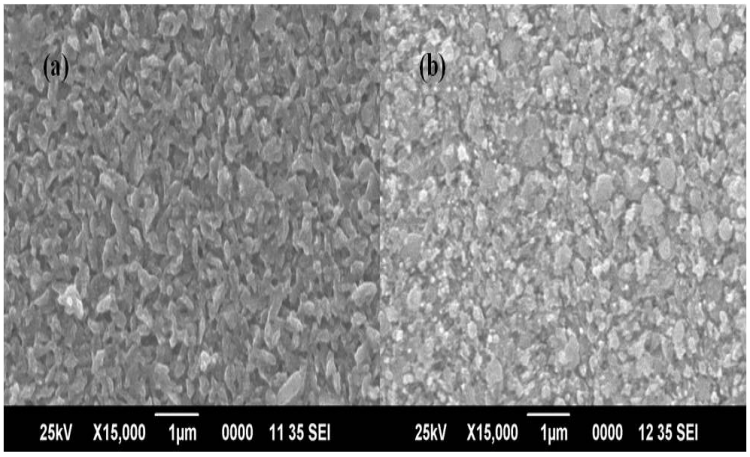

Fig.4.2 SEM images of different spray rates [(a) 3ml/min, (b) 7 ml/min]

4.3.3 Electrical studies

Electrical measurements were done after giving electrical contacts using silver paint in the form of two end contacts, having a distance of 1cm between them. In this study, the resistivity is calculated using the following equation,

$$\rho = R_s d \qquad (4.5)$$

where ρ is the resistivity, Rs is the sheet resistance (Ω/sq) and d is the sample thickness.

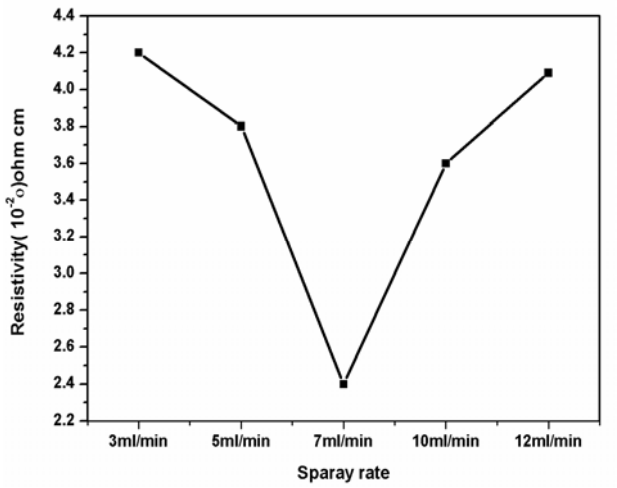

Fig.4.3 Electrical resistivity of ZnO thin film at different spray rate

Variation of resistivity with spray rate is depicted in Fig.4.3. Resistivity was observed to be the least for sample prepared at 7ml/min. L. Martinez Perez et al. [23] claimed that electrical resistivity of the order of 2.7×10^{-2} Ω cm was measured at room temperature for the best H_2-annealed undoped ZnO film. From our study, the resistivity could be brought down to $2.4x10^{-2}$ ohm cm without any doping or annealing. This may be due to the better crystallinity of the films prepared at this spray rate and/or presence of defect states helping creation of carriers. Such defects strongly influence the resistance of the film. Photoluminescence (PL) analysis included in the following section, gives more explanation about such defects in the film.

4.3.4 Optical studies

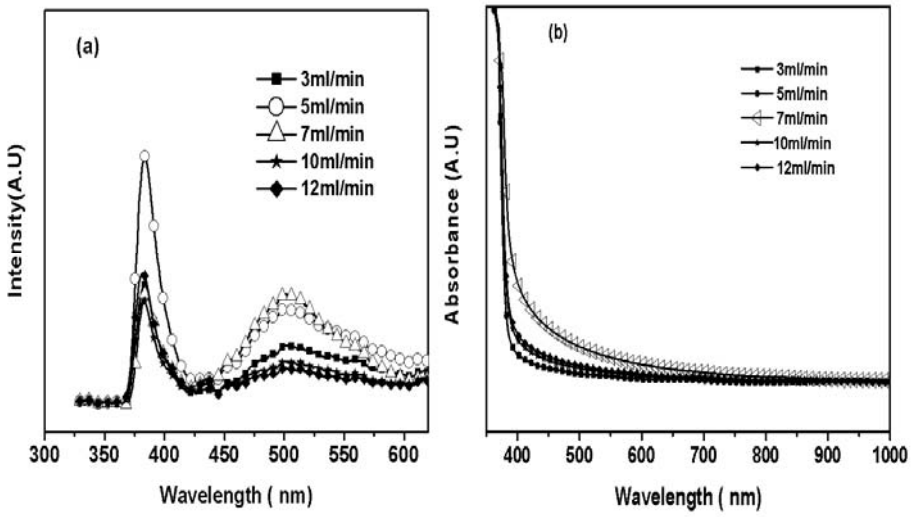

Fig.4.4 (a) PL Spectra (b) Absorbance Vs. Wavelength plot of ZnO thin films prepared at different spray rates.

Fig.4.4 (a) & (b) depict the PL spectra and absorbance Vs wavelength plot of the samples prepared at different spray rates respectively. Here it is quite obvious that the 'Blue-Green emission' centred at 503 nm is the most intense for samples prepared at the spray rate of 7ml/min whereas the band- edge (excitonic) emission [centred at 380] is maximum for sample prepared with spray rate of 5ml/min. Previous reports suggest that the PL emission of ZnO thin films in the blue-green region is strongly dependent on stoichiometry of the film [24, 25]**.** Studenikin et al.[2] argued that oxygen vacancies and porosity of the film are the reasons behind this emission. Ratheesh kumar et al. [26]

concluded that the origin of the blue-green emission was due to transition from conduction band to the acceptor level corresponding to the antisite of oxygen. Hur et al. [27] also made similar observations on the green emission.

In the present case, the most accepted reason for the green emission appears to be the presence of oxygen antisite (O_{zn}). Interestingly, in the present work, the only reason for the change in orientation as well as the introduction of antisite defects appears to be the variation of spray rate. Through increasing the spray rate, we are increasing the quantity of zinc (Zn) ions available at the substrate surface to build the grains. Up to the spray rate of 5 ml/min, the grains oriented along (101) direction can accommodate the Zn ions available at the substrate surface from that spray rate. But as the spray rate becomes 6 ml/min, the growth direction has to change to include the increased quantity of Zn ions and hence the grains get oriented along (002) plane. According to S. Amirhaghi et al [28], the 2-dimensional Zn atom population is highest in the (002) plane of the wurtzite structure. The present result is very well agreeing with this observation.

However at the beginning stage of building up of the (002) plane, there can be vacancies as the spray rate may not be able to supply enough Zn ions to fill the plane fully. Naturally, this leads to the formation of oxygen antisites (O_{zn}) in these films, resulting in the green emission with high intensity. But as the spray rate is further increased beyond 7 ml/min, the Zn vacancies are filled as more Zn ions are available at the substrate surface leading to the fading of the green emission. More over, for the samples prepared at the spray rate of 5 ml/min, [when the (101) orientation has maximum possible Zn atoms] the ultraviolet emission has maximum intensity. This is in agreement with the observation of Ratheesh kumar et.al. [29] where it is observed that intensity of this emission depends on the metal to oxygen ratio. Again it is observed that the optical absorption of the sample deposited at 7 ml/min [having maximum intensity for the green emission] starts from ~ 600 nm indicating that there are defect levels in the region 2-2.5 eV below the conduction band and this very well corresponds to the position of O_{zn}. The low resistivity of this sample may also be due to the excitation of carriers through this absorption.

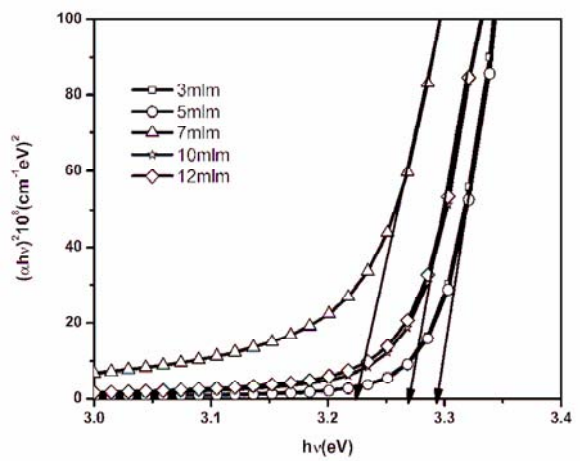

Fig.4.5 $(\alpha h\upsilon)^2$ vs. hυ plot of ZnO with different spray rate

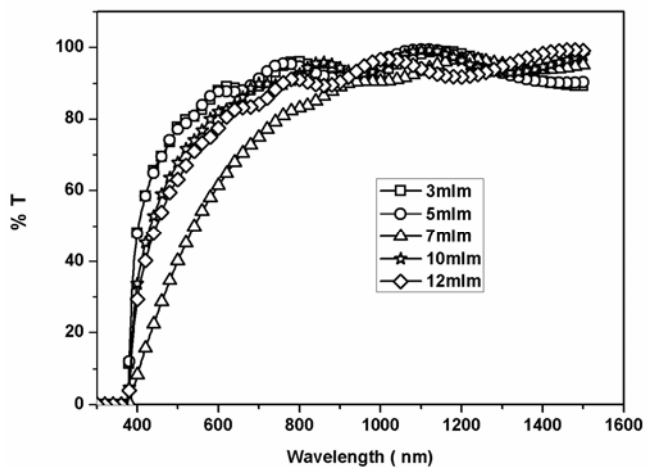

Fig.4.6 Transmission curves for ZnO with different spray rate

Optical absorption spectra were recorded in the wave length rage 350-1000nm. Absorption edge varied with different spray rate. Band gap was determined from $(\alpha h\upsilon)^2$ vs. hυ plot and it decreased from 3.25 eV to 3.20eV as spray rate increased from 3ml/min to 7 ml/min. After this, it increased with increasing spray rate. Interestingly the sharpness of the absorption edge is lost on increasing spray rate up to the optimum values [i.e., up to 7 ml/min]. Optical transmission spectra were recorded for all samples in the wavelength rage 350-1600 nm (Fig.4.6). 'Interference fringe-like' pattern of the transmittance curve

recognized the smooth and reflecting nature of the film. Transmittance of the film decreased as the spray rate increased from 3ml/min to 7 ml/min after which it increased.

4.4 Effect of variation of molarity

4.4.1 Experimental details

Keeping the spray rate at 7 ml/min, as it was showing lowest resistivity and better crystallinity, samples were prepared using different molarities of Zinc acetate solution [from 0.2 M to 0.6 M]. Here the samples were named as 0.2 M, 0.3M,0.4 M,0.5M,0.6M with variation of molarity. These films were characterized using structural, optical and electrical measurements.

4.4.2 Structural properties

XRD patterns of ZnO prepared with spray solutions of different molarities are shown in Fig. 4.7. At the lower molarity, samples exhibited poly crystalline nature with the planes orienting along (002) and (101) plane. After reaching the 0.3M, intensity of peak corresponding to the plane (101) decreased while that of the plane (002) increased.

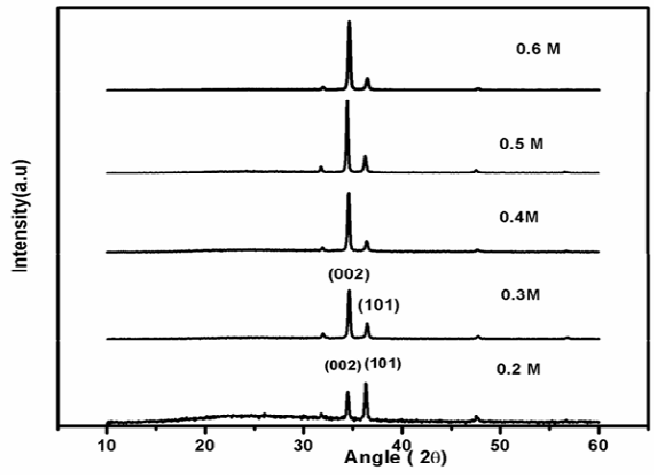

Fig.4.7 XRD pattern of ZnO thin film sample with different molarity.

Growth rate of ZnO films is explained using two mechanisms viz., Rideal-Elay mechanism and Langmuir –Hinshelwood mechanism [30]. According to the former one, ZnO films grow continuously with the molarity of Zn precursor and the formation of ZnO is through the reaction with absorbed water molecules. In spray pyrolysis it is difficult to control the incorporation of O_2 into the film during the growth process because the film is deposited in

the atmospheric condition. Hence in the case of sprayed samples, growth rate as well as stoichiometry of the film can be controlled only through Zn-concentration as oxygen is easily available from the atmosphere. At the lower molarity, the film has both (101) and (002) orientations; but as the molarity increased, the (002) plane orientation is improved which is due to the dense content of Zn atoms from precursor solution. As mentioned earlier, according to S. Amirhaghi et.al. [28], population of Zn atom is highest in the (002) plane of the wurtzite structure. The crystallinity is also improved with the increase in molarity. Values of texture coefficient calculated for different orientations namely (100), (002), (101) and (102) are shown in table 4.4 for different molarity .

Molarity	Texture Co-efficient			
	(100)	(002)	(101)	(102)
0.2M	0.49	1.68	0.96	0.86
0.3M	0.20	3.14	0.29	0.31
0.4M	0.22	3.32	0.33	0.33
0.5 M	0.23	3.22	0.28	0.31
0.6M	0.14	3.44	0 .26	0.18

Table. 4.4 Variation of Texture co-efficient with molarity.

sample name	lattice parameters a (Å)	c(Å)	c /a	Strain %	Stress(GPa)
0.2 M	3.25	5.18	1.59	-0.38	1.74
0.3 M	3.22	5.18	1.60	-0.38	1.74
0.4 M	3.25	5.18	1.59	-0.38	1.74
0.5 M	3.22	5.20	1.61	-0.11	0.49
0.6 M	3.24	5.18	1.59	-0.76	1.74

Table.4.5 Variation of lattice parameters, strain, stress as a function of molarity

Molarity	Resistivity(10^{-2} Ω cm)	Thickness (nm)	Grain Size(nm)
0.2	1.8	400	33.55
0.3	2.4	600	33.65
0.4	3.08	750	39.69
0.5	3.37	1050	33.50
0.6	5.18	1200	34.17

Table.4.6 Resistivity , Grain Size, Thickness as a function of molarity.

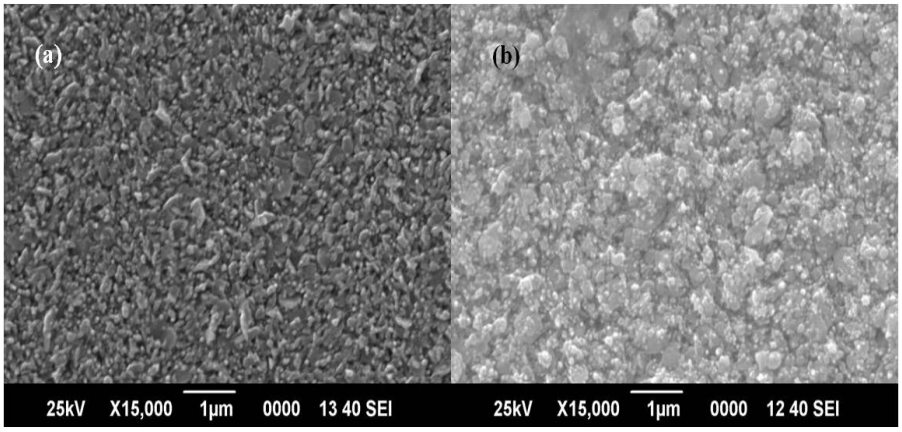

Fig.4.8 SEM micrograph of films Molarity (a) 0.2M ,(b)0.6M.

4.4.3 Optical studies

Optical band gap of the ZnO film was calculated from optical absorption studies. The $(\alpha h\upsilon)^2$ vs hυ plot for the ZnO thin films deposited at different molarities is presented in the Fig.4.9 . Band gap of the film deposited at lower molarity of 0.2M is 3.28 eV which decreased as the molarity of the solution increased up to 0.4 M (3.19 eV) and then increased on further increasing the molarity beyond 0.4M. Interestingly sharpness of the absorption edge is lost on increasing molarity up to the optimum values [i.e., up to 0.4 M)]. Transmittance of the film decreased as the molarity increased from 0.2 M to 0.6 M (Fig.4.10).

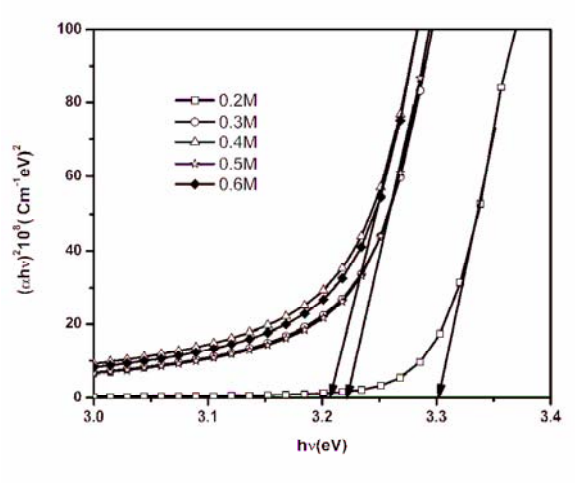

Fig.4.9 $(\alpha h\upsilon)^2$ vs. hυ plot of ZnO at different molarity

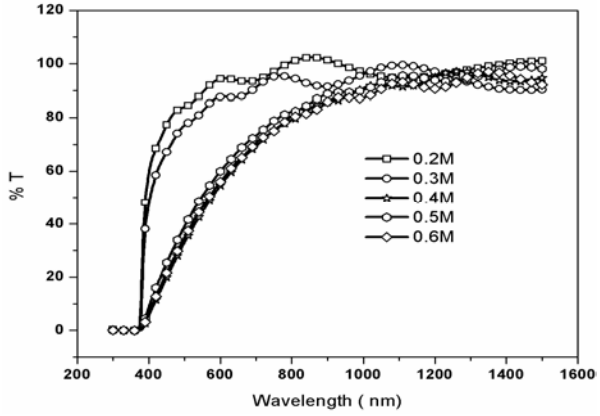

Fig.4.10 Transmission curves for ZnO at different molarity

4.4.4 Electrical studies

Electrical Resistivity measurements were carried out on all samples using two-probe method. The measurements proved that resistivity of the samples increased with increasing the molarity of the solution. (Fig.4.11)

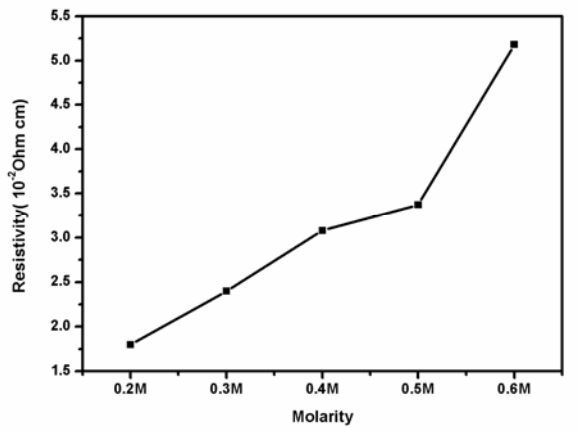

Fig.4.11 Electrical resistivity of ZnO thin film at different molarity

4.5 Effect of Precursor Medium

4.5.1 Experimental details

Molarity of Zinc acetate was fixed at 0.3 M, since it was showing better structural, optical and electrical properties. Spray rate and temperature were always held constant [at 7ml/min and 450 $\pm 5^0$C respectively] hereafter. Usually deionized water is used as the solvent for preparing the precursor solution in spray pyrolysis technique. But in order to obtain films with higher conductivity, it is essential that the complete oxidation of metal is avoided. This is generally achieved by adding the appropriate reducing agent such as propanol (2-,Propanol; C_3H_7OH), ethyl alcohol (ethanol; C_2H_6O) in the precursor of Zn. Decomposition products of these organic materials lead to the reduction of the oxide film, thereby creating the anion vacancies. In the present study, precursor solution containing 0.3 M Zinc acetate [$Zn(CH3COO)_2 .2H_2O$] is prepared by dissolving it in the deionised water. This salt of Zn is used due to its high vapour pressure at low temperature. In this work two types of spray solutions were prepared. In the first one, this aqueous solution was mixed with ethanol while in the other type the aqueous solution was mixed with propanol. Volume

of alcohol added to the aqueous solution was varied as 0,20,30,50,60 and 70 ml so that the total volume of spray solution was always 100 ml. Using these two types of spray solutions, two sets of ZnO thin film samples were prepared and these were named as Z-E0,Z-E20,Z-E30,Z-E50,Z-E60,Z-E70 [for samples prepared using Ethanol based solution] and Z-P0,Z-P20,Z-P30,Z-P50,Z-P60,Z-P70 [for the samples prepared using Propanol based solution].

4.5.2 Structural studies

XRD patterns of ZnO thin films with various ethanol and propanol concentrations [2θ angle in the range of 10–60 deg] are depicted in Fig. 4.12(a) and 4.12 (b).

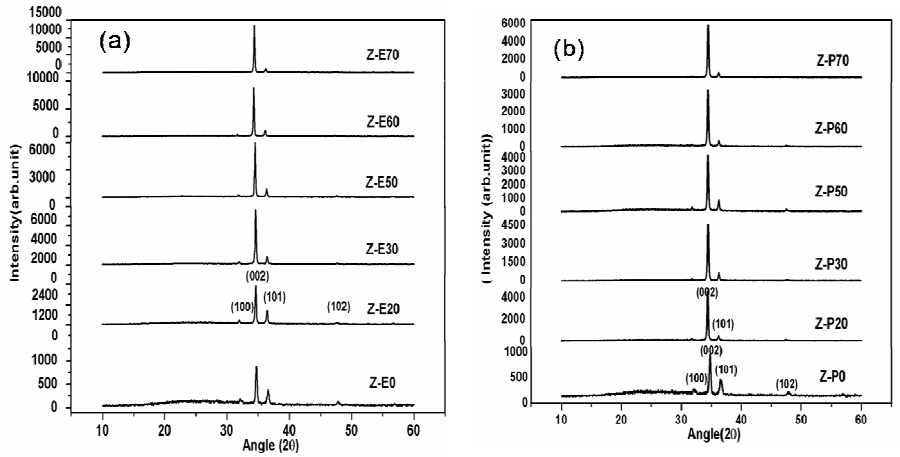

Fig 4.12 a) XRD pattern of different ethanol concentration b) propanol concentration

Sample name	Ethanol Concentration (ml)	Texture Co-efficient(TC)			
		TC (100)	TC (002)	TC(101)	TC(102)
Z-E0	0	0.40	2.43	0.47	0.68
Z-E20	20	0.27	2.89	0.48	0.35
Z-E30	30	0.10	3.43	0.33	0.24
Z-E50	50	0.14	3.39	0.24	0.23
Z-E60	60	0.12	3.47	0.20	0.19
Z-E70	70	—	3.69	--	—

Table.4.7 Variation of Texture co-efficient (TC) with ethanol concentration

Sample name	Propanol Concentration (ml)	Texture Co-efficient(TC)			
		TC(100)	TC(002)	TC (101)	TC (102)
Z-P0	0	0.40	2.43	0.47	0.68
Z-P20	20	—	3.56	0.18	0.15
Z-P30	30	0.12	3.51	0.22	0.14
Z-P50	50	0.20	3.19	0.29	0.30
Z-P60	60	0.12	3.55	0 .16	0.16
Z-P70	70	—	3.64	0.15	—

Table.4.8 Variation of Texture co.efficient (TC) with propanol concentration

Values of texture coefficient calculated for different orientations namely (100), (002), (101) and (102) are shown in table 4.7 and 4.8 for the two different spray solutions having different concentrations of ethanol and propanol respectively. These results imply that the solvent used to prepare precursor solution influences the crystallinity and preferential orientation of the spray pyrolysed thin film samples very much. However thickness of the sample decreased with increasing the percentage of alcohol (Table 4.9).

Propanol(ml)	Thickness(nm)	Ethanol(ml)	Thickness(nm)
P-0	1400	E-0	1400
P-20	1150	E-20	1050
P-30	900	E-30	750
P-50	550	E-50	500
P-60	500	E-60	425
P-70	400	E-70	375

Table. 4.9 Variation of thickness with alcohol concentration.

Fig.4.13 gives the variation of grain size and FWHM of the two sets of samples due to the change in the concentration of ethanol and propanol in spray solutions. When grain

size enhanced from 22 nm to 45 nm with the increase of the ethanol concentration, the variation of propanol did not effect the grain size much. The increase in grain size with the variation in the precursor solution concentration may be due to the difference in the boiling points between the two alcohols used in this work resulting in the 'residence time' of the drop on the hot substrate [31].

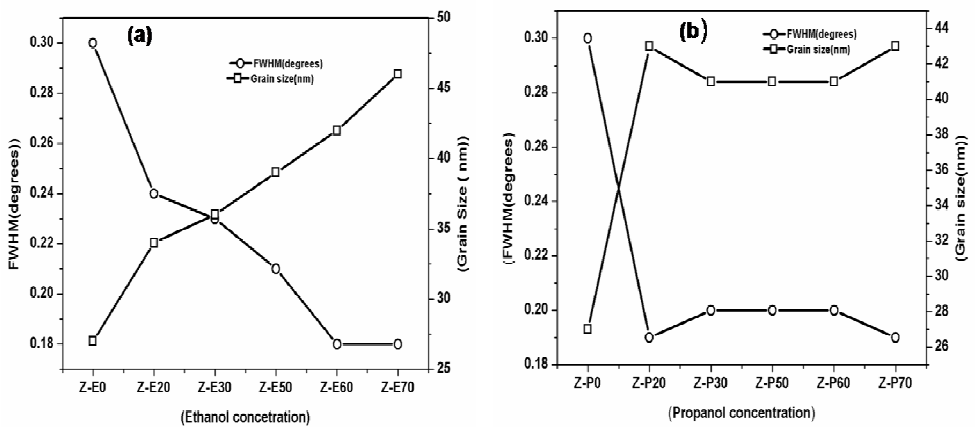

Fig.4.13 Variation of FWHM (degrees) and Grain size with a) ethanol concentration b)propanol concentration.

Strain could be positive (tensile) or negative (compressive) according to the equation (4.3) (Table. 4.10 & Table.4.11). The total stress in the film commonly consists of two components: one is the intrinsic stress introduced by impurities , defects and lattice distortions in the crystal, and the other , is the extrinsic stress introduced by the mismatch between crystalline ZnO and amorphous glass substrate and thermal expansion coefficient mismatch between the film and substrate.

Sample name	Ethanol concentration (ml)	lattice parameters a (Å)	c(Å)	c /a	Strain %	Stress(GPa)
Z-E0	0	3.19	5.16	1.61	-0.76	3.44
Z-E20	20	3.17	5.16	1.62	-0.76	3.44
Z-E30	30	3.22	5.18	1.60	-0.38	1.72
Z-E50	50	3.20	5.22	1.63	0.38	-1.72
Z-E60	60	3.20	5.22	1.63	0.38	-1.72
Z-E70	70	3.21	5.18	1.61	-0.38	1.72

Table. 4.10 Variation of lattice parameters, strain, stress as a function of ethanol Concentration

sample name	Propanol concentration (ml)	lattice parameters a (Å)	c(Å)	c /a	Strain %	Stress(GPa)
Z-P0	0	3.19	5.16	1.61	-0.76	3.44
Z-P20	20	3.22	5.18	1.60	-0.38	1.72
Z-P30	30	3.22	5.18	1.60	-0.38	1.72
Z-P50	50	3.21	5.22	1.62	0.38	-1.72
Z-P60	60	3.21	5.22	1.62	0.38	-1.72
Z-P70	70	3.21	5.22	1.62	0.38	-1.72

Table.4.11 Variation of lattice parameters, strain, stress as a function of propanol concentration

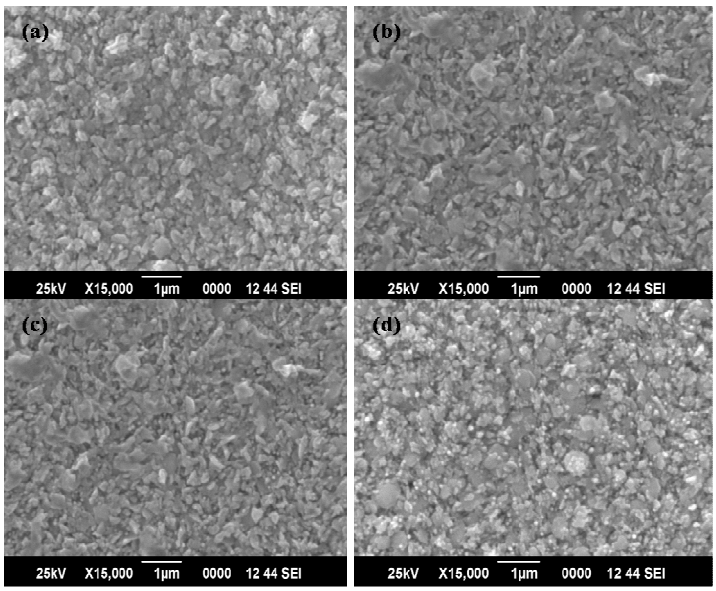

Fig.4.14 SEM micrograph of films with different alcoholic concentration (a) Z-P20(b)Z-P70 (c)Z-E20 and (d)Z-E70.

From the results of SEM analysis (Fig.4.14 (a), (b), (c) and (d)) it is quite clear that the surface nature of the films is greatly influenced by the variation of alcohol concentration. Increase in the percentage of ethanol changes the film surface from 'spindle like' structure to uniform orientation.

4.5.3 Optical studies

Optical absorption and transmission spectra were recorded in the wavelength region of 350–1200 nm. In order to determine the optical band gap, "$(\alpha h\upsilon)^2$ vs. hυ graph" was plotted (Fig 4.15). The intercepts of this plot on the energy axis give the energy band gap of the material. Effects of ethanol and propanol concentrations on the optical transmittance and band gap (Eg) values of the ZnO thin films have been studied. (Fig4.15, Fig.4.16 & Table4.12) But the optical transmittance in the visible range increased with increasing the alcohol concentration (Fig4.17). Increase of the transmittance may be due to the decrease of film thickness which occurred due to the increase of the alcohol concentration in the precursors.

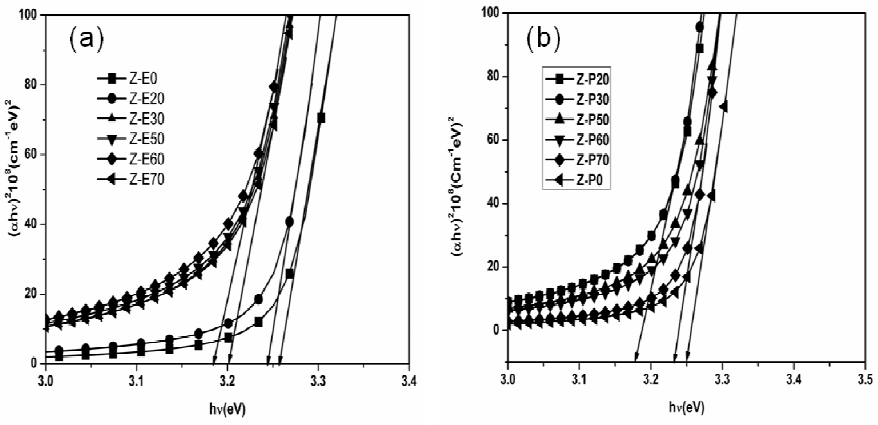

Fig.4.15 (a) $(\alpha h\upsilon)^2$ vs hυ plot of Variation of Z-E (b)Z-P

Ethanol concentration (ml)	Bang gap Eg(eV)	Propanol Concentration (ml)	Band gap Eg (eV)
E-0	3.26	P-0	3.26
E-20	3.24	P-20	3.24
E-30	3.19	P-30	3.21
E-50	3.19	P-50	3.22
E-60	3.18	P-60	3.21
E-70	3.24	P-70	3.24

Table .4.12 Variation of energy gap with ethanol and propanol concentration

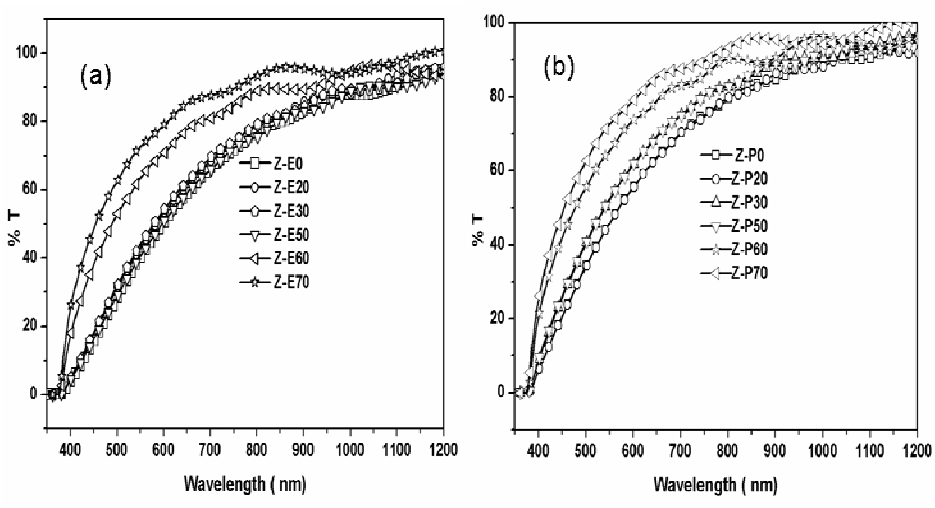

Fig.4.16 Transmission spectra a) Z-E b) Z-P based solvent.

4.5.4 Photoluminescence (PL) measurements

PL spectra of both Z-E and Z-P samples, at room temperature recorded in the range of 350–625 nm, showed two emission peaks centred at 377nm and 500 nm (Fig.4.17), in which the peak at 377 nm was corresponding to the 'Near Band Edge' (NBE) emission while the one at ~500 nm was corresponding to the characteristic 'blue-green emission'. The NBE emission is well understood [32] and had been attributed to free-exciton annihilation [33, 34]. Some efforts were also made to correlate crystallinity with the intensity of NBE emission [35, 36]. In the present work, it was clear from the PL spectra that the intensity of NBE emission changed with the variations of concentrations of the alcohols in the precursor solutions. This is in good agreement with our results from the XRD analysis [Sec4.5.2] which proved that the degree of the crystallinity increased with the increase in alcohol concentration in spray solution. Here one can also see that maximum height of NBE peak is for the samples prepared using spray solutions having 70% propanol. The same samples were having minimum blue-green emission. But in the case of E-series samples, having maximum NBE, there was minimum alcohol concentration. Hence intensity of the PL emission may have a clear dependence on the type of the alcohol used in the precursor solution.

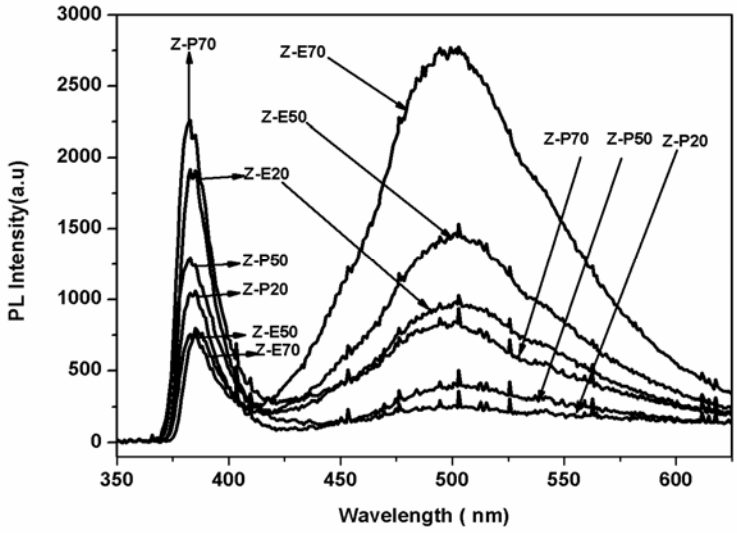

Fig.4.17 Room temperature PL spectra of different ethanol and propanol concentration

PL emission centred at ~503 nm is the characteristic emission of ZnO thin films and was extremely broad. This might be due to phonon-assisted transition [37]. But the exact reason for this emission is not clearly understood. Bylander put forward a model, which suggested that the blue-green emission was due to electronic transition from an interstitial Zn to a Zn vacancy [38]. Sekiguchi et al. reported the effect of hydrogenation on the luminescence of ZnO crystals and found that hydrogen treatment strongly reduced the green emission, through the passivation of levels causing the green emission [39]. It was also seen that the band edge emission intensity increased considerably after the hydrogen treatment. Lin et al tried to explain the origin of blue-green emission, in undoped ZnO thin film [40]. In these samples, two emissions were observed with energies 3.18eV and 2.38 eV. It was concluded that the green emission was corresponding to the local levels caused by oxygen antisites and the transition was from the conduction band to deeper acceptor level of oxygen antisite (O_{zn}). Here the intensity of blue- green emission of the sample Z-P series is very much less compared to that of sample Z-E series. This is in good agreement with the resistivity measurement studies. Intensity of blue-green emission decreased due to the decrease of oxygen antisite and naturally the resistivity will also be decreased due to this.

4.5.5 Electrical studies

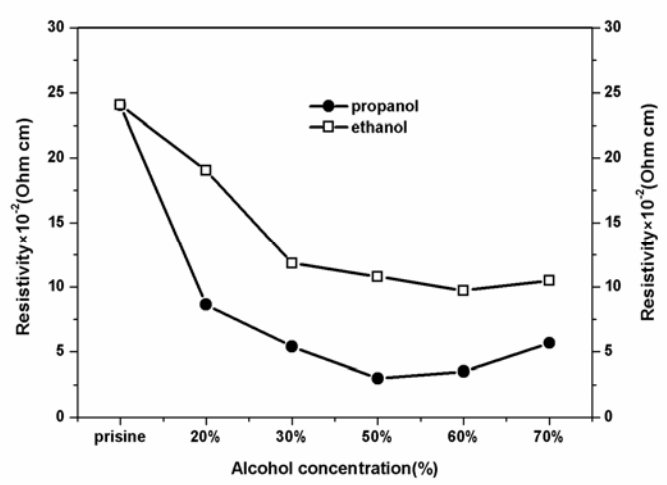

Fig.4.18 Electrical resistivity of ZnO thin film at different alcoholic concentration.

Variation of resistivity with concentration of precursor solution is presented in the Fig.4.18. It is very clear that resistivity of the sample decreased with increase of concentration of both the alcohols and the lowest resistivity of 2.4×10^{-2} Ω cm was obtained for samples prepared in propanol medium. This was achieved without any doping and annealing. From Fig.4.18, it is also clear that Z-P (propanol based) series samples have lower resistivity than the Z-E (ethanol based) series samples. From the PL studies also the peak intensity of blue-green emission from samples of Z-P series was lower than that of samples of Z-E series which is supporting the results from the electrical studies.

4.6 Effect of pH Variation

4.6.1 Experimental Details

Systematic study was conducted on the samples deposited by varying the pH of the precursor solution from pH-3 to pH-6. These samples were prepared after fixing the spray rate and molarity at the optimum value and were named as pH-3, pH-3.5, pH-4, pH-4.5, pH-5 and pH-6. A few drops of acetic acid were added to the solution to prevent the formation of hydroxides. Here pH of the precursor solution was varied by changing the volume of acetic acid in the precursor solution.

4.6.2 Structural properties.

In the present study, it is very clear that the samples, prepared at different pH, possess polycrystalline hexagonal wurtzite structure (a=3.250, c=5.206Å), with peaks appearing at $2\theta=31.77^0$, 34.42^0 and 36.25^0 corresponding to (100), (002) and (101) phases respectively. From the pH-3.5 to pH-4, the orientation is shifted to (002) direction. But in the case of lower and higher pH, (101) is the preferential orientation(Fig.4.19). Variation of crystallite size with variation in the pH of the precursor solution is presented in the Fig.4.20.Crystallite size sharply increased up to pH-4 and decreased with further increase of pH value .

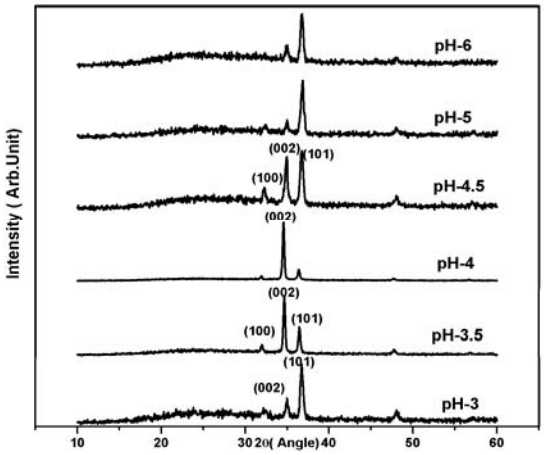

Fig.4.19 XRD pattern of ZnO thin film sample with different pH of the solution.

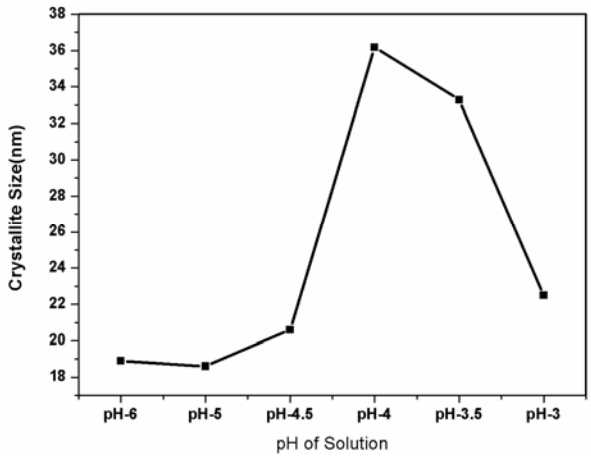

Fig.4.20 Variation of crystallite size with pH of the solution.

4.6.3 Optical properties

Optical band gap of the ZnO film was calculated from the optical absorption studies. Band gap was determined from $(\alpha h\upsilon)^2$ vs. hυ plot and no significance variation in the band gap was observed(Fig.4.21)

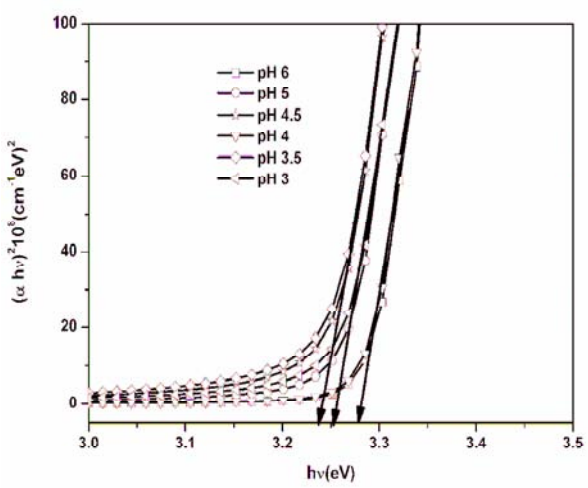

Fig.4.21$(\alpha h\upsilon)^2$ vs hυ plot of Variation of pH of the solution.

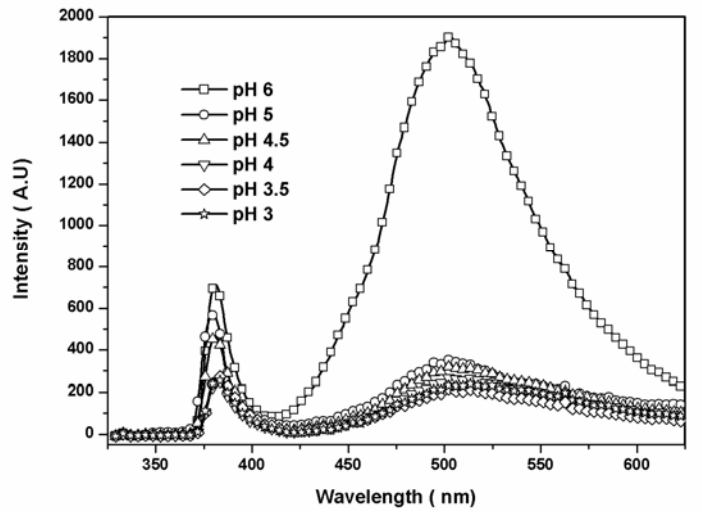

Fig. 4.22 Room temperature PL spectra of different pH of the solution

From the PL measurement (Fig.4.22) all the samples [from pH-3 to pH-6] showed two emission peaks centred at 377nm and ~503 nm, which were already described in

section 4.5.4. Here the intensity of blue- green emission of samples decreased with the increase in the acidic nature of the film. Transmittance of the film also decreased with the pH of the solution.

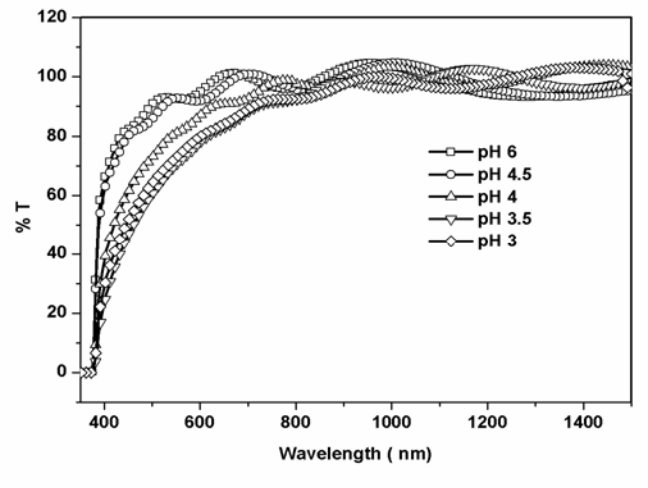

Fig.4.23 Transmission curves for ZnO with various pH of the solution

4.6.4 Electrical properties

Electrical resistivity of the film decreased with increasing the acidic nature of the solution. The precursor solution with pH-4 exhibited the lowest value of resistivity in the order of $2\times10^{-2}\,\Omega$ cm.

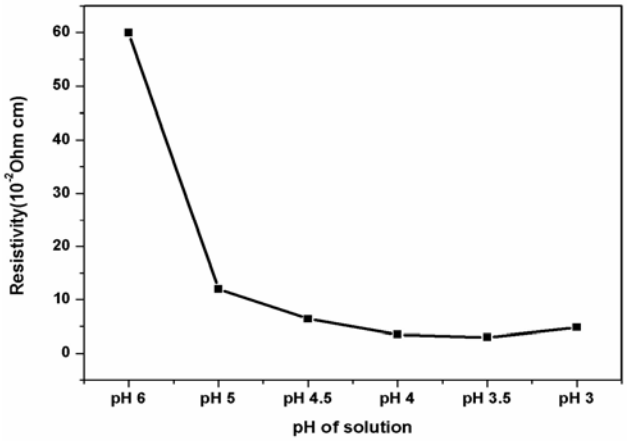

Fig.4.24 Electrical resistivity of ZnO thin film at different pH of the solution

4.7 Conclusions

The studies presented in this chapter describe the processes done for optimizing the deposition parameters of ZnO thin films like molarity, spray rate, precursor medium and pH of the solution, to get the good quality and large area thin films using CSP technique. The structural analysis proved that on increasing the spray rate, orientation of grains changed from (101) to (002). Intensity of Blue- Green emission decreased after the orientation of grains shifted to (002) plane.

Crystallite size, Optical transmission and electrical conductivity of the films enhanced with increase of alcohol concentration. Intensity of blue-green emission varied with percentage as well as with the type of alcohol used in the precursor solution supporting electrical and optical properties. Propanol based samples had lower resistivity than the ethanol based samples. The lowest value of $2\times10^{-2}\Omega$ cm was obtained for the sample prepared using water and propanol in 1:1 (Z-P50).

Spray rate was fixed 7ml/min and molarity of the spray solution, at 0.3M. The precursor medium was selected as the one having deionised water and propanol in the ratio 1:1 and having pH equal to 4. We used these optimised condition for the preparation of doped ZnO thin film for the further studies which are presented in the following chapters of the thesis.

References

[1] J Aranovich, A Ortiz and R.H Bube J.Vac.Sci.Technol. **16** (1979) 994.

[2] S. A. Studenikin, N. Golego and M. Cocivera, J. Appl. Phys. **83** (1998) 2104.

[3] B. Joseph, K. G. Gopachandran, P. K. Manoj, P. Koshy and V. K. Vaidyan, Bull. Mat. Sci.**22** (1999) 921.

[4] D. J. Goyal, C. M. Agashe, B. R. Marathe, M. G. Takwale and V. G. Bhide, J. Mater. Sci. Lett. **11** (1992) 708.

[5] T. Prasada Rao, M.C. Santhosh Kumar, S. Anbumozhi Angayarkanni and M. Ashok J.Alloys and Compounds.**485** (2009) 413.

[6] T.PrasadaRao, M.C.Santhosh Kumar , A.Safarulla ,V.Ganesan ,S.R.Barman and C. Sanjeeviraja, Physica B **405** (2010) 2226.

[7] A.E Hichou, M.Addou,J.Ebothe and M.Troyon J.of Luminescence **113**(2005)183.

[8] D. J. Goyal, C. Agashe, M. G. Takwale, B. R. Marathe and V. G. Bhide, J. Mater. Sci. **27**(1992) 4705.

[9] M. Krunks and E. Mellikov, Thin Solid Films **270**(1995) 33.

[10] A. Zaier, F.Oum El az, F.Lakfif , A.Kabir , S.Boudjadar and M.S.Aida Materials Science in Semiconductor Processing **12** (2009) 207.

[11] B. J. Lokhande**,** P. S. Patil and M. D. Uplane Material letters **57**(2002) 573.

[12] A. Maldonado**,** R. Asomoza**,** J. Cañetas-Ortega**,** E.P. Zironi**,** R. Hernández **,**R. Patiño and O. Solorza-Feria**.** Sol.Ener. Mater. and Solar cell **57**(1999) 331.

[13] T. Prasada Rao and M.C. Santhoshkuma, Appl. Surf. Sci.**255**(2009) 4579.

[14] R. Ayouchi, D. Leinen, F. Martin, M. Gabas, E. Dalchiele and J. R. R. Barrado, Thin Solid Films **426** (2003) 68.

[15] Sang-Hum Jeong, Bong-Soo Kim and Byung-Teak Lee, Appl. Phys. Letter. **82** (2003) 2625.

[16] M. J. Brett and R.R Parsons,J.Mater.Sci.**22** (1987) 3611**.**

[17] M. Matsuoka and K.Ono,Appl.Phys.Lett.**53** (1988)1393.

[18] G. K. Willamson and R. E. Smallman, Philos Mag1(8)(1956) 34.

[19] R. Romero, D. Leinen, E.A. Dalchiele, J.R. Ramos-Barrado and F. Martin,Thin Solid Films. **515 (**2006) 1942.

[20] D. N. Lee,Thin Solid Films **434** (2003) 183.

[21] C. Suryanarayana, M. Grant Norton, X-ray Diffraction –A Practical Approach, Plenum Press, New York and London(1998) p.125.

[22] M.K. Puchet, P.Y.Timbrell and R.N. Lamb, J. Vac. Sci. Technol.A.**14** (1996) 2220**.**

[23] L. Martínez Pérez, M. Aguilar-Frutis, O. Zelaya-Angel and N. Muñoz Aguirre, phys. stat. sol. (a) **203** (2006)2411.

[24] K. Vanheusden, C. H. Seager, W. L. Warren, D. R. Tallant and J. A. Voigt, Appl.Phys.Lett. **68** (1996) 403.

[25] Z. K. Tang, G.K.L.Wong, P.Yu, M. Kawasaki,A. Ohtomo,H. Koinuma and Y.Segawa, Appl.Phys.Lett.**72** (1998)3270.

[26] P. M.Ratheesh kumar, K. P. Vijayakumar and C. Sudha Kartha, J.Mater.Sci.**42** (2007) 2598.

[27] T. B. Hur, G. S. Jeen,Y-H Hwang and H. K. Kim,J.Appl. Phys.**94** (2003) 5787**.**

[28] S.Amirhaghi,V. Cracium, D. Creacium, J. Elders and I. W. Boyd, Microelecron. Eng. **25** (1994) 321.

[29] P. M. Ratheesh Kumar , C. Sudha Kartha and K. P. Vijayakumar,J.Appl.Phys.**97** (2005) 13509,1.

[30] S.Nakao,K. Saitosh,M. Ikeyama,H. Niwa,S. Tanemura,Y. Miyagamaand and S. Miyagama, Thin Solid Films **281** (1996) 10.

[31] A.Maldanoda , M. de . Olevera, S. Tirado Guerra and R. Asomoza , Sol. Energy. Mater.Sol. Cells. **82** (2004) 75

[32] C. Klingshirn, Phys, Status Solidi. B.**71** (1975) 547.

[33] P. Zu, Z. K. Tang, G. K. L. Wong, M. Kawasaki, A. Ohtomo, H. Koinuma and Y. Segawa, Solid. State. Commun.**103** (1997) 459.

[34] S. Cho, J. Ma, Y. Kim, Y. Sun, G. K. L. Wong and J. B. Ketterson, Appl.Phys. Lett.**75** (1999) 2761.

[35] K. Ozaki and M. Gomi, Jpn. J. Appl. Phys.**41** (2002) 5614.

[36] F. K. Shan, B. I. Kim, G. X. Liu, Z. F. Liu, J. Y. Sohn, W. J. Lee, and B.C. Shin, J. Appl. Phys. **95** (2004) 4772.

[37] D. C. Reynolds, D. C. Look, B. Jogai and H. Mokoc, Solid State Commun **101** (1997) 643.

[38] E. G. Bylander, J.Appl. Phys.**49** (1978) 1188.

[39] T. Sekiguchi,N. Ohashi and Y.Teranda, Jpn.J.Appl.Phys.**36** (1997) L289.

[40] B.Lin,Z.Fu and Y.Jia,Appl.Phys.Lett.**79** (2001) 943.

Chapter 5

Effect of doping on spray pyrolysed ZnO thin film

5.1 Introduction

The density of impurities in semiconductors is one of the major parameter that can control position of Fermi level. It is often possible to impart some desirable properties to semiconductor by introducing a controlled quantity of suitable impurity elements into it either during its preparation or diffusing them afterwards through thermal or other treatments. This process is called 'doping' and the impurities are known as 'dopants'. Doping of impurities in wide band gap semiconductors often induces dramatic changes in electrical and optical properties. Doping of ZnO with the atoms of elements of higher valency results in replacing Zn^{2+} atoms and hence improvement in the electrical conductivity. ZnO can be doped with a wide variety of atoms to meet the demands of several applications. Various dopants such as F^{1-}, Cu^{1+}, Ag^{1+}, Ga^{3+}, Al^{3+},In^{3+}, Sn^{4+} and Sb^{5+} has been already tried [1-10] and efficiency of the dopant depends on its electro-negativity and ionic radius. In the present work, the technique we used for film preparation is very simple viz., CSP and it is rather easy to vary the concentrations of Zinc ion or dopant in this technique and hence to vary / control the properties of the films.

ZnO is a potential candidate for various applications in the field of opto-electronic devices in short-wavelength. In order to achieve this, high quality n- and p-type ZnO are indispensable. Interestingly, n-type doping is relatively easy compared to that for the p-type. When ZnO is doped with group III elements, [such as Al, Ga and In], the dopants substitute Zn atoms while the group VII elements [such as Cl and F] substitute O atoms; these two doping lead to n-type. P-type doping in ZnO may be possible by substituting Zn site using group-I elements (Li, Na and K) or substituting O using group-V elements (N,P and As).

The prime objective of this work was to decrease the resistance of ZnO layer deposited using CSP technique through doping. This chapter describes the effects of both 'Ex-situ' and 'In-situ' doping using different elements and the details of these two processes are given in following sections. Ex-situ doping was done through thermal diffusion using Tin and Indium while the in-situ doping was using Indium and Aluminium. Variations in

structural, electrical and optical properties of the samples due to these two are also described in detail in respective sections.

5.2 Effect of doping of ZnO thin film: A review

Benny Joseph et al. studied the variation of structural , morphological , electrical and optical properties of ZnO film prepared using CSP technique due to doping with Aluminum [11]. The films were highly transparent in visible region [97% at 550 nm] and electrically conductive [resistivity of 2.45×10^{-2} Ω cm]. XRD studies – shoed that the films were polycrystalline in nature with (002) preferred orientation.

Aluminium Doped Zinc Oxide(AZO) thin films of 100 nm thickness were prepared by systematically changing the number of "Diethyl Zinc(DEZ, $Zn(C_2H_5)_2$)- Distilled-water cycles" [at 150 °C] in 'Atomic Layer Deposition' (ALD) method [12]. ZnO films grown without any TMA- Distilled water cycle exhibited a polycrystalline nature having (100), (002),(101), and (110) orientation. But AZO films crystallized preferentially along the (100) direction as a result of doping with Al. The lowest resistivity of 4.5×10^{-3} Ω cm was observed for AZO films ~100 nm thick and grown with Al doping of 3.0 at. %.

In-doped (2 mol%) ZnO films on glass substrates were deposited using the spray pyrolysis method at 500 °C [13]. Samples were annealed under N_2 atmosphere between 100 and 600 °C for 5 min.XRD spectra indicated that the *c*-axis intensity to *a*-axis is slightly increased with the increase in annealing temperature, along with degree of crystallinity. Average surface roughness and average grain size were almost constant with increasing annealing temperature. Electrical resistivity decreased to 4.0×10^{-2} Ω cm when electron mobility and carrier concentration were 3.0 cm $V^{-1}s^{-1}$ and 7.0×10^{19} cm^{-1} respectively at annealing temperature of 450 °C.

Effect of variation of precursors on the c-axis orientation in pure and doped ZnO films deposited using spray pyrolysis technique was also studied [14]. These authors used aluminium nitrate and aluminium chloride as precursors for aluminium doping and also the different ratios of the ZnO precursors were tried (zinc chloride, zinc acetate and the ratio of zinc chloride and acetate). Films obtained from zinc chloride and zinc chloride /zinc acetate ≥0.5 had the largest crystalline sizes of 46 nm. The preferential orientation changed by changing the deposition condition viz., the substrate temperature, precursor solution composition or by introducing aluminium.

In yet another work, the dependence of electrical and optical properties of the temperature of substrate and target had been studies for Al- and Si- doped ZnO films, prepared using R.F. sputtering [15]. The lowest resistivity was obtained for substrate temperature in the range 180-220^{o}C, mainly due to the improvement in crystallanity.

When comparing the resistivity of undoped ZnO thin films with Sn-doped ZnO thin films, it is found that the resistivity decreases. The decrease in resistivity may be explained as follows: since the ionic radius of tin (r_{Sn}^{4+} = 0.38 °A) is smaller than that of the zinc ion (r_{Zn}^{2+} = 0.6 °A),tin atoms doped into ZnO lattice act as donors by supplying two free electrons when the Sn^{4+} ions occupy Zn^{2+} ion sites. This in turn increases the free carrier concentration and hence, decreases the resistivity. The mechanism of the conduction can be described by the following equation:

$$SnO_{2\,ZnO} \rightarrow Sn^{ll}Z\_n + O^{x}_{O} + 1/2O_2 + 2e^{l} \qquad (5.1)$$

Sn^{4+} ions substituted Zn^{2+} ions in the lattice induce positive Sn^{ll}_{Zn} charges in the material. In order to maintain electrical neutrality, two negative electrons are induced to compensate the excess positive charges. Hence the resistivity decreases due to increasing free electrons in the film. Sn-doped ZnO (SZO) films, prepared using SILAR technique, were used as NO_2 gas sensor and the results were reported [16]. Experimental results showed that the sensitivity of ZnO films increased on Sn doping

Y.Caglar et al. [17] prepared undoped and SZO thin film using spray pyrolysis. Effect of Sn doping on structural and morphological properties of ZnO films was investigated using XRD and SEM. XRD patterns confirmed that the film had polycrystalline nature[(100),(002),(101),(102) and (110). While pristine ZnO had the (101) preferred orientation, Sn doped ZnO films were having (002) orientation.

Nano structured pure and SZO synthesized for gas sensing application by thermal evaporation technique [18].SEM images indicated change in the growth pattern from nano-wire [for pure ZnO] to tetra pods [for SZO]. The response towards different gases for Pure and SZO were recorded. Pure ZnO nano-wires exhibit selective response towards acetone vapour while for SZO, the response decreased. The deviation from stoichiometry and the morphology of ZnO are probably responsible for such a difference in gas response. Pure and Sn doped ZnO showed nearly same crystallite size.

M.R Vaezi et al. [19] reported the preparation of SZO films from a Zinc complex solution containing tin ions on to pyrex glass substrate using two-stage chemical deposition process. Resistance of the undoped ZnO films is high and reduces to a value $4.2x10^{-2}$ ohm cm when 2.5% Sn is incorporated. All of the ZnO films have above 80% transmittance in a rage of 400-700 nm. The optical energy gap (Eg) increases with the increase of doping amount of Sn in the films.It varied from 3.05 to 3.18 eV depending on the amount of Sn incorporated.

NO_2 gas sensor was fabricated by successive ionic layer adsorption and reaction (SILAR) technique and rapid photo thermal processing (RPP) of the SZO film [20]. Influence of variation of Sn concentration in the chemical bath and the RPP temperature on NO_2 sensitivity of thin film sensor elements was investigated in this work. Higher sensitivity was obtained at 5–10 at %, Sn concentration in the solution of ions and RPP temperature of 550–650^oC. Another report was on preparation of Al or Sn doped ZnO films using spray pyrolysis [21] . These films were deposited on either indium tin oxide (ITO) coated or bare glass substrates. $ZnCl_2$, $AlCl_3$ and $SnCl_2$ were used as precursors. The properties of the films have been studied before and after annealing 4 h at 400^0C in vacuum (10^{-3} Pa). Here the lowest electrical resistivity achieved was due to doping with Sn ($3x10^3$ Ohm cm) and this was further lowered by 2-3 order of magnitude after the vacuum annealing (0.9 Ohm cm).

Paraguay et al. [22] prepared sprayed ZnO film and doped with different elements, Al, In, Cu, Fe and Sn. Sensitivity of the films were studied in two steps: first as a function of their temperature (435-675 K) for a fixed ethanol concentration (40 ppm) and the next case was as a function of ethanol concentration (4-100 ppm) for a fixed temperature (675 K). A better sensitivity can be observed for Sn- and Al-doped films, with a dopant/Zn ratio of 0.4 at.% and 1.8 at.%, respectively.

Bougrene et al. deposited ZnO:Sn films using spray pyrolysis technique on glass substrates and physico-chemical properties of these films were studied [23] Crystallinity and optical transmittance improved on doping. Lowest resistivity obtained was $5x10^{-2}$ ohm cm. Olvera and Maldonado reported the deposition of high quality ZnO:Ga films using CSP technique[24] . Two different precursors were used for the deposition. Lowest resistivity obtained was $4.5x10^{-3}$ ohm cm and the average optical transmittance in the visible region was about 85 %.

5.2.1 Summary of best results

Different group tried to deposit ZnO films using different technique. Hahn et al. deposited highly conductive polycrystalline ZnO films using MOCVD technique with resistivity of the order of $3x10^{-4}$ ohm cm. Average optical transmittance was nearly 85%[25]. Minimum resistivity of $1.4x10^{-4}$ ohm cm was obtained with Al doping [26] by Jeong et al. These films exhibited an average of 95% in the visible region. Chen et al could get lowest resistivity of $8.54x10^{-5}$ ohm cm in films deposited using PLD technique, which showed an average optical transmittance of 88% [27]. Chemical spray pyrolysis technique generally resulted in resistive films compared to the samples from physical method like sputtering and PLD. S.Major et al. [28] reported the lowest resistivity of $8\text{-}9\times10^{-4}$ Ω cm in Indium-doped spray pyrolysed ZnO thin films .H. Gómez-Pozos et al. [29] recently achieved the lowest resistivity of Al –doped spray pyrolysed ZnO thin film (4.3×10^{-3} Ω cm). They achieved this by doping the samples using 'Aluminum 2,4 pentanedionate' followed by high temperature vacuum annealing treatment.

5.3 Experimental details

The ZnO films for doping studies were prepared using CSP technique. Spray solution was prepared by dissolving 0.3M of the Zinc acetate in the solvent containing equal volume of isopropyl alcohol and deionised water. The typical value of pressure used for this deposition was ~5psi and the substrate temperature was kept at 450 ± 5^{0}C.The sample is removed easily after the deposition and cooled using post deposition treatment called 'Zero-energy process' (Discussed in the chapter-3, Secion-3.2.2). For further reduction of the resistance material like Aluminium, Indium and Tin were doped with different doping method (In-situ and Ex-situ doping). The structural, optical and electrical properties of the samples was studied by X-Ray diffraction (XRD), Spectrophotometer and Photoluminescence (PL) ('as described in chapter (4) Section (4.3.1). The carrier concentration and Hall mobility were measured using the Hall Effect instrument with magnetic field of 0.57T (Model-HMS-3000, 'Ecopia',).

5.3.1 Ex-situ doping

In 'ex-situ doping', a thin layer of In/Sn was deposited over the undoped ZnO thin films using vacuum evaporation [Pressure ~ 2×10^{-5} mbar] method and this bilayer films were annealed in vacuum [Pressure ~ 2×10^{-5} mbar; Temperature-100 ^{0} C; Time- 60 min].

Different masses of In/Sn (2, 4, 6, 8 and 10 mg) were deposited over the surface of ZnO sample. These samples were annealed in vacuum for diffusing the In/Sn in to the ZnO layer. Evaporation of In/Sn and annealing did not affect thickness of the sample. The samples were named as Z-2mg-In, Z-4mg-In, Z-6mg-In, Z-8mg-In, Z-10mg-In [Indium doped samples] and Z-2mg-Sn, Z-4mg-Sn, Z-6mg-Sn, Z-8mg-Sn, Z-10mg-Sn[Tin doped samples] respectively.

5.3.2 In-situ doping

In order to reduce the resistivity further, Indium was doped by adding the required quantity of Indium nitrate in the spray solution itself and this was denoted as 'in-situ doping'. Doping percentage of Indium was varied from 0.5 to 2.5% and the samples were named as Z-0.5In, Z-1In, Z-1.5In, Z-2In, Z-2.5In respectively. All other spray parameters are kept constant.

Next we tried the 'In-situ doping' of Aluminum, by adding the required quantity of aluminum 2,4 pentanedionate in the spray solution itself. Doping percentage of Aluminum was varied from 0.5 to 3.5% and the samples were named as AZ-0.5,A Z-1, AZ-1.5, AZ-2,A Z-2.5 respectively.

5.4 Results and discussion

5.4.1 Effect of Sn doping through ex-situ technique

5.4.1.1 Structural properties

X-ray diffraction patterns of undoped and doped ZnO thin films prepared at optimum parameters are exhibited in Fig 5.1 The diffraction peak corresponding to (002) orientation is located at $2\theta = 34.45^{\circ}$. It was observed that all the samples had the preferential orientation along (002) plane and intensity of peak corresponding to this orientation increased with Sn doping concentration. The c -axis of the grains became uniformly perpendicular to the substrate surface. No new phases were observed, even when the mass of evaporated Sn was increased up to 10 mg, indicating that incorporation of Sn neither could change the 'wurtzite' structure of ZnO nor resulted in the formation of SnO_2.

Mean crystallite size was calculated using the (002) diffraction peak using Debye-Scherrer formula, $D=.9\lambda/\beta Cos\ \theta$, [Where D is the diameter of the crystallite, λ wave length of CuKα line (λ = 1.5404 Å), β is the full width at half maximum in radians and θ is the

Bragg angle]. This result is depicted in Fig .5.2. Bougrine et al. [23] reported that the peak intensity of the Sn doped ZnO films was higher than that of the undoped samples, and Sn doped ZnO films had (002) as the preferred orientation. However Navale et al. [18] reported that Sn doped ZnO thin films had (101) as the preferred orientation.

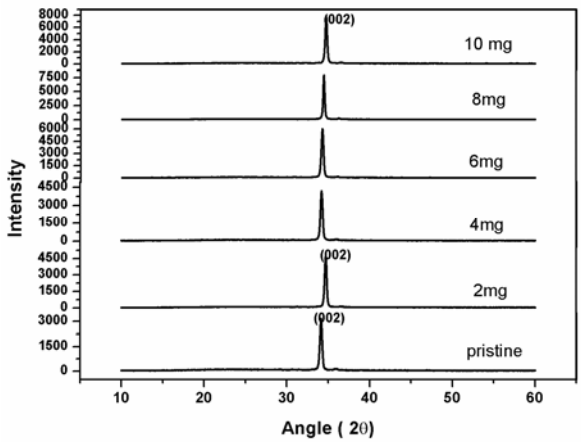

Fig.5.1 XRD pattern of pristine and Sn doped [using Ex-situ method] ZnO thin films

The crystallite size increases initially with the increase of Sn content and reached a maximum value of 38 nm and reduced afterwards (Fig. 5. 2). Probably there might be substitution of oxygen due to Sn anions in Zn sites, leading to a partial healing of the crystalline structure [23]. This can be also considered to be the 'effect of crystallization process with doping' [30].

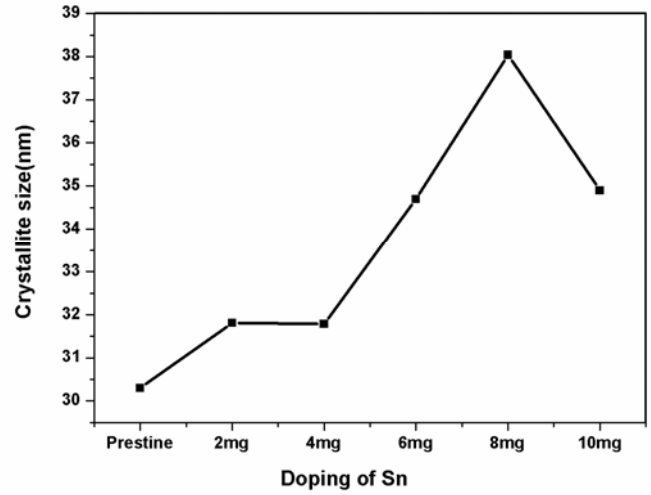

.

Fig.5.2 Variation of crystallite size of Sn doped ZnO film with doping percentage

5.4.1.2 Optical properties

Optical absorption spectra were recorded in the wavelength region 200 -1200 nm. In order to determine the optical band gap, $(\alpha h\nu)^2$ against hν graph was plotted (Fig. 5. 3) as described earlier. The band gap of the pristine sample was 3.28 eV and remained almost the same for the doped samples too.

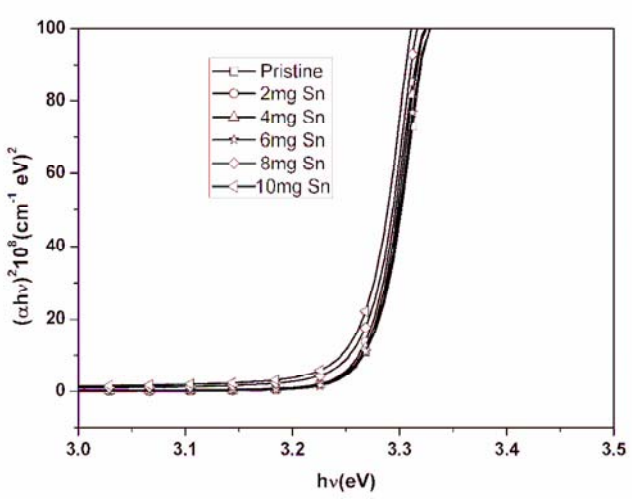

Fig. 5.3 $(\alpha h\upsilon)^2$ versus hυ graph for the Sn doped ZnO thin films

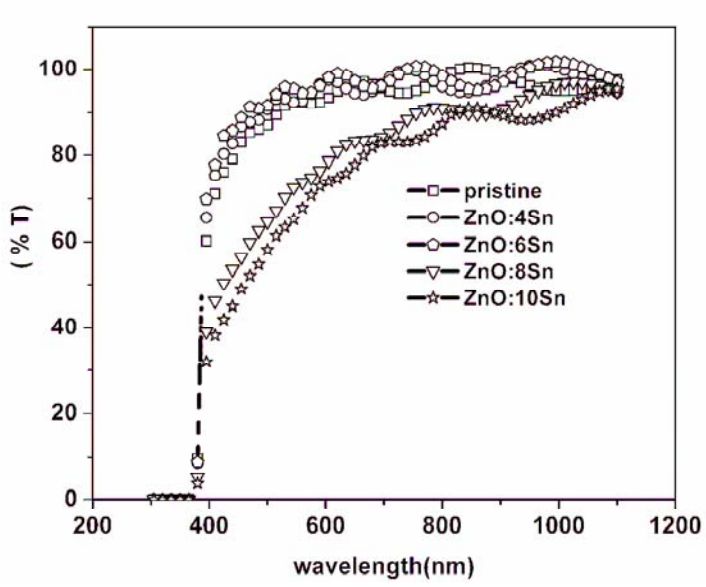

Fig.5.4 Transmission spectra of ZnO (Sn doped and pristine) thin films

Fig.5.4 makes it clear that the percentage of transmission decreased with increasing the doping concentration. The sample ZnO-6mg-Sn attained transmission above 80%. In fact the 'metal to oxygen ratio' decided the transmission [31, 32] .If the sample is metal rich, it will have low transmission. Here it is quite clear that as doping percentage increased, the (Zn+Sn)/O ratio is also increased, leading to the reduction in optical transmission.

5.4.1.3 Electrical resistivity measurement

Electrical Resistivity measurements were carried out using two – probe method. The pristine sample had a resistivity of 2.8 $\times 10^{-2}$ Ω cm. When the doping percentage increased the resistivity decreased and ZnO-10mg-Sn had the lowest resistivity of 8×10^{-3}Ω cm. As pointed out in the many works [33,34] the main factor affecting the resistivity of sprayed ZnO thin films is zinc interstitial and /or oxygen vacancies and quantity of dopant diffused into the ZnO lattice. The decrease in the resistivity must be due to the donor action of tin, through replacement of Zn atoms and / or occupying the interstitial position.

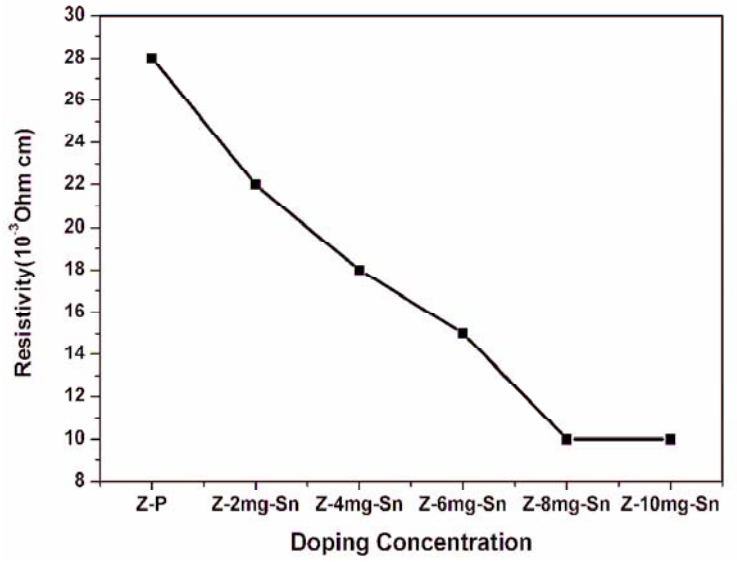

Fig.5.5 Variation of electrical resistivity of Sn doped ZnO with doping percentage.

5.4.2 Effect of ex-situ doping using Indium Diffusion

5.4.2.1 Structural properties

Fig.5.6 shows XRD pattern of the ZnO thin films doped with different indium concentrations. It was found that all the films had preferential orientation along (002) plane.

Zn can be easily substituted by In without any lattice distortion due to the similarity in their atomic sizes (Atomic radii of Zn and In atoms are r_{Zn}^{2+}=0.074 nm and r_{In}^{3+}=0.080 nm respectively). Hence one could state that, due to indium diffusion, oxygen concentration was also not varying much in the sample. Again, the doped samples maintained the (002) orientation, indicating that the c -axis of the grains became uniformly perpendicular to the substrate surface. In the case of indium doping also no new phases were observed, even when mass of evaporated In was increased up to 10 mg, indicating that incorporation of indium neither could change 'wurtzite' structure of ZnO nor resulted in the formation of In_2O_3 or In_2S_3.

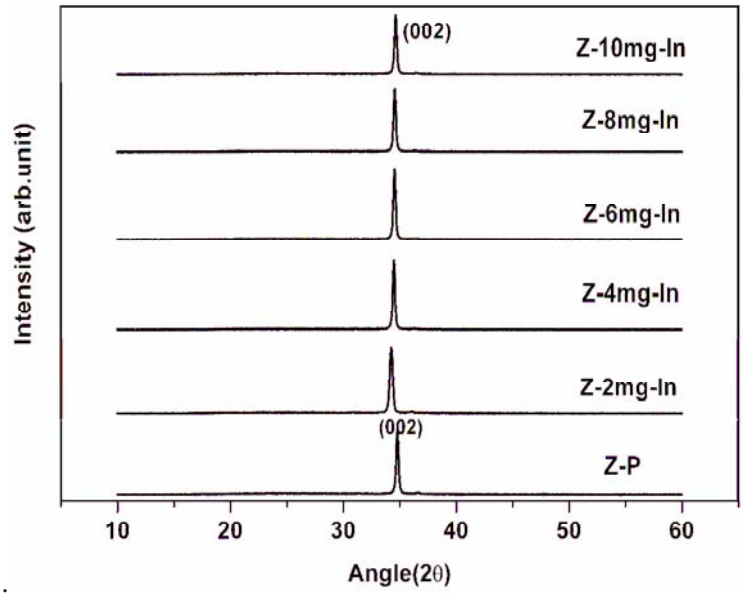

Fig.5.6 XRD pattern of pristine and-In doped [Ex-situ method] samples

When indium is incorporated into the ZnO thin films through ex-situ method, the crystallite size increased as the mass of the dopant increased from 2 mg to 6 mg. However when the mass of indium diffused was above 6 mg, reduction in the crystallite size was observed. Similar variation of crystallite size was observed in the case of tin diffusion and here the optimum mass was 8 mg.

sample name	lattice parameters a (Å)	c(Å)	c /a	Strain %	Stress(GPa)
Z-P	3.24	5.20	1.60	-0.11	0.49
Z-2mg-In	3.26	5.22	1.60	0.38	-1.72
Z-4mg-In	3.23	5.18	1.60	-0.38	1.72
Z-6mg-In	3.23	5.18	1.60	-0.38	1.72
Z-8mg-In	3.26	5.18	1.58	-0.38	1.72
Z-10mg-In	3.23	5.16	1.59	-0.76	3.44

Table.5.1 Variation of lattice parameters, strain, stress as a function of Ex-situ doping

5.4.2.2 Optical properties

Optical absorption spectra were in the wavelength region 200 -1200 nm. In order to determine the optical band gap, $(\alpha h\nu)^2$ against hν graph was plotted (Fig. 5. 7). Pristine sample has band gap of 3.22 eV; however in the case of Indium doping, the band gap increased with doping percentage. Transmittance decreased at high doping level and this may be due to the increase in scattering of photon by crystal defects created by doping or probably due to the increase in the metal to oxygen ratio (Zn+In)/O [35].

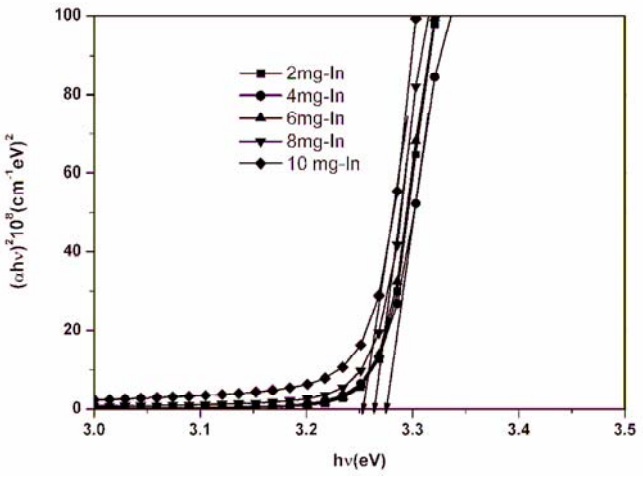

Fig. 5.7 $(\alpha h\upsilon)^2$ versus hυ graph of In doped [through Ex-situ method] samples

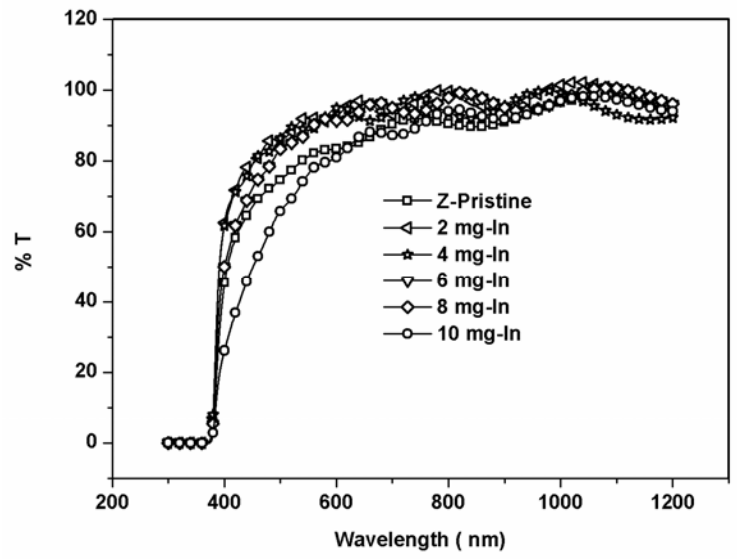

Fig.5.8 Transmission spectra of ZnO [In doped (through Ex-situ method) and pristine] thin films

5.4.2.3 Photoluminescence measurement

The luminescence of ZnO films typically has 'near band edge emission' and 'blue-green emission'. Owing to these properties, ZnO can be used to make devices for UV or blue emission. Since these films find great application in the areas of optics and opto electronics, it is important to investigate the optical properties of ZnO films. Researchers have considered that the UV emission could be due to the excitonic transition. But still controversy exists in the explanation of the origin of blue-green emission.

Ortiz et al. reported the PL spectra of undoped and $TbCl_3$ doped ZnO films. The undoped film had emission at 510 nm, while doped sample exhibited the emission at 550 nm [36,37]. However the exact origin of the blue green emission (510 nm) was not given. This emission was assumed to be due to the transition within a self activated center formed by doubly ionized zinc vacancy and ionized zinc interstitial. Another detailed experimental evidence was given to explain the origin of blue green emission in ZnO phosphor powder [38]. It was suggested that the green emission was due to the recombination of electron in

the singly occupied oxygen vacancies (V_o^+) with photo excited holes in the valence band. Hur et al. discussed the variation in the PL emissions of ZnO due to different annealing conditions in air and found that the concentration of antisite oxygen increased when ZnO ceramics were in O-rich conditions [39]. It was also seen that, as the concentration of O-antisite increased, intensity of green emission also increased. Hence in this report, it was proposed that the green emission resulted from the transition from conduction band to the acceptor level of antisite oxygen. However band edge emission intensity reduced when ZnO was in O-rich condition. In an interesting paper, Lin et al. tried to explain the origin of blue-green emission, in undoped ZnO films [40]. In these samples, two emissions were observed with energies 3.18 eV and 2.38 eV. It was concluded that the green emission was corresponding to the local levels composed by oxygen antisites and the transition was from the conduction band to deep acceptor level of oxygen antisites (O_{Zn})

The PL emission centered at ~510 nm [Blue-Green Emission (BGE)] is the characteristic emission of ZnO thin films. This emission is extremely broad and this might be due to phonon-assisted transition [41]. But the exact reason for this emission is not clearly understood. Ratheesh kumar et al. [35] concluded that this was due to the transition from conduction band to the acceptor level corresponding to the oxygen antisite [O_{Zn}].

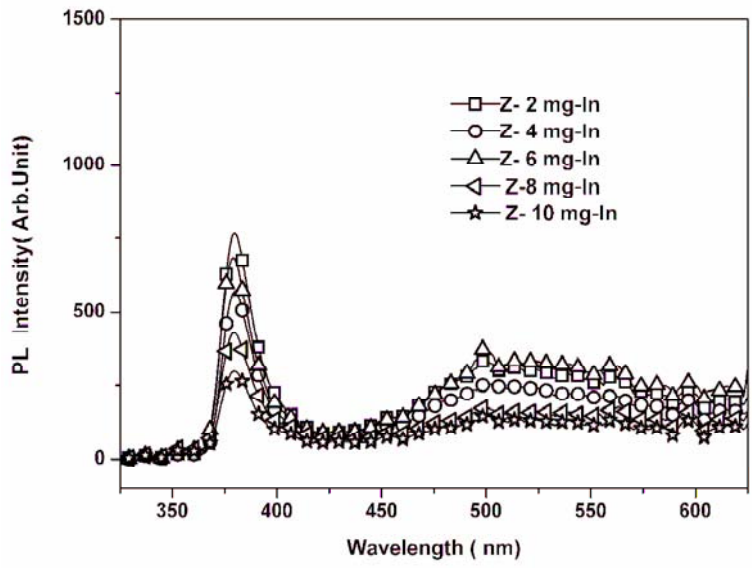

Fig.5.9 Photoluminescence spectra of Indium doped sample [Ex-situ doping]

5.4.2.4 Electrical resistivity measurement

The undoped ZnO sample has resistivity of $2.4\times10^{-2}\ \Omega$ cm. But in the case of samples which were doped using the 'ex-situ method', the resistivity decreased (Fig. 5.10) and the lowest resistivity of $8\times10^{-3}\ \Omega$ cm was obtained for the sample Z-8 mg-In. Resistivity slightly increased as the mass of indium evaporated increased beyond 8 mg.

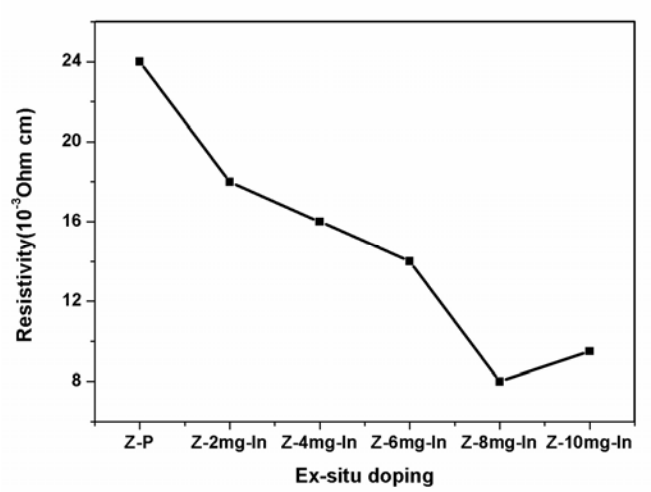

Fig.5.10 Electrical Resistivity of Ex-situ doped Indium in ZnO thin films.

Reason for the variation of resistivity can be explained using the results from XRD and PL analysis of doped samples. Here we find that there is no change in grain orientation due to 'Ex-situ' doping process as revealed by the analysis using XRD technique (Fig. 5.6). After the ex-situ doping of indium its (Zn+In/O) metal to oxygen ratio increased. Metal to oxygen ratio increases density of free carriers for conduction hence the reduction in resistivity. When the metal to oxygen ratio increased, the band edge emission also decreased [39]

5.4.3 Studies on samples doped with Indium through in-situ doping

5.4.3.1 Structural analysis

Fig.5.11 shows XRD pattern of pristine and in-situ doped samples with different Indium concentration. Pristine sample had only peak corresponding to (002) orientation [$2\theta=34.42^0$]. But for the doped samples, another peak corresponding to the orientation of (101) also developed right from the Z-0.5-In onwards. On increasing the doping percentage further, the intensity of peak corresponding to the plane (002) decreased and that of (101)

increased. Finally for the sample Z-2.5-In, the (101) peak was the prominent one. Similar behaviour has been reported in many other works [35, 22].

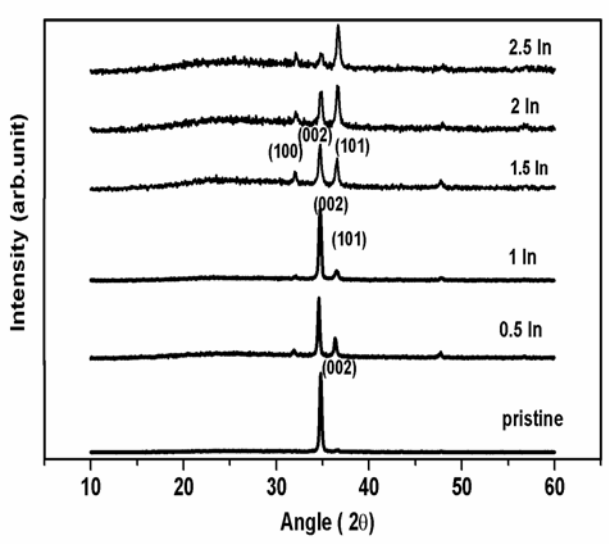

Fig 5.11 XRD pattern of pristine and In doped [In-situ] ZnO thin films

Variation of crystalline size of the doped films, with doping concentration of indium, is shown in the Fig.5.12. In the case of in-situ doping, the crystallite size decreased from 30 nm to 20 nm when the doping concentration of Indium increased.

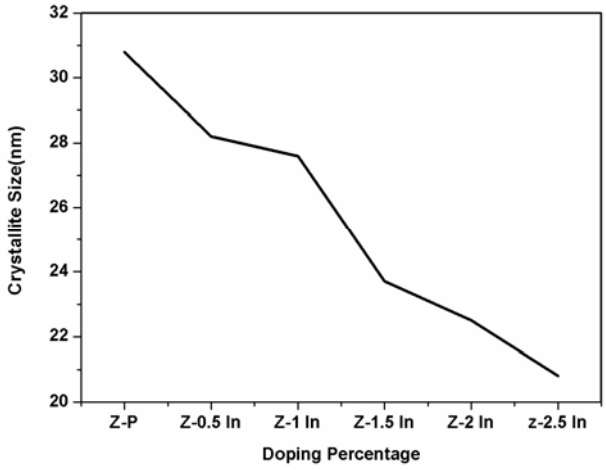

Fig.5.12 Crystallite Size of Indium doped ZnO thin films, through in-situ method.

sample name	lattice parameters a (Å)	c(Å)	c /a	Strain %	Stress(GPa)
Z-P	3.24	5.20	1.60	-0.11	0.49
Z-0.5 In	3.21	5.16	1.60	-0.76	3.44
Z-1 In	3.19	5.16	1.61	-0.38	3.44
Z-1.5 In	3.19	5.16	1.61	-0.38	3.44
Z-2 In	3.19	5.14	1.61	-0.38	3.44
Z-2.5In	3.18	5.14	1.61	-0.76	3.44

Table.5.2 Lattice parameters of In-situ doped In-ZnO thin films.

5.4.3.2 Optical studies

Optical absorption and transmission spectra were recorded in the wavelength region of 350–1200 nm. Optical band gap of the samples is determined using the following equation,

$$\alpha h\upsilon = A(h\upsilon - E_g)^{1/2} \qquad (5.2)$$

Where hυ is the photon energy, E_g is the optical band gap and A is the constant. In order to determine the optical band gap, "$(\alpha h\upsilon)^2$ vs. hυ graph" was plotted (Fig.5.13) . No significant variation in the band gap was observed. In the case of samples which had undergone in-situ doping, optical transmission was above 80% in the visible region (Fig.5.14)

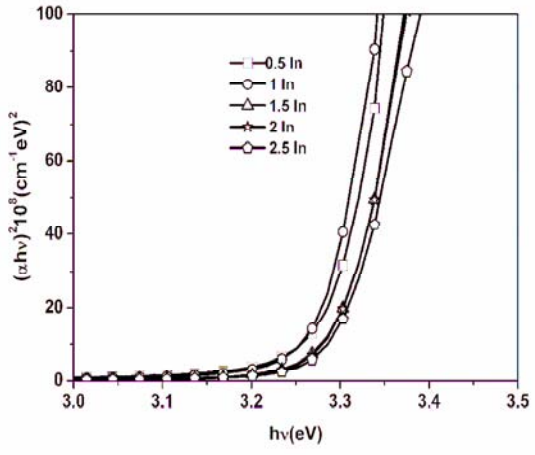

Fig.5.13 $(\alpha h\upsilon)^2$ versus hυ graph for the In doped films [in-situ method]

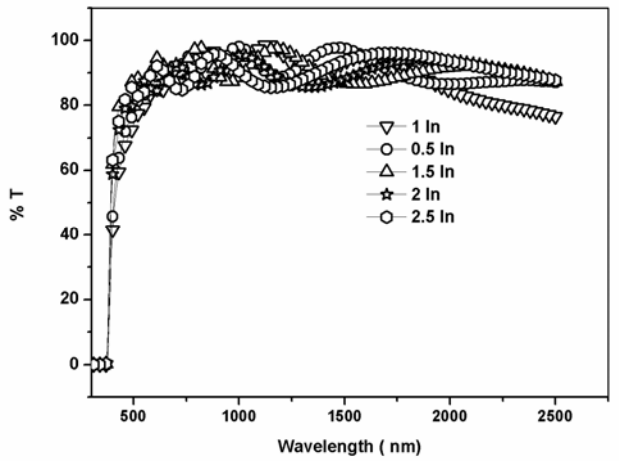

Fig.5.14 Transmission spectra of In-ZnO thin films [in-situ doped]

5.4.3.3 Photoluminescence Measurements

Interestingly the BGE is not present in the case of samples doped through the in-situ process and it is this set of samples which exhibits the lowest resistivity after doping. In-situ doping results in a clear variation of grain orientation from (002) to (101); more than that, just by introducing 1% of indium itself, the resistivity comes to the lowest value of 2x 10^{-3} ohm.cm. Similar observation had been reported by several groups in connection with indium doping in ZnO [42, 40, 22].

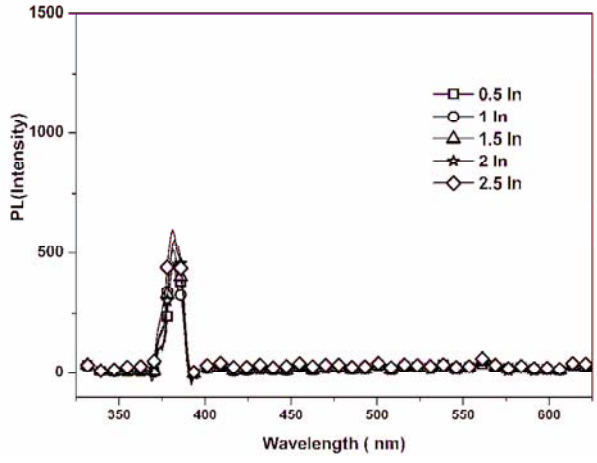

Fig.5.15 PL Spectra of In-situ doping of Indium

5.4.3.4 Electrical resistivity measurement

In the case of in-situ doping also resistivity of the samples decreased on increasing the doping concentration up to 1% of indium and it was 2 $\times 10^{-3}$ Ω cm. This is probably one of the lowest reported resistivity values obtained for Indium doped spray pyrolysed ZnO thin films; it is to be specifically noted here that the samples prepared in our lab are having area of 30 cm^2 . More over the resistivity is uniform over ~80% of the area of the sample (Fig.5.17). In the case of doping of sprayed ZnO samples using indium, Benouis et al. recently reported that 2% doping resulted in the resistivity of 6 $\times 10^{-3}$ Ω cm [43] while Kenji Yoshino et al.[44] reported the lowest resistivity of 4 $\times 10^{-2}$ Ω cm could be achieved in Indium doped samples by annealing in vacuum at 450^0C.

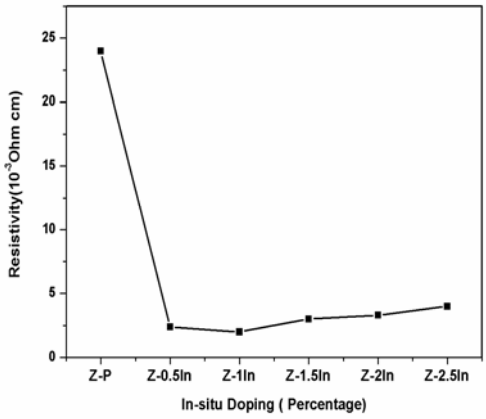

Fig.5.16 Electrical resistivity of ZnO thin film in In-situ doping of Indium

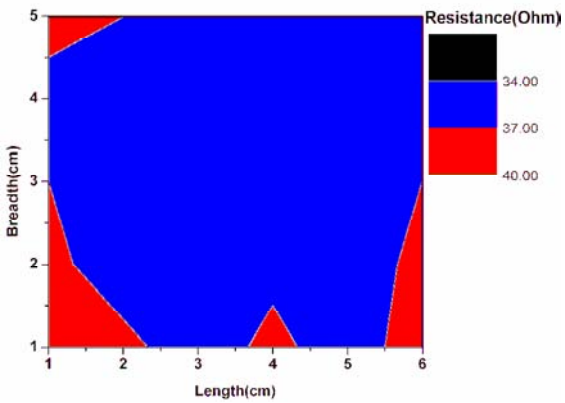

Fig.5.17 Surface mapping of sheet resistance of sample over an area of 30 cm^2 (Z-1%In) The blue region indicates resistance in the range, 34 Ω to 37 Ω / square while the red region indicates the resistance in the range, 37 Ω to 40 Ω / square. Maximum variation ~15%].

5.4.4 In-situ doping of Aluminum

5.4.4.1 Structural Analysis

Fig.5.18 depicts XRD patterns of AZO having different doping percentages. All the AZO samples are having (002) peak (angle 34.42^0) as the prominent one. Intensity of (002) plane increases up to 2.5 % of doping and decreased on further increase in doping percentage. However no extra phases, corresponding to either aluminum or aluminum oxide, were detected.

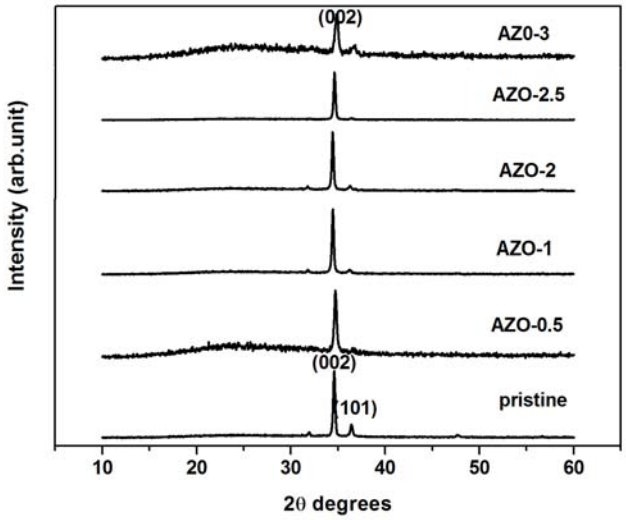

Fig.5.18 XRD pattern of ZnO at different Aluminium concentration .

. .

Sample Name	Plane	FWHM	Crystallite Size(nm)
Pristine	(002)	0.26	31.9
AZO-0.5	(002)	0.30	27.0
AZO-1	(002)	0.22	37.8
AZO-2	(002)	0.22	37.1
AZO-2.5	(002)	0.23	36.5
AZO-3	(002)	0.34	24.7

Table.5.3 preferentially oriented planes and grain size variations of AZO at different doping percentages

When the doping percentage of aluminium increased from 0.5 % to 2.5 %, the grain size also increased from 27 nm to 36 nm and further increasing of doping percentage resulted in decrease of crystallite size

SEM analysis (Fig 5.19) clearly shows that there is a change in the surface morphology of ZnO films due to the presence of Aluminium. Pristine film has hexagonal grains on the surface. But as the doping percentage of Al increased, the structure becomes 'triangular shaped' and this resembles the AZOl thin film samples deposited using a dc-magnetron sputtering [45].

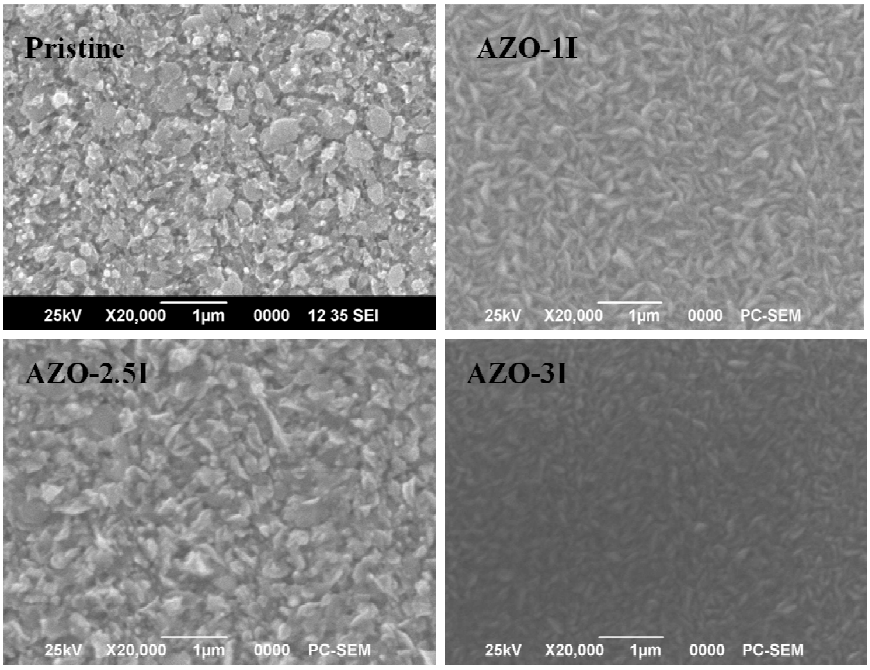

Fig.5.19 SEM micrograph of films with different doping percentage Of AZO

5.4.4.2 Optical studies

Optical absorption and transmission spectra were recorded in the wavelength region of 300–1100 nm. In order to determine the optical band gap, "$(\alpha h\upsilon)^2$ vs $h\upsilon$ graph" was plotted. Plot of "$(\alpha h\upsilon)^2$ vs $h\upsilon$ is linear over a wide range of photon energies, indicating direct band to band transition. Values of the band gaps are given in the table 5.4 which shows that it increased from 3.25 eV to 3.30 eV after the doping. Fig. 5.20 shows that all the films have transmission above 80%.

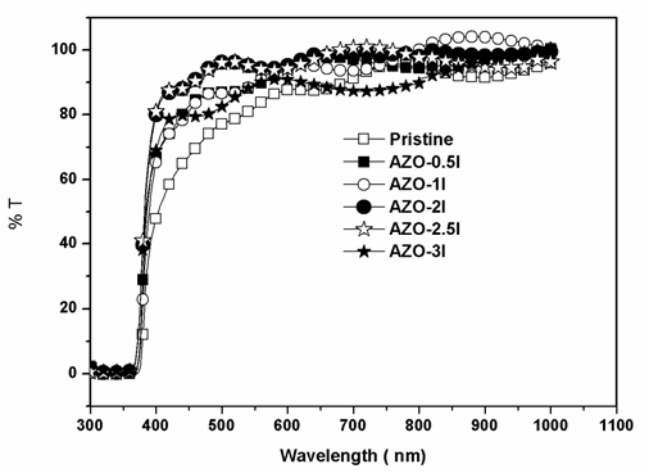

Fig.5.20 Transmission spectra of pristine and AZO samples.

In the case of a transparent conducting oxide film, optical transmission as well as electrical conductivity has to be as large as possible for the application in the opto-electronic devices. 'Figure of merit' is given by the expression, Φ_{TC} = T/Rs where Rs is the sheet resistance of the film and T is the optical transmittance [31].

Sample name	Band Gap(eV)	Figure of merit(Ω^{-1})
Pristine	**3.25**	**9.4×10^{-1}**
AZO-0.5	**3.28**	**4.1×10^{-1}**
AZO-1	**3.29**	**6.0×10^{-1}**
AZO-2	**3.31**	**1.2**
AZO-2.5	**3.30**	**2.4**
AZO-3	**3.30**	**1.2**

Table.5.4Variation of Band gap and figure of merit in AZO-I thin film with different doping concentration

This parameter was calculated for all the samples at wavelength λ=540 nm and it is given in the table. 5.4. The highest value of Φ_{TC} [2.4 Ω^{-1}] was obtained for AZO films doped with 2.5% of aluminum. AZO-2.5 samples have highest transmittance in the whole visible

region. The transmittance of AZO is better than SZO and IZO. Hence from the studies, it was observed that the film could be used as transparent conducting electrode for device like solar cells, flat panel displays etc.

5.4.4.3Photoluminescence measurements

PL spectra, at room temperature, were recorded in the range of 350–625 nm. All the AZO-I samples showed two emission peaks centred at 377nm and 520 nm (Fig.5.21), in which the peak at 377 nm was corresponding to the NBE while the one at ~520nm was corresponding to the characteristic BGE.

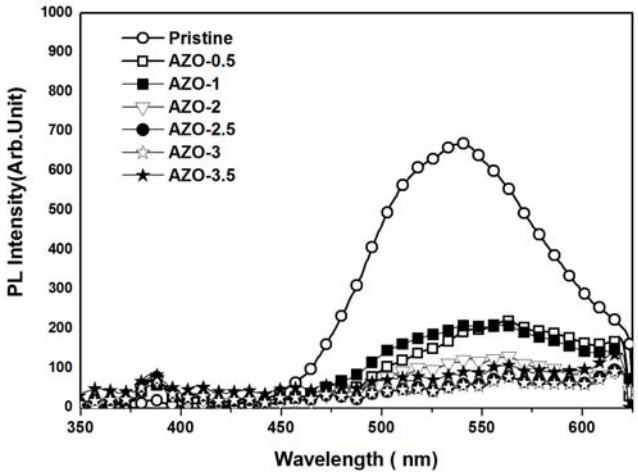

Fig.5.21 Photoluminescence spectra of pristine, AZO samples with different doping concentration.

As stated earlier, PL emission centred at ~ 520 nm [BGE] is characteristic emission of ZnO thin films. This emission was extremely broad and might be due to phonon-assisted transition. Bylander put forward a model, suggesting that the emission was due to electronic transition from interstitial Zn to Zn vacancy [46]. It was also seen that the intensity of NBE emission increased considerably after the hydrogen treatment. Lin et al. tried to explain the origin of BGE, in undoped ZnO thin film [47]. In these samples, two emissions were observed with energies 3.18eV and 2.38 eV .

PL properties depend on the growth conditions, including growth temperature and ambience. In our case, the growth temperature is kept constant and hence the film properties depend on the ambient condition. In CSP technique there is strong possibility of O-rich

condition and oxygen is incorporated in the sample from the atmosphere.PL spectra of these samples also have both UV [NBE] and blue-green emission [BGE]. In the case of ZnO, donors are oxygen vacancy [V_o] and Zinc interstitial [Z_{ni}]. When the sample is kept in the oxygen atmosphere [which usually happens in CSP technique] the oxygen concentration increases. In this condition, quantity of oxygen diffusing into the sample increases reducing oxygen vacancies. Hence the Oxygen antisite (O_{zn}) in the oxygen rich condition is easily formed from the interstitial oxygen (Oi) and zinc vacancies (V_{zn}). More over Oxygen antisite has relatively low formation energy [48].

In CSP method, as air is used as the carrier gas, there is every chance for the enhancement of concentration of oxygen antisite in ZnO film. This condition results in the increase of BGE intensity which is due to the transition from the conduction band to antisite oxygen (O_{zn}). However intensity of the BGE decreased with the increase in the doping percentage of aluminium. When the Aluminium was doped in the film, it was assumed that some of aluminium atoms occupied the zinc lattice site, reducing the probability of oxygen occupying the zinc site. Hence the density of oxygen antisite would be less in the film. This might be the reason for the decrease in the intensity of BGE due to doping. Resistivity of the film decreased with aluminium doping at lower concentration, which proved the occupancy of Aluminium at zinc site. After reaching the optimum percentage of doping, intensity of this peak started increasing. It is also worth mentioning here that the resistivity became minimum at the optimum doping percentage.

5.4.4.4 Electrical studies

Electrical measurements were done employing 'two probe technique' and for this two electrical contacts using silver paint [in the form of two end contacts having distance of 1cm between them] were used. In this study, the sheet resistivity is calculated by the following equation $\rho=R_s d$. Where ρ is the resistivity, R_s is the sheet resistance (Ω/sq) and d is the sample thickness (nm). The undoped ZnO sample had resistivity of $2.4\times10^{-2}\Omega$ cm. After doping, resistivity of the sample decreased and Fig. 5.22 shows that the lowest resistivity of 1.5×10^{-3} Ω cm is obtained for AZO-2.5 sample. Four probe measurements were also in good agreement with the electrical resistivity values measured using two probe method (1.2×10^{-3} Ω cm).

Sample	Bulk Carrier concentration (cm^{-3})	Sheet carrier concentration(cm^{-2})	Mobility (cm^2/Vs)	Hall Co efficient (cm^3/C)
AZO-1	-1.326E+19	-1.326E+15	1.601E+01	-4.707E-01
AZO-2	-1.473E+19	-1.473E+15	1.622E+01	-4.239E-01
AZO-2.5	-1.866E+19	-1.866E+15	1.655E+01	-3.346E-01
AZO-3	-1.625E+19	-1.625E+15	1.191E+01	-3.840E-01

Table.5.5 Hall co-efficient, mobility and carrier concentration of AZO samples with different percentage of doping.

After doping, resistivity of the AZO thin films decreased due to the gradual replacement of Zn^{+2} ions by Al^{+3} ions, releasing a free electron to the conduction band for every Al ion incorporated into the lattice. In order to verify this, Hall measurement was conducted on the doped samples. This clearly proved that carrier concentration in doped samples was increasing as doping concentration increased. In addition to this, the Hall measurement has also indicated that the mobility of carriers was increasing up to the optimum doping concentration (Table.5.5). Hence the increase of carrier concentration and mobility resulted in the decrease of resistivity of the doped samples. However carrier concentration and Hall mobility are increasing only up to the doping percentage of 2.5% after which both start decreasing. Enhancement of concentration of aluminium atoms in the film beyond the optimum value [2.5%] may be resulting in the action of these dopant atoms as 'scattering centres' [49], leading to the lower carrier mobility.

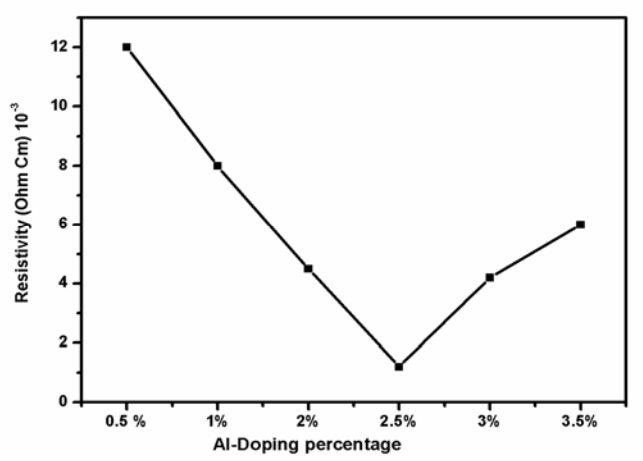

Fig.5.22 Variation of electrical resistivity of AZO thin film with doping percentage.

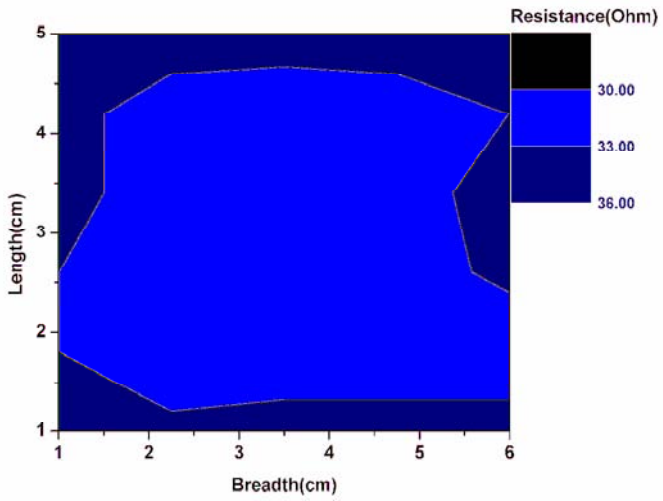

Fig. 5.23 Surface mapping of sheet resistance of AZO-2.5 sample over an area of 30 cm^2 (Z-2.5%Al) .The blue region indicates resistance in the range, 30Ω to 33 Ω / square while the navy blue region indicates the resistance in the range, 33Ω to 36 Ω / square.

5.4.4.5 Annealing Effect

In order to reduce the resistivity of doped film further, the film having the lowest resistivity [Z-2.5Al] was annealed at 450^0C for 2 hours at pressure of 2×10^{-5} mbar, with heating and cooling rate as 5^0C/min. Crystallanity improved after the annealing. Electrical resistivity also reduced drastically by one order, to $6\times10^{-4}\Omega$ cm. The reason for the reduction of resistivity may be attributed to desorption of oxygen leading to the annihilation of the oxygen acceptor state in the sample [41].

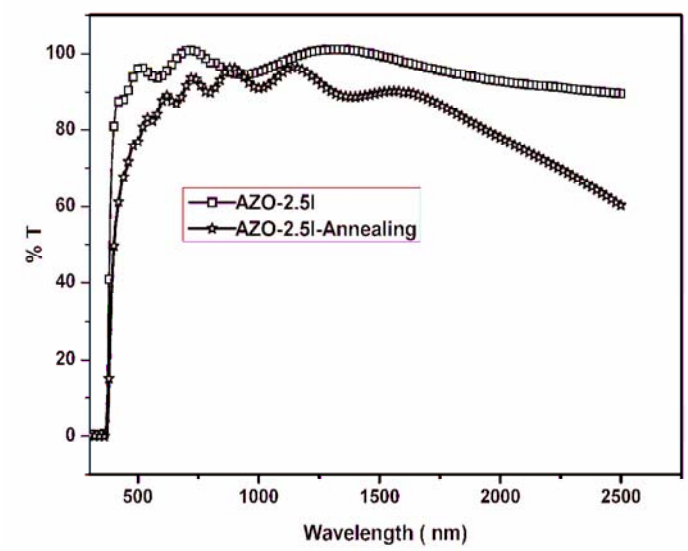

Fig.5.24 Transmission spectra of AZO and AZO- annealed samples.

Fig.5.24 shows that the transmission spectrum of AZO film before and after vacuum annealing. Transmission in the NIR region considerably decreased after the vacuum annealing. This is probably due to the free carrier absorption, a phenomenon that is common in all transparent conductors with higher carrier concentration [51]. The absorption in NIR region is usually not seen in ZnO films and this makes it difficult to do 'laser scribing' using IR lasers. This results hints that this will become possible provided we fully optimise the NIR absorption.

5.5 Conclusions

Large area Zinc oxide thin films having good opto-electronic properties can be prepared using CSP technique through optimisation of deposition parameters and proper

doping. In the present work, ZnO films were doped with tin through thermal diffusion. Successive annealing 100 ^{0} C in vacuum resulted in diffusion of the whole tin in to the sample. There is small variation of band gap after the doping. Resistivity of the sample reduced from 28×10^{-3} Ω cm to 8×10^{-3} Ω cm. Transmittance of the sample decreased when the doping percentage increased.

Doping using Indium was carried out in two ways such as in-situ as well as ex-situ method. In-situ doping using Indium is an excellent method for enhancing the conductivity of the sample. Incorporation of 1% Indium through in-situ method resulted in giving the lowest resistivity of 2×10^{-3} Ω cm and >80% transmission in visible region. PL analysis also supported the results from electrical characterisation studies of the samples.

Aluminum was doped by adding the required quantity of aluminum 2,4 pentanedionate in the spray solution itself [In-situ method]. Doping percentage of Aluminum was varied from 0.5 to 3.5%. Samples doped with aluminium in the range 2 to 2.5 % had lowest resistivity of 1.5×10^{-3} Ω cm[having large area- 30cm^2]. Annealing of these samples in vacuum further lowered the resistivity [6×10^{-4} Ω cm], with optical transmittance [in visible region] remaining in the range 85 to 90%.

Transmission in the NIR region decreases after the vacuum annealing; this is common in all other transparent conductors [like ITO] with higher carrier concentration. Room temperature PL revealed that the intensity of the blue-green emission (520 nm) decreased in these samples. Lowest intensity for the PL emission was also obtained for the sample having the optimum doping. The 'zero-energy process' was found to be very useful to large area samples too and hence suited for photovoltaic device applications.

References

[1] S. Ilican, Y. Caglar , M. Caglar and F. Yakuphanoglu, Appl. Surf. Sci. **255** (2008) 2353.

[2] F. Yakuphanoglu, Y. Caglar, S. Ilican and M. Caglar, Physica B **394** (2007) 86.

[3] X.B. Wang, C. Song, K.W. Geng, F. Zeng and F. Pan, Appl. Surf. Sci. **253** (2007) 6905.

[4] V.S. Khomchenko, T.G. Kryshtab, A.K. Savina, L.V. Zavyalova, N.N. Roshchina, V.E. Rodionov, O.S. Lytvyn, V.I. Kushnirenko, V.B. Khachatryan and J.A. Andraca-Adame, Superlattices Microstruct. **42** (2007) 94.

[5] D.Y. Chen and C.-Y. Hsu, Superlattices Microstruct. **44** (2008) 742.

[6] S. Venkatachalam, Y. Iida and Yoshinori Kano, Superlattices Microstruct. **44** (2008) 127.

[7] Y. Caglar, S. Ilican, M. Caglar and F. Yakuphanoglu, Spectrochim. Acta A **67** (2007) 1113.

[8] M.R. Vaezi and S.K. Sadrnezhaad, Mater. Sci. Eng. B **141** (2007) 23.

[9] S. Ilican, Y. Caglar, M. Caglar, F. Yakuphanoglu and J. Cui, Physica E **41** (2008) 96.

[10] M. Caglar, S. Ilican, Y. Caglar and F. Yakuphanoglu, J. Mater. Sci.,Mater. Electron. **19** (2008) 704.

[11] Benny Joseph **,** P.K. Manoj and V.K. Vaidyan,Ceramics International **32**(2006) 487.

[12] Parag Banerjee,Won-Jae Lee, Ki-Ryeol Bae,Sang Bok Lee and G.W. Rubloff,Journal of Applied Physics **108** (2010)043504.

[13] Kenji Yoshino, Satoshi Oyama, Masahiro Kato, Minoru Oshima,Minoru Yoneta and Tetsuo Ikari, Journal of Physics: Conference Series **100** (2008) 082019.

[14] R. Romero, D. Leinen , E.A. Dalchiele , J.R. Ramos-Barrado , and F. Martín ,Thin Solid Films **515** (2006) 1942.

[15] T. Minami, H. Sato, T. Sonoda, H. nanto and S. Takata, Thin Solid Films **171** (1989) 307.

[16] S. T. Shishiyanu, T. S. Shishiyanu and O. I. Lupan, Sensors and Actuators **107** (2005) 379.

[17] Yasemin Caglar , Seval Axsoy,Saliha Illican and Mujdat Caglar, Super lattice and Microstructure **46** (2009) 469.

[18] S.C. Navale and I.S. Mulla, Mater. Sci. Eng. C **29** (2009) 1317.

[19] M.R.Vaezi and S.K. Sadrnezhaad, Materials Science and Engineering B **141** (2007) 23.

[20] S.T. Shishiyanu, T.S. Shishiyanu and Oleg I. Lupan, Sensors and Actuators B, **107** (2005) 379.

[21] F. Kadi Allah , S. Y. Abe , C.M. Nunez , A. Khelil , L. Cattin, M. Morsli,J.C. Bernede A. Bougrine , M.A. del Valle and F.R. Dıaz, Applied Surface Science **253** (2007) 9241.

[22] F. Paraguay D. M. Miki-Yoshida , J. Morales, J. Solis and W. Estrada L. Thin Solid Films **373** (2000)137.

[23] A. Bougrene, M. Addou, A. Kachouane, J. C. Bernede and M. Morsli, Mater. Chem. Phys. **91** (2005) 247.

[24] M. de la L. Olvera and A. Maldonado, Phys. Stat. Sol. (a) **196** (2003) 400.

[25] B. Hahn, G. heindel, E. P. Schoberer and W. Gebhaardt, Semicond. Sci. Technol.**13** (1998) 788.

[26] W.J. Jeong, S.K. Kim and G.C. Park, Thin Slid Films **506-507** (2006) 180.

[27] M. Chen, Z. L. Pei, X. Wang, C. Sun and L. S Wen, J. Vac. Sci. Technol. A, **19** (2001) 963.

[28] S.Major, A.Banerji and K. L.Chopra , Thin Solid Films **108** (1983) 333.

[29] H Gómez-Pozos, A Maldonado and M de la L. Olvera, Materials Letters **61**(2007) 1460.

[30] P.K. Manoj, Benny Joseph, V.K. Vaidyan, and D. Sumangala Devi Amma, Ceram. Int. **33** (2007) 273.

[31] H.L.Hartnagel,A.L.Dawar, A.K.Jain and C.Jagadish, Semiconducting transparent thin films.(Bristol and Philadelphia,Inst.phys.pub)(1995)p 306.

[32] P.M. Ratheesh Kumar, C.Sudha Kartha , K.P. Vijayakumar, F.Singh and D.K. Avasthi, Material Science and Engineering B**117** (2005) 317.

[33] A. Rodrı´guez-Ba`ez, A. Maldonado, G. Torres-Delgado, R. Castanedo-Pe`rez and M.de la L. Olvera, Mater. Lett. **60** (2006) 1594.

[34] D.J. Goyal, C. Aagashe, M.G. Takwale, B.R. Marathe and V.G. Bhide, J.Mater. Sci. **27** (1992) 4705.

[35] P. M. Ratheesh Kumar, C.Sudha Kartha, K. P. Vijayakumar, T.Abe, Y.Kashiwaba F. Singh and D.K Avasthi, Semiconductor. Sci.Technol.**20** (2005) 120.

[36] A.Ortiz,C.Falcony,M.Garcia and A.Sanchez, J.Phys.D:Appl.Phys.**20** (1987) 670.

[37] C.Falcony, A.Ortiz, M.Garcia and J.S.Helman, J.Appl.Phys.**63** (1988) 2378.

[38] K. Vanheusden, W. L. Warron, C. H. Seager, W. L. Warren, D.R. Tallant, J. A. Voigt and B. E. Gnade, J. Appl. Phys. **79** (1996) 7983.

[39] T. B. Hur, G. S. Jeen, Y. H. Hwang and H. K. Kim, J. Appl. Phys.**94** (2003) 5787.

[40] B. Lin, Z. Fu and Y. Jia, Appl. Phys. Lett. **79** (2001) 943.

[41] D. C. Reynolds, D. C. Look, B. Jogai and H. Mokoc, Solid State Commun. **101** (1997) 643.

[42] Miki-Yoshida M, Paraguay-Delgado F, Estrada-Lopez W and Andrade , Thin Solid Films **376** (2000) 99.

[43] C.E. Benouisa, M. Benhalilibaa, A. Sanchez Juarezb, M.S. Aidac, F. Chamid and F. Yakuphanoglue, J. Alloys and Compounds **490** (2010) 62**.**

[44] Kenji Yoshino, Satoshi Oyama, Masahiro Kato, Minoru Oshima,Minoru Yoneta and Tetsuo Ikari, J.Phy. Conference Series **47** (2008) 8170.

[45] H Sato, T .Minami, Y .Tamura, S .Sakata, T .Mouri and N. Ogawa , Thin solid films **246** (1994) 65.

[46] E. G. Bylander, J. Appl. Phys. **49** (1978) 1188.

[47] B.Lin,Z.Fu and Y.Jia,Appl.Phys.Lett. **79** (2001) 943.

[48] E.C.Lee, Y.S.Kim, Y.G.Jin and K.J.Chang, Physica B **308-310** (2001) 912.

[49] Y.Igasaki and H.Saito J. Appl.Phys. **70** (1991) 3613.

[50] P. Nunes, A.Malik, B. Fernades, E .Fortunato, P .Vilarinho and R .Martins, Vacuum **52 (**1999) 45.

[51] Mizuhashi M, Thin Solid Films **70** (1980) 91.

Chapter 6

Effect of co-doping in spray pyrolysed ZnO thin film

6.1 Introduction

6.1.1 Co-doping of ZnO: A Review

A brief review is presented in the following paragraphs covering some of the important results obtained through co-doping. Much of the studies on doped ZnO films have been carried out by using cationic dopants like Al [1, 2], Ga [3,4] and In[5]. Among these Al is the most widely studied dopant [6]. Anionic dopant like fluorine, although there have been much fewer reports than the cases of metallic dopants, is also attractive because substitution of oxygen by fluorine is known to perturb the valence band mostly, leaving the conduction band relatively free of scattering. Feasibility of forming ZnO films with very high mobility was proved via CVD technique at high temperature [7,8], and also PVD techniques like vacuum arc plasma evaporation and sputtering could give possibility of fabricating ZnO films co-doped with fluorine and metallic dopants with better electrical properties [9,10].

Fluorine doped ZnO (FZO) films were deposited on Corning glass using radio frequency (rf) magnetron sputtering of pure ZnO target in CF_4 containing gas mixtures, and the compositional, electrical, optical, and structural properties of the as-grown as well as the vacuum-annealed films were investigated[11]. The fluorine content in FZO films increased with increasing CF_4 content in sputter gas. Three FZO films were prepared by using three different volumetric flow rates of CF_4 gas in an order of increasing CF_4 content in sputtering gas mixture. FZO films deposited at elevated temperature of 150^0C had considerably lower fluorine content and showed a poorer electrical properties than the films deposited at room temperature. Electrical properties of FZO films fabricated at 150^0C were poorer than those grown at room temperature. The lowest resistivity of FZO films deposited at 150^0C was 4.4×10^{-3} Ω cm .The as-deposited film (Room Temperature) had resistivity of 7.84×10^{-2} Ω cm, Hall mobility of 4.7cm^2/Vs, and carrier concentration of 1.7×10^{19}cm^{-3}. While these values after vacuum-annealing were 3.6×10^{-3} Ω cm, 30.5cm^2/Vs and 5.6×10^{19}cm^{-3}, respectively.

Highly transparent and conducting FZO thin films were deposited on glass substrate using Pulsed laser Deposition (PLD)[9]. Structural, electrical and optical properties of the films were investigated as a function of oxygen pressure ranging from 0.01 to 0.5Pa. All the films had highly preferential c-axis orientation (002). The films were dense and very smooth with a typical columnar structure. A minimum resistivity of 4.83×10^{-4} Ω cm, with carrier concentration of 5.43×10^{20} cm^{-3} and Hall mobility of 23.8cm^2/Vs was obtained for FZO film prepared at optimal oxygen pressure of 0.1Pa . The average optical transmittance in the entire visible wave length region was higher than 90%.

In yet another work, FZO transparent conducting films were prepared using radio frequency magnetron sputtering at 150 °C on glass substrate [13]. Thermal annealing in vacuum was used to improve the optical and electrical properties of the films. X-ray diffraction patterns indicated that (002) preferential growth was observed. Grain size of FZO films calculated from the full-width at half-maximum of the (002) diffraction lines is in the range of 18–24 nm. The average transmittance in visible region is over 90% for all specimens. The specimen annealed at 400 °C has the lowest resistivity of 1.86×10^{-3} Ω cm, the highest mobility of 8.9 cm^2 /Vs, the highest carrier concentration of 3.78×10^{20} cm^{-3}, and the largest band gap of 3.40 eV. Resistivity of FZO films increases gradually to 4.58×10^{-3} Ω cm after annealing at 400 °C for 4hrs.

A.Z. Juarez et al. reported the deposition of FZO films onto glass using the CSP, with zinc acetate and NH_4F as precursors [14]. Role of F/Zn atomic ratio, in the starting solution and the substrate temperature were investigated and the optimum deposition conditions have been summarized.XRD of the films showed that there is incorporation of F atoms in the film. The FZO films are of polycrystalline nature with a preferential growth along (0 0 2) plane parallel to the surface of the substrate for temperatures higher than 400^0C. It is observed that fluorine incorporation in the films affects the grain size, which decreased as the F/Zn atomic ratio increases, for the same substrate temperature. The films were uniform and exhibit an optical transmittance above 85% in the visible region.

L.Casteneda et al. [15] recently studied effect of acetic acid content in the starting solution on the composition, morphology, and PL properties of the FZO using CSP. Fluorine content in the samples increases as the acetic acid content in the solutions

increases. Morphology of the FZO thin films changes drastically with the variation of acetic acid content. PL spectra revealed the presence of high defect content in the films.

In another report, M. Olevera [16] et al. revealed the effect of fluorine and aging of the starting solution on electrical, optical, structural and morphological properties of spray pyrolysed FZO films. Two sets of samples were deposited,using fresh and a two-day old starting solution prepared from zinc acetyl acetonate and ammonium fluoride dissolved in a mixture of water and alcohol. Films with a resistivity as low as 2×10^{-2} Ω cm, mobility up to 5 $cm^2/(V\ s)$, carrier concentration in the range $1.5–5.7\times10^{20}$ cm^{-3} and a transmittance in the range 75–90% were achieved with the old solution. Films were polycrystalline, growing preferentially along the (0 0 2) and (1 0 0) directions, depending on the fluorine concentration in the starting solution.

The same group investigated effect of zinc acetate molarity combined with substrate temperature of spray pyrolyzed FZO [17].The lowest value of resistivity was obtained with solutions of 0.2 M. In this case, the resistivity obtained for a film 325-nm thick was 5.5×10^{-2} Ω cm, decreasing to a value of 6.7×10^{-3} Ω cm for films 1400-nm thick. Mobility values were approximately 7 cm^2/VS. Transmittance in the visible is near 90% at 550 nm. All the films showed a preferred (002) crystalline orientation irrespective of the deposition conditions. Finally, the grain size increased as the molarity of the solution decreased.

Effect of the zinc precursor type (zinc acetate and zinc pentanedionate), aging of the starting solution,substrate temperature and a vacuum-annealing treatment on the electrical, morphological, structural and optical properties was studied [18]. Resistivity values of FZO thin films deposited from aged solutions were lower than those films obtained from fresh solutions. The lowest resistivity values of as-grown films deposited at 500^0C, using a two-day aged starting solution of zinc acetate and zinc pentanedionate, were 1.4×10^{-2} and 1.8×10^{-2} Ω cm respectively. After a vacuum annealing treatment performed at 400 ^{0}C for 30 min a decrease in the resistivity was obtained, reaching a minimum value of 6.5×10^{-3} Ω cm for films deposited from an aged solution of zinc acetate. The films were polycrystalline, with a (0 0 2) preferential growth orientation in all the cases. Micrographs from SEM show a uniform surface coverd by rounded grains. No other change in the surface morphology was observed with the different precursors used. The transmittance of films in the visible region was higher than 80%.

Highly transparent and conducting fluorine-doped zinc oxide thin films, consisting of spherical nano meter-sized grains, were synthesized onto soda-lime glass substrate using CSP [19]. Effect of fluorine concentration in starting solution was investigated. Both doped and undoped films were preferentially oriented along [002] direction. Electrical resistivity decreased from 5.7 x 10^{-2} to 8.6 x 10^{-3} Ω cm after 1 at.% fluorine doping, however on further increasing the doping concentration. Surface morphology of films obtained at 3 at.% fluorine doping appeared smooth and uniform.

Altaminaro et al. developed a low resistive ZnO film using sol-gel technique by doping it with fluorine and aluminum [20]. NH_4 F and aluminum nitrate monohydrate were used as the precursors for fluorine and aluminium. All films were thermally pre-heated at 100^0C and then subjected to an annealing process at 450^0C in two different : open air and H_2/N_2 gas mixture. The advantage of doping of both Al and F was that, it maintained good transparency since only very small quantity was present in these films. In this study, Al and F were doped individually and simultaneously. When doped individually, films were showing a slight preferred orientation along (002) plane. Grain size was less for Al-doped film than the F-doped one. These films showed good adherence to the glass substrate and exhibited optical transmittance >90% for 400nm -1200nm.The lowest resistivity obtained was $8.6x10^{-3}$ ohm cm for annealed and co-doped films in H_2/N_2 atmosphere. Carrier concentration and mobility for the best film were $3x10^{19}$ cm^{-3} and 27 cm^2/Vs,respectively.

Fluorine and hydrogen co-doped AZO films were prepared using RF magnetron sputtering of ZnO targets containing 1 wt.% Al_2O_3 on Corning glass at substrate temperature of 150 ◦C with $Ar/CF_4/H_2$ gas mixtures. Structural, electrical and optical properties of the 'as-deposited' and the vacuum-annealed films were investigated [21]. XRD analysis revealed large lattice relaxation with increasing hydrogen and fluorine content, and such lattice expansion was restored upon vacuum annealing. The lowest resistivity of the 'as-deposited' films was about $3.9–4\times10^{-4}$ Ω cm; but very low absorption loss enabled to have fairly high figure of merit of $3.47\Omega^{-1}$. Vacuum-annealing at 300 ◦C resulted in improvement of electrical properties largely due to enhanced Hall mobility without deteriorating the optical properties, yielding minimum resistivity of 2.9×10^{-4} Ω cm and figure of merit as high as 4 Ω^{-1}.

Fluorine and Aluminum doped zinc oxide thin films,Z:Al-F were prepared on soda–lime glass substrates using the sol–gel method and repeated dip-coating. Effect of ageing of the solution and film thickness on the physical characteristics of the films was studied [22]. As deposited Z:Al-F films had high electrical resistivity (order of GΩ), after vacuum annealing, the resistance decreased, to the order of 12 kΩ in the case of the thickest films (520 nm). Structural, optical, and morphological characterizations were carried out in vacuum-annealed films. X-ray diffraction (XRD) patterns revealed that both 'as-deposited' and vacuum-annealed Z:Al-F thin films were polycrystalline having hexagonal wurtzite-type structure with a well-defined (002) diffraction peak, irrespective of the ageing time of the starting solution. Films presented an average optical transmittance in the visible range (400–700 nm) in the order of 90%, as well as a band gap of 3.3 eV.

AZO films with varying fluorine content were prepared through RF magnetron sputtering at a room temperature to investigate doping effects of fluorine on the structural, the optical, and the electrical properties [10]. Small quantity of fluorine addition to AZO films resulted in beneficial effect on the electrical conductivity by improving the direct current (dc) Hall mobility, and the minimum specific resistivity was as low as 5.9×10^{-4} Ω cm. With increasing fluorine content in AZO films, optical absorption loss in the visible range decreased regardless of carrier concentration in the films. X-ray diffraction and scanning electron micrograph analyses showed that the crystallinity of AZO films was deteriorated by addition of fluorine. Small amount of fluorine addition to AZO film resulted in decrease of absorption loss as well as increase in Hall mobility.

Co-doping of Al and F on ZnO nano-powder was successfully achieved by a soft chemical method [23]. An aqueous solution (0.2 M) of zinc acetate (ZnAc) was used as the host precursor. Aluminum nitrate ($Al(NO_3)_3$) and ammonium fluoride (NH_4F) were used as dopant precursors. Four sets of nano-powder samples were synthesized from starting solutions having Al+F in the following proportions: 5+10, 10+20, 15+30 and 20+40 at.%. Triethonalamine (TEA) was added as surfactant and required quantity of NH_3OH solution was added to maintain the pH value as 7.The strong X-ray diffraction peaks revealed the high crystallinity of the synthesized nano-powder and the XRD profiles showed that the material has hexagonal wurtzite structure. The lattice parameters a and c were calculated as 3.258 Å and 5.180 Å respectively. EDAX results confirmed the presence of Al and F and

from the quantitative analysis it was observed that there was a systematic increase in both dopants in the final product as they were included in the starting solution. The SEM images showed that the Z:Al-F powders have nano-rod structure with hexagonal cross section. Co-doping enhanced the carrier concentration of the ZnO nano-powders indicated by the higher IR reflectivity.

Z:Al-F films of 200 nm thicknesses were prepared on glass substrates by co-sputtering targets composed of 2 wt.% Al_2O_3,1.3 wt.% ZnF and pure ZnO targets, respectively [24]. After annealing in vacuum (pressure of 10^{-6} Torr at 300 ◦C for 2 h) resistivity of the films decreased down to 4.75×10^{-4} Ω cm. Interestingly the ZnO film which composed of AZO (25%) and FZO (75%) by volume fraction showed the highest mobility of 42.2 cm^2/V s. All the 'as-deposited' and the annealed films exhibited strong (0 0 2) peaks of preferred orientation, together with relatively weak (1 0 1) and (1 0 3) peaks. It can be concluded that dual doping of F and Al might be a plausible method for getting transparent conducting ZnO films with better performance.

Chemically sprayed fluorine- indium doped ZnO(Z:In-F) thin films were deposited on the glass substrate [25]. Resistivity of the sample decreased with increasing the substrate temperature, reaching the minimum value of 1.2×10^{-2} Ω cm for the samples deposited at 500^0C. XRD patterns revealed that the films were polycrystalline in nature having hexagonal wurtzite type (Preferential orientation in (002) direction).

Recently, A. Maldonado et al. [26]studied the effect of the dopant concentration ratio in the starting solution, as well as the substrate temperature on the electrical, morphological, structural, and optical properties of spray pyrolysed ZnO:In - F thin films . A minimum electrical resistivity, in the order of 3.4×10^{-3} Ω cm, for as-grown films deposited at 475 ◦C from a starting solution containing [In]/[Zn] = 3 and [F]/[Zn] = 20 at.%, was obtained. All the films were polycrystalline, and some differences in the intensity of the peaks and preferential growth, depending on the doping ratios, were observed. The deposited Z:In -F thin films showed an average optical transmittance in the order of 85%, in the visible region (400–700 nm). Band gap values oscillated around 3.35 and 3.39 eV. Surface morphology of the films was also strongly affected by the dopant concentration ratio, since a variation in both geometry and grain size was observed.

T.Minami et al. [9] described the high rate deposition of Ga and F-co-doped ZnO (Z:Ga-F) and ZnO–In_2O_3 multi-component oxide thin films on large area substrates attained by "Vacuum Arc Plasma Evaporation (VAPE)" method using oxide fragments as low-cost source material. Highly transparent and conductive Z:Ga-F and Zinc Oxide – Indium Oxide multicomponent Oxide(Zn_x–In_{1-x}–O)thin films were prepared on substrate at a low temperature of 100^0C. A resistivity of 4.5×10^{-4} Ω cm was obtained in ZnO:Ga, F films deposited at 100^0C using ZnO fragments co-doped with 1 wt.% $ZnF_2$and 1 wt.% Ga_2O_3 as the source material. The ZnO–In_2O_3 thin films having Zn/(In+Zn) atomic ratio of approximately 10–30 at.% deposited on substrates at 100^0C exhibited amorphous nature and smooth surface as well as a low resistivity of $3–4\times10^{-4}$ Ω cm.

Conductive and transparent fluorine and zirconium co-doped zinc oxide[Z:Zr-F)] thin films deposited on sodocalcic glass substrates using CSP [27]. Effects of ageing of starting solution and the substrate temperature on the transport, structural and morphological properties of as-deposited Z:Zr-F) thin films were studied. A decrease in the electrical resistivity values was observed as the starting solution used was aged, reaching a minimum resistivity of the order of 1.3×10^{-2} Ω cm in samples deposited from a 17-day-aged solution. However the resistivity started increasing in samples deposited using solutions aged beyond this. The X-ray diffraction patterns revealed that the Z:F-Zr thin films are polycrystalline in nature, fitting well with a hexagonal wurtzite structure, and showing the preferential growth along (002) direction in all the films. The average optical transmittance, measured in the near UV–visible region, was of the order of 75% in all the cases.

6.2 Experimental details

6.2.1 Co-doping of Indium and Fluorine

In the present work, 'co-doping' of both Indium and fluorine were done by adding required quantities of indium nitrate and ammonium fluoride in to the spray solution; here percentage of Indium in the solution was kept constant (1% of In) while the concentration of fluorine was varied from 0.2 % to 3% and for this, quantity of ammonium fluoride added to the spray solution was varied in calculated quantities. These samples were named as Z:In-0.2F, Z:In-0.5F, Z:In-1F and Z:In-3 F respectively.

6.2.2 Co-doping of Aluminum and Fluorine

In the case of 'co-doping' of both Aluminum and fluorine, required quantities of Aluminum 2,4 pentanedionate and ammonium fluoride were added into the spray solution; here percentage of aluminium in the solution was kept constant (2.5% of Al) while the concentration of fluorine was varied from 0.5 % to 3% and for this, ammonium fluoride was added to the spray solution in calculated quantities. These samples were named as Z:Al-0.5 F, Z:Al-1F, Z:Al-2F and Z:Al-3 F respectively.

6.3 Results and discussions

6.3.1 Effect of co-doping of Indium and Fluorine

6.3.1.1 Structural properties

Fig.6.1 shows XRD pattern of ZnO samples co-doped with indium and fluorine. All the films had peaks at $2\theta=34.42^0$ corresponding to the preferential orientation of (002) plane (JCPDS data card 36-1451). This indicates that the C-axis of the grains becomes uniformly perpendicular to the substrate surface. No fluorine and indium compounds were detected under the resolution limit of the XRD diffraction technique, even when a high percentage of fluorine was used as the dopant during the deposition process. From this figure it is also clear that the intensity of (002) peak decreased after the co-doping of indium and fluorine. Z-In-1F has higher peak compared with other fluorine doped samples.

Mean crystallite size was calculated for the (002) diffraction peak using Debye-Scherrer formula, $D=.9\lambda/\beta Cos\ \theta$, [Where D is the diameter of the crystallite, λ wave length of CuKα line (λ = 1.5404 Å)], β is the full width at half maximum (in radians) and θ is the Bragg angle. After the co doping of indium and fluorine, the crystallite size decreased from 30 nm to 20nm.

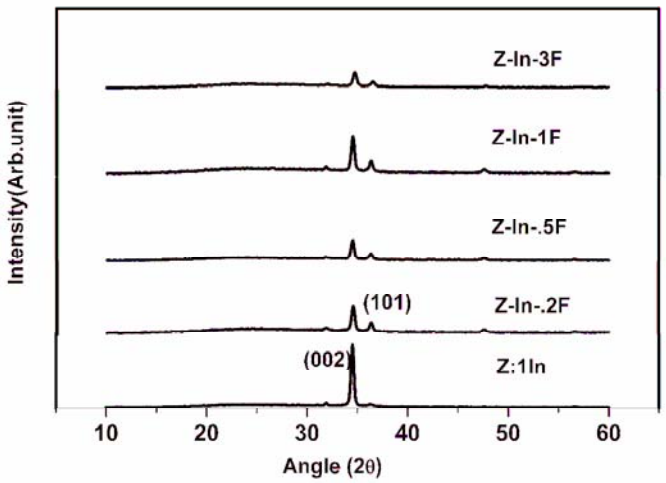

Fig.6.1Variation of XRD with Z:In-F samples at different doping percentage.

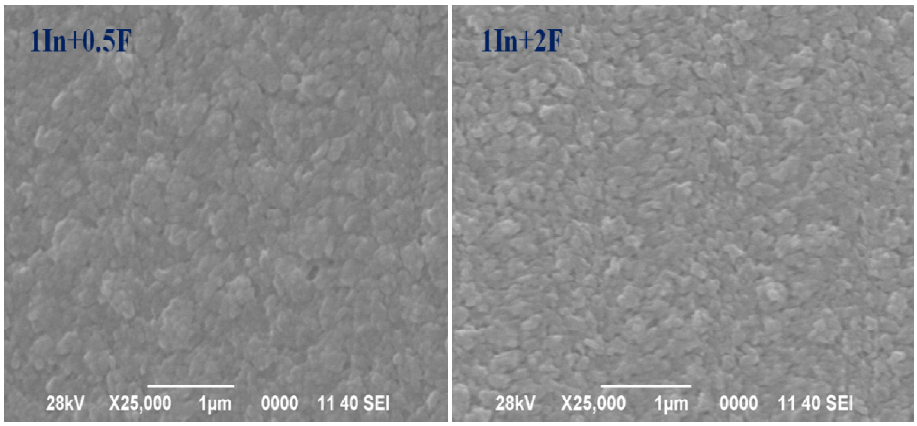

Fig.6.2 SEM micrograph of films with different doping 1) Z:1In-0.5F 2) Z:1In-2F.

Fig.6.2 illustrates electron micrographs showing the morphology of Z:In-F thin films deposited with different doping percentages of fluorine. Uniform, compact and nonporous films with reasonable uniform grain size distribution is observed for the samples deposited with different doping percentage of fluorine.

6.3.1.2 Optical properties

Optical absorption spectra were in the wavelength region 300 -1200 nm. In order to determine the optical band gap, $(\alpha h\nu)^2$ against hν graph was plotted (Fig.6.3). There is slight variation of band gap from 3.25 eV to 3.29 eV after the co-doping.

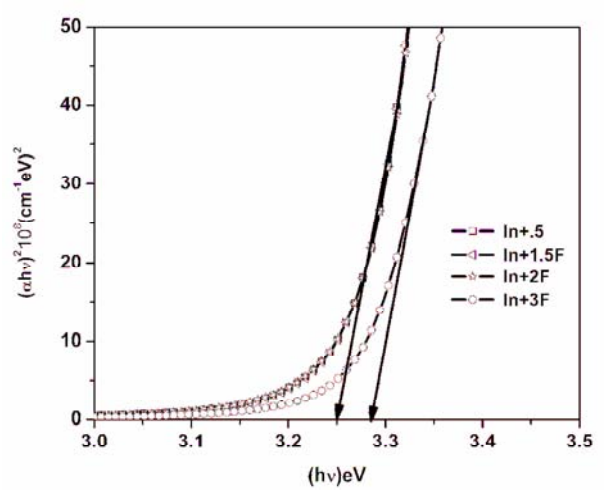

Fig.6.3 $(\alpha h\upsilon)^2$ versus hυ graph for the Z:In-F samples at different doping percentage.

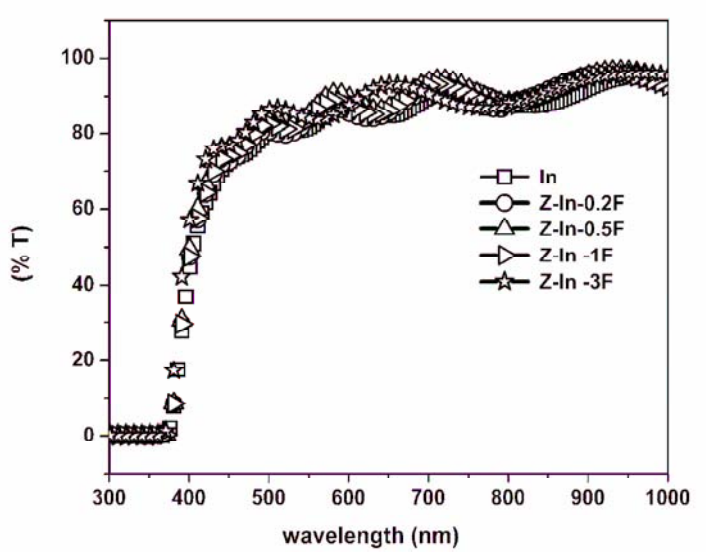

Fig.6.4 Transmission spectra of Z:In-F samples at different doping percentage

Optical transmittance spectra were also recorded in the wavelength range 300 nm to 1200 nm (Fig.6.4). Both Indium doped and Indium-Fluorine doped films showed interference fringe pattern in transmission spectra. This revealed the smooth reflecting surfaces of the films that prevented scattering loss at the surfaces. All the films had high transmittance [> 80%]. Co-doped samples exhibited increased optical transmission in the visible and NIR region and this was good for device fabrication.

6.3.1.3 Electrical properties

Electrical resistivity was measured using two-probe method. It was found that resistivity slightly increased from $2\times10^{-3}\Omega$ cm to $10\times10^{-3}\Omega$ cm (Fig.6.5) in Z:In-F.

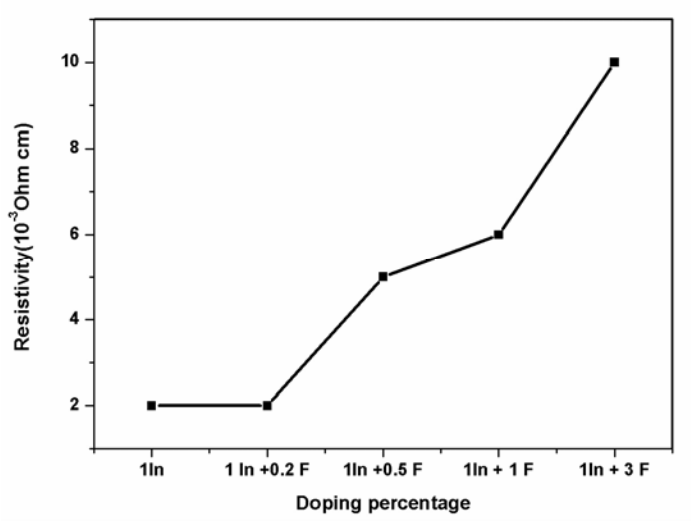

Fig.6.5 Electrical resistivity of Z:In-F at different doping percentage

6.3.2 Effect of co-doping of Aluminum and Fluorine

6.3.2.1 Structural properties

Fig.6.6 shows XRD pattern of ZnO samples co-doped with Aluminum and Fluorine. Details of the doping concentrations and chemicals used are given in Section 6.2.2. All the films had peaks at $2\theta=34.42^0$ corresponding to the preferential orientation of (002) plane, indicating that the C-axis of the grains are uniformly perpendicular to the substrate surface. No compounds related to fluorine and aluminium were detected under the resolution limit of

the XRD diffraction technique, even when a high percentage of fluorine was used for doping process. From Fig.6.6 it is clear that the intensity of (002) plane has no observable variation after the incorporation of fluorine. However the intensity of (101) (2θ=36.80) varied due to the incorporation of fluorine in the film, becoming minimum at 2.5% F. After that the intensity increased. Crystallite size also increased [from 25 nm to 35 nm] with the increase of fluorine concentration up to 2.5 % F and thereafter it slightly decreased.

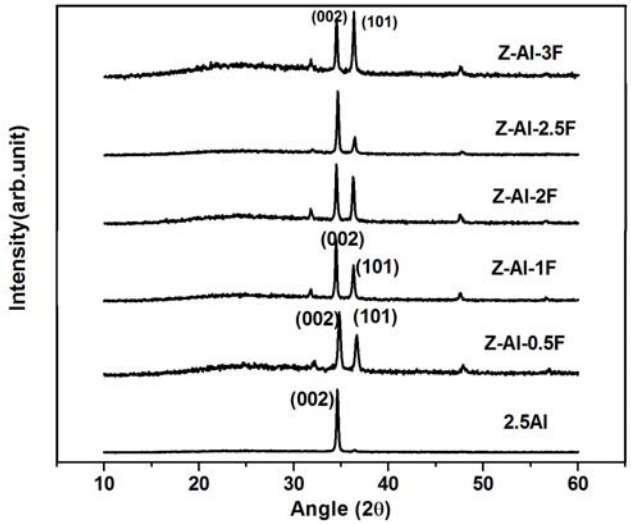

Fig.6.6 Variation of XRD with Z:Al-F at different doping percentage.

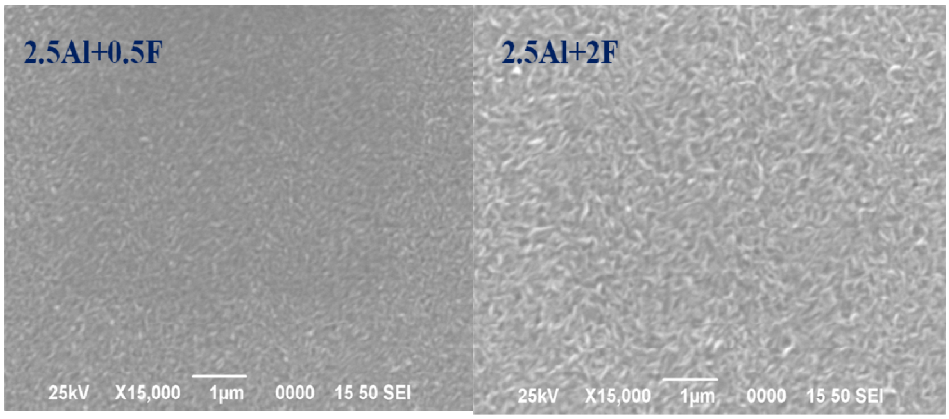

Fig.6.7 SEM micrograph of films with different doping 1) Z:2.5 Al -0.5F 2) Z:2.5Al-2F

6.3.2.2 Optical properties

Optical absorption spectra were recorded in the wavelength region 300 -1200 nm. In order to determine the optical band gap, $(\alpha h\nu)^2$ against hν graph was plotted (Fig.6.8). Small variation of band gap was observed after the co doping of fluorine.

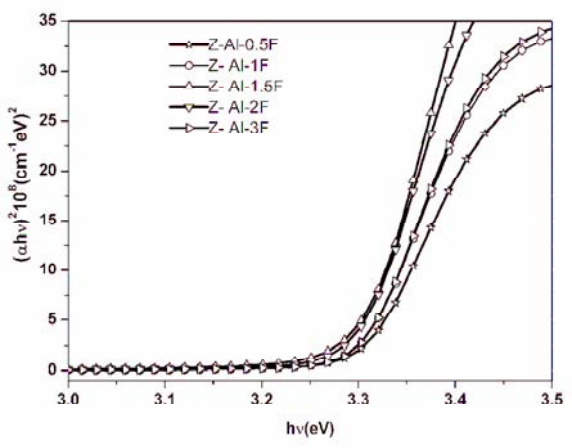

Fig.6.8 $(\alpha h\upsilon)^2$ versus hυ graph for the Z:Al-F samples at different doping percentage

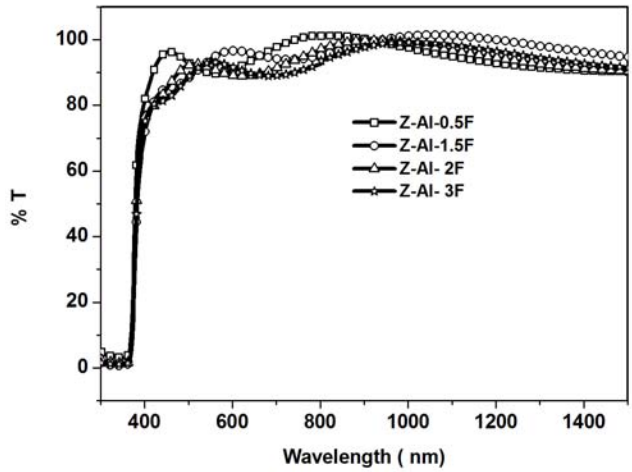

Fig.6.9 Transmission spectra of Z:Al-F samples at different doping percentage

Optical transmittance spectra were also recorded in the wavelength range 300 nm to 1500 nm (Fig.6.9). Z:Al-F films showed high transmittance [> 80%] in transmission spectrum. The transmittance of Z:Al-F was higher than Z:In-F.

6.3.2.3 Electrical properties

Electrical resistivity measurement using 'two-probe' method proved that resistivity increased slightly [from 1.5 $\times 10^{-3}\Omega$ cm to $7\times 10^{-3}\Omega$ cm] with fluorine doping (Fig.6.10). Juarez et al .reported that Z:Al-F films has the lowest resistivity of 8.6 $\times 10^{-3}\Omega$ cm in darkness and 5.6 $\times 10^{-3}\Omega$ cm under controlled illumination of samples prepared using sol-gel method [16].

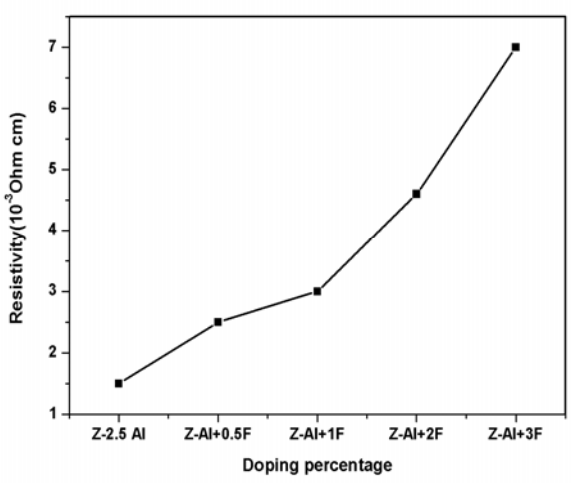

Fig.6.10. Electrical resistivity of Z:Al-F samples at different doping percentage

6.4 Conclusions

We have deposited Z:In-F and Z:Al-F thin film using CSP technique. Here two elements were simultaneously doped into the ZnO thin film. After the study, dopant concentration ratio of Z:In-F and Z:Al-F in the solution were optimized. Intensity of (002) plane peak decreased and crystallite decreased after the co-doping of indium and fluorine.Z:In-F exhibited increase optical transmission. But the electrical resistivity slightly increased after the co- doping of fluorine and Indium. In the case of Z:Al-F film the crystallite size increased and also there was observable variation in (101) plane. Here resistivity was increased after the co-doping of Aluminum and Fluorine. Z:Al-0.5F sample had lowest resistivity and highest transmittance.

Reference

[1] J. Krˇc, M. Zeman, O. Kluth, F. Smole and M. Topic, Thin Solid Films **426** (2003)296.

[2] R. Groenen, J.L. Linden, H.R.M. van Lierop, D.C. Schram, A.D. Kuypers, and M.C.M.van de Sanden, Appl. Surf. Sci. **173** (2001) 40.

[3] S.M. Park, T. Ikegami and K. Ebihara, Thin Solid Films **513** (2006) 90.

[4] T. Yamada, A. Miyake, S. Kishimoto, H. Makino, N. Yamamot and T. Yamamoto,Surf. Coat. Technol. **202** (2007) 973.

[5] Yu Bin Xiao, Seon Mi Kong, Eun Ho Kim and Chee Won Chung ,Sol. Ener. Mat. & Solar Cells **95**(2011) 264.

[6] K. Ellmer, J. Phys. D: Appl. Phys. **34** (2001) 3097.

[7] J. Hu and R.G. Gordon, Solar Cells **30** (1991) 437.

[8] R.G. Gordon, MRS Bull. **25** (2000) 52.

[9] T. Minami, S. Ida, T. Miyata and Y. Minamoto, Thin Solid Films **445** (2003) 268.

[10] I.H. Kim, K.S. Lee, T.S. Lee, J.-H. Jeong, B. Cheong, Y.J. Baik and W.M. Kim, J. Appl. Phys. **100** (2006) 063701.

[11] H.S. Yoon, K.S. Lee, T.S. Lee, B. Cheong, D.K. Choi, D.H. Kim and W.M. Kim, Sol. Energy Mater. Sol. Cells **92** (2008) 1366.

[12] Ling Cao,Liping Zhu, Jie Jiang,Ran Zhao,ZhizhenYe and Buihui Zhao,Sol. Energy Mat. & Solar Cells **95** (2011) 894.

[13]Yu-Zen Tsai , Na-Fu Wang and Chun-Lung Tsai ,Thin Solid Films **518** (2010) 4955.

[14] A. Sanchez-Juarez, A. Tiburcio-Silver and A. Ortiz ,Sol. Energy Mat. and Solar Cells **52** (1998) 301.

[15] L. Castaneda , A.Maldonado, J.Rodrıguez-Baez, J.C.Cheang-Wong , M. Lo pez-Fuentes and M. delaL.Olvera, Materials Science in Semiconductor Processing(Article in press)

[16] M. de la L. Olvera, A. Maldonado and R. Asomoza, Sol. Energy Mat. & Solar Cells **73** (2002) 425.

[17] M. de la L. Olvera, A. Maldonado, R. Asomoza, O. Solorza and D.R. Acosta ,Thin Solid Films **394(**2001) 242.

[18] A. Maldonado, S.Tirado-Guerra, M. Melendez-Lira and M. de la L. Olvera Sol.Energy. Mat. And Solar Cells **90** (2006) 742.

[19] B.N. Pawar, Duk-Ho Ham, R.S. Mane, T. Ganesh, Byung-Won Cho and Sung-Hwan Han ,Applied Surface Science **254** (2008) 6294.

[20] D.C. Altamirano-Juárez, G. Torres-Delgado, S. Jiménez-Sandoval, O. Jiménez-Sandoval and R. Castanedo-Pérez, Sol. Energy Mater. Sol. Cells **82** (2004) 35.

[21] Y.H. Kima,c, J. Jeongb, K.S. Leea, J.K. Parka, Y.J. Baika, T.-Y. Seongc, W.M. KimApplied Surface Science **256** (2010) 5102.

[22] A. Maldonado, S. Tirado-Guerra, J.M. Cázares and M. de la L. Olvera ,Thin Solid Films **518** (2010) 1815.

[23] K. Saravanakumar, B. Sakthivel and K. Ravichandran, Materials Letters **65** (2011) 2278.

[24] B.G. Choi, I.H. Kim, D. H Kim, K.S. Lee, T.S. Lee, B. Cheong, Y.-J. Baik and W.M. Kim, Journal of the European Ceramic Society **25** (2005) 2161.

[25] O. G. Morales-Saavedra, L Casteneda, J.G.Banuelos and R.Ortega- Martinez. Laser Physics **18** (2008) 283.

[26] A. Maldonado,J. Rodríguez-Baez, and M. de la L. Olvera ,Materials Chemistry and Physics **129** (2011) 109.

[27] A. Maldonado, S.Tirado-Guerra , and M. delaL.Olvera, J. of Phy. and Chem. of Solids **70** (2009) 571.

Chapter 7

Summary and Conclusions

Present work is on the development of highly conductive and transparent Zinc Oxide (ZnO) thin film using Chemical Spray Pyrolysis (CSP). First we introduced an innovative post deposition treatment for enhancing the conductivity of ZnO, which we called as "Zero-Energy Process". Further work was on enhancing the conductivity by doping of different elements Aluminum (Al), Indium (In), Tin (Sn) and co-doping using Indium & Fluorine (In+F) and Aluminum & Fluorine (Al+F).

ZnO thin films were deposited on soda lime glass substrate with following parameters kept as constant [Temperature- 450^0C ± 5^oC, Molarity- 0.3M, Volume-100 ml and spray rate -7ml/min]. After the deposition of the film, two type of post deposition treatments were tried on the samples. One is 'Regular cooling (Z-R)' and the other is 'Inversion cooling (Z-I)'. X-ray photo-electron spectroscopy analysis showed that Zn/O ratio increased after the inversion process and the ratio is uniform throughout the thickness of the samples. All films had orientation along (002) plane. Above all electrical resistivity of Z-I decreased from 80 Ω cm to 2.4 $\times 10^{-2}$ Ω cm. Photoluminescence studies revealed that the intensity of 'Blue-green emission' [which was due to the transition to the Oxygen antisite (O_{zn})] was decreased after the inversion. The process could also enhance the crystallinity and the optical transmittance. Vacuum annealing does not bring any further changes in electrical properties of Z-I samples. But After the vacuum annealing of Z-R, resistivity decreased from 80Ω cm to 1.8×10^{-2} Ω cm. Thus the Zero-Energy process resulted in samples of high electrical conductivity and optical transmission avoiding the post deposition [and energy consuming] processes like vacuum annealing.

Deposition parameters of ZnO thin films like molarity, spray rate, precursor medium and pH of the solution were optimised to get the good quality and large area thin films. The samples were prepared at different spray rate, varied from 3 ml/min to 12 ml/min after fixing all the other parameters constant. Structural analysis proved that with increasing the spray rate from 5 ml/min to 7ml/min, orientation of films tuned from (101) to (002). By the variation of spray rate we could fine tune the intensity of 'Blue- Green emission'; it

decreased after the orientation of grains shifting to (002) plane. The film with spray rate of 7ml/min achieved the lowest resistivity of 2.4×10^{-2} Ω cm. Keeping the spray rate at 7 ml/min, samples were prepared using different molarities of Zinc acetate solution [from 0.2 M to 0.6 M]. At the lower molarity, samples exhibited poly crystalline nature with the planes orienting along (002) and (101) directions. After reaching 0.3M, intensity of peak corresponding to the plane (101) decreased while that of the plane (002) increased. Resistivity of the samples increased with increasing the molarity of the solution. After optimizing spray rate (7ml/min) and molarity (0.3M), next move was to vary the precursor medium. In this work two types of spray solutions were used. In the first one, this aqueous solution was mixed with ethanol while in the other type the aqueous solution was mixed with propanol. Volume of alcohol added to the aqueous solution was varied as 0,20,30,50,60 and 70 ml so that the total volume of spray solution was always 100 ml. Crystallite size, optical transmission and electrical conductivity of the films enhanced with increase of alcohol concentration. Intensity of Blue-green emission varied with percentage as well as with the type of alcohol used in the precursor solution, supporting the results from electrical and optical characterisations. Propanol based samples had lower resistivity than the ethanol based samples. The lowest value of $2\times10^{-2}\Omega$ cm was obtained for the sample prepared using water and propanol in 1:1. In the next step, pH of the solution was varied from pH-3 to pH-6. From the pH-3.5 to pH-4, the orientation of grains was shifted to (002) direction. But in the case of lower and higher pH, (101) was the preferential orientation. Precursor solution with pH-4 exhibited the lowest value of resistivity in the order of $2\times10^{-2}\,\Omega$ cm. Finally spray rate was fixed 7ml/min and molarity of the spray solution, at 0.3M. The precursor medium was selected as the one having deionised water and propanol in the ratio 1:1 with pH equal to 4. We used these optimised condition for the preparation of doped ZnO thin film for the further studies.

For doping studies we tried various methods and elements with the aim of reducing the resistivity of the sample. In 'ex-situ doping', a thin layer of In/Sn was deposited over the undoped ZnO thin films using vacuum evaporation [Pressure ~ 2×10^{-5} mbar] method and this bilayer films were annealed in vacuum [Pressure ~ 2×10^{-5} mbar; Temperature-100 ^{0} C; Time- 60 min]. Different masses of In/Sn (2, 4, 6, 8 and 10 mg) were deposited over the surface of ZnO sample. There was small variation of band gap after the doping. Resistivity

of the Z-8mg-In reduced from 28 $\times 10^{-3}$ Ω cm to 8×10^{-3} Ω cm. Transmittance of the sample decreased when the doping percentage increased. In-situ doping using Indium (indium nitrate) was an excellent method for enhancing the conductivity of the sample. Incorporation of 1% Indium through in-situ method resulted in giving the lowest resistivity of 2 $\times 10^{-3}$ Ω cm and >80% transmission in visible region. PL analysis also supported the results from electrical characterisation studies of the samples.

Aluminum was doped by adding the required quantity of aluminum 2, 4 pentanedionate in the spray solution itself [In-situ method]. Doping percentage of Aluminum was varied from 0.5 to 3.5%. Samples doped with aluminum in the range 2 to 2.5 % had resistivity of 1.5×10^{-3} Ω cm. Annealing of these samples in vacuum further lowered the resistivity [6×10^{-4} Ω cm], with optical transmittance [in visible region] remaining in the range 85 to 90%. Transmission in the NIR region decreases after the vacuum annealing. A phenomenon that is common in all other transparent conductors [like ITO] with higher carrier concentration. Room temperature PL revealed that the intensity of the blue-green emission (520 nm) decreased in these samples. Lowest intensity for the PL emission was also obtained for the sample having the optimum doping.

In the case of 'co-doping' of both Aluminum and fluorine, required quantities of Aluminum 2,4 pentanedionate and ammonium fluoride were added into the spray solution; here percentage of aluminum in the solution was kept constant (2.5% of Al) while the concentration of fluorine was varied from 0.5 % to 3% and for this, ammonium fluoride was added to the spray solution in calculated quantities. In the case of Z:Al-F film the crystallite size increased and also there was observable variation in (101) plane. Here the transmittance and resistivity were increased. Co-doping of both Indium and fluorine was done by adding required quantities of indium nitrate and ammonium fluoride in to the spray solution; here percentage of Indium in the solution was kept constant (1% of In) while the concentration of fluorine was varied from 0.2 % to 3%.Intensity of (002) plane peak decreased and crystallite decreased after the co-doping of indium and fluorine. Z:In-F exhibited increase in optical transmission. But the electrical resistivity slightly increased after the co doping using fluorine and indium. Fig.7.1 shows resistivity value through various stages of ZnO film.

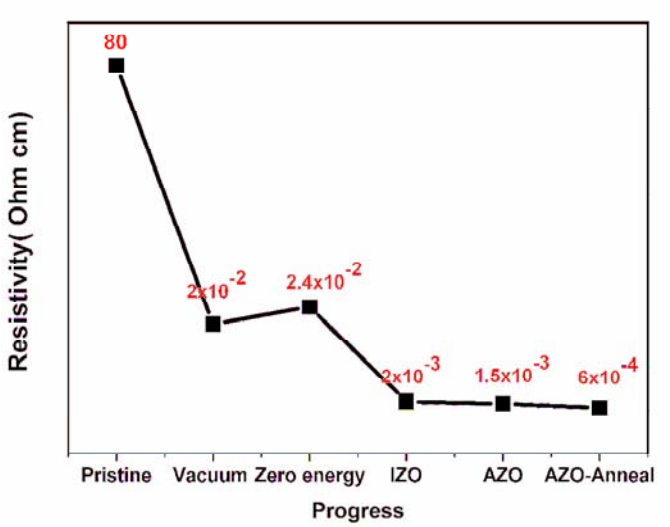

Fig.7.1.Resistivity values of ZnO thin films achieved in the present work.

Future scopes

1) Automation of Inversion process has to be done as it guarantees more than 95% uniform resistance over the sample surface.

2) Development of nano ZnO using chemical spray pyrolysis.

3) Fabrication ZnO/nano ZnO based all sprayed Thin film solar cell.

Main aim of our research work is the fabrication of very low cost and eco-friendly thin film solar cells using easily available materials. In our lab, thin films of In_2S_3, $CuInS_2$ are prepared using Chemical Spray Pyrolysis technique. Suitable combinations of these compounds, in bilayer thin film structure, can form p-n junction ($ZnO/In_2S_3/CuInS_2/Ag$) and hence find application in solar cell technology with sprayed ZnO as the electrode instead of high cost ITO. Development of 'Extremely Thin Absorber [ETA]' layer solar cells having ZnO [possibly with nano rods] as the TCO layer [using spray pyrolysis for the deposition of all the three layers] will be the ideal aim in this type of work.